

Symmetry Energy I: Semi-Infinite Matter

Paweł Danielewicz^{1,2} and Jenny Lee¹

*¹National Superconducting Cyclotron Laboratory and
Department of Physics and Astronomy, Michigan State University,
East Lansing, Michigan 48824, USA*

*²Kavli Institute for Theoretical Physics
University of California, Santa Barbara, CA 93106*

arXiv:0807.3743v2 [nucl-th] 29 Oct 2008

Abstract

Energy for a nucleus is considered in macroscopic limit, in terms of nucleon numbers. Further considered for a nuclear system is the Hohenberg-Kohn energy functional, in terms of proton and neutron densities. Finally, Skyrme-Hartree-Fock calculations are carried out for a half-infinite particle-stable nuclear-matter. In each case, the attention is focused on the role of neutron-proton asymmetry and on the nuclear symmetry energy. We extend the considerations on the symmetry term from an energy formula to the respective term in the Hohenberg-Kohn functional. We show, in particular, that in the limit of an analytic functional, and subject to possible Coulomb corrections, it is possible to construct isoscalar and isovector densities out of the proton and neutron densities, that retain a universal relation to each other, approximately independent of asymmetry. In the so-called local approximation, the isovector density is inversely proportional to the symmetry energy in uniform matter at the local isoscalar density. Generalized symmetry coefficient of a nuclear system is related, in the analytic limit of a functional, to an integral of the isovector density. We test the relations, inferred from the Hohenberg-Kohn functional, in the Skyrme-Hartree-Fock calculations of half-infinite matter. Within the calculations, we obtain surface symmetry coefficients and parameters characterizing the densities, for the majority of Skyrme parameterizations proposed in the literature. The volume-to-surface symmetry-coefficient ratio and the displacement of nuclear isovector relative to isoscalar surfaces both strongly increase as the slope of symmetry energy in the vicinity of normal density increases.

PACS numbers: 21.10.Dr, 21.10.Gv, 21.60.Jz, 21.65.-f, 21.65.Cd, 21.65.Ef

Keywords: symmetry energy, half-infinite matter, nuclear matter, Hohenberg-Kohn functional, Skyrme-Hartree-Fock model, nuclear surface, isovector density, surface symmetry coefficient

I. INTRODUCTION

Nuclear symmetry energy ties different areas of nuclear physics, including structure of ground-state nuclei, dynamics of central nuclear reactions, physics of giant collective excitations and physics of neutron stars. Recently, the interest in symmetry energy has been stirred up by novel astrophysical observations and by the availability of exotic beams in accelerators, with greater span of asymmetries for given nuclear mass than for stable beams. Particularly important in the different areas, and simultaneously uncertain, is the density dependence of symmetry energy in uniform matter. As situation in the literature progresses, an increasing wider range of theoretical conclusions is getting made on that density dependence, as well as on some associated nuclear characteristics. In that situation, not unfamiliar from other contexts, rather than increasing claim statistics, it may be useful to take a step back and examine in detail the chain of implications following from the symmetry energy, to better understand the connections and to see how firmly any conclusions can be reached. We hope to make such a progress here within nuclear structure.

Two main directions are advanced in our paper. One is in extending and combining symmetry-energy considerations from nuclear energy formula and from uniform nuclear matter, within the nuclear energy functional of the Hohenberg-Kohn type [1]. Another direction is in carrying calculations of semi-infinite nuclear-matter within the Skyrme-Hartree-Fock approach [2]. The framework developed in considering the energy functional is employed in analyzing the Hartree-Fock calculations. In the past, an analysis pertaining to the symmetry-energy, in the context of Hohenberg-Kohn functional, has been carried out by Farine [3]. Semi-infinite asymmetric matter has been examined before in the Hartree-Fock approach, in particular by Kohler [4, 5] and by Pearson *et al.* [6, 7, 8], and in the relativistic Hartree approach by Del Estal *et al.* [9]. Also, a number of Thomas-Fermi calculations for the half-infinite asymmetric matter have been done [10, 11, 12, 13, 14, 15, 16]. Since the latest detailed Hartree-Fock studies by Pearson *et al.* [8] have been done over two decades ago, there is potential for computational progress in these calculations, aside from our differing strategy in analyzing the results.

In the following, Sec. II reviews the basic nuclear energy formula, emphasizing the symmetry energy. Section III extends the symmetry-energy considerations to the context of a continuous nuclear Hohenberg-Kohn energy-functional. The limit of uniform matter is

discussed there too. In Sec. IV, details of our numerical calculations of half-infinite matter are presented and the results analyzed. Overall conclusions are presented in Sec. V.

II. ENERGY FORMULA

A. Elementary Formula

The first basic context within which the nuclear symmetry energy is encountered is the empirical nuclear energy formula. In its most elementary textbook form, the formula contains just four macroscopic terms:

$$\begin{aligned} E(N, Z) &= E_{\text{mac}} + E_{\text{mic}} = E_V + E_S + E_a + E_C + E_{\text{mic}} \\ &= -a_V A + a_S A^{2/3} + a_a \frac{(N - Z)^2}{A} + a_C \frac{Z^2}{A^{1/3}} + E_{\text{mic}}. \end{aligned} \quad (1)$$

Here, N and Z are the neutron and proton numbers, respectively, $A = N + Z$ is the mass number and a_V , a_S , a_a and a_C are the volume, surface, symmetry and Coulomb coefficients. The microscopic energy E_{mic} contains shell and pairing energy corrections. In spite of its simplicity, the energy formula is extremely powerful both in describing nuclear masses and in giving access the nature of nuclear interactions. When the microscopic corrections are disregarded, and the macroscopic coefficients are fitted to the data set on energies of over 3100 $A \geq 10$ nuclei, to yield $a_V = 15.3$ MeV, $a_S = 16.1$ MeV, $a_a = 22.5$ MeV and $a_C = 0.69$ MeV, the rms deviation of the formula from data turns to be just 3.6 MeV, to be compared to the span of energies for the nuclei of over 2000 MeV. The nuclear energies are dominated by the volume term, responsible for nuclear binding, with binding energies reduced by the surface, symmetry and Coulomb terms.

Regarding the nature of nuclear interactions, the dominance in E of the negative volume term E_V , proportional to A , tells that the attractive nuclear interactions are short-range. The invariance of the symmetry term E_a with respect to neutron-proton interchange demonstrates that the nuclear interactions possess such an interchange symmetry, commonly termed charge symmetry. The positive value of a_a suggests that neutron-proton interactions are more attractive than like-nucleon interactions; the Pauli principle effects contribute positively to that coefficient as well. The surface term E_S scales with A as in proportion to the surface of a nucleus with fixed volume per nucleon, represented as $4\pi r_0^3/3$, or, equivalently,

with fixed density $\rho_0 = 3/(4\pi r_0^3)$. The reduction in the binding proportional to the surface may be thought of as one associated with the fact that nucleons at the surface experience less attraction than the nucleons in interior; the curvature of nuclear wavefunction at the surface also, in fact, contributes to that reduction. The form of the Coulomb term E_C is such as expected for a uniformly charged sphere, specifically $(3/5)(Ze)^2/4\pi\epsilon_0 R$, where $R = r_0 A^{1/3}$.

Quantitatively, the fitted Coulomb parameter provides an estimate of the nuclear radius parameter, $r_0 \simeq (3/5)e^2/(4\pi\epsilon_0 a_c) = 1.25$ fm. With necessarily enhanced error, due to the raising of r_0 to cube power, the parameter further implies an estimate for the nuclear density ρ_0 . Under changing nuclear density ρ , the nuclear energy should minimize at ρ_0 , reaching the value of $-a_V$ per nucleon for $N = Z$ and in absence of Coulomb interactions or boundaries. Given the surface term, one can estimate the nuclear surface tension, which is the energetic cost of creating the surface per unit area, or tension, $\sigma = \partial E/\partial \Sigma = a_S/4\pi r_0^2 \simeq 0.8$ MeV/fm², again with a deteriorated expected accuracy due to the power of radius and due to combining of parameters. In the tension, Σ is nuclear surface area taking on the value of $4\pi r_0^2 A^{2/3}$ for a spherical shape. It is apparent that the energy formula can provide a wealth of information on nuclei. Naturally, this can be expected to extend to the changes in nuclear properties with changes in the relative neutron-proton asymmetry, $\eta = (N - Z)/A$.

The success of the energy formula may be extended by modifying terms and incorporating new ones, with or without new parameters, including the microscopic terms. The terms may be guided by physics or *ad hoc*. The formula success can be perceived in at least two different ways. One is in terms of a better predictive power of the formula for net energy. In fact, by adding different terms and parameters, the rms deviation from fitted nuclear can be reduced by a factor of order of 5 [17, 18, 19, 20, 21]. Another measure of success is in enhanced access to fundamental nuclear properties. The advances in the two directions do not necessarily go hand in hand. Thus, obviously, adding an *ad hoc* term may throw off the value of a parameter that has a physical meaning, while helping though to reduce the rms error [20]. Even when a term of genuine physical meaning is added, problems can occur when many terms and parameters are present [22]. As an example, one can envision that the range of variation of N and Z for measured nuclei may not be suffice to make two terms in an energy formula distinct, with different parameter combinations yielding comparable agreement with data and a parameter expected *a priori* to be obscure, eating into a major parameter. Another example might be a term introduced to improve the description

of one N - Z region (e.g. low A) that gets its parameters determined, in an unguided fit, by the prevalence of nuclei in another N - Z region (such as high A). The problems with multiparametric fits are known from other areas and the developed remedy is to introduce as many prejudices [23] into the fit as possible. The prejudices may, in fact, include the qualitative features of fitted functions, following from physical considerations, common-sense limits on region for parameter determination and the use of constraints on the parameters from auxiliary investigations. The latter constraints, in the case of an energy formula, could e.g. involve information on the proton and neutron densities, ρ_p and ρ_n [20, 24, 25].

B. Surface Symmetry Energy

Examining the symmetry term in the basic formula (1), one can notice that this term has a volume character, i.e. it changes in proportion to A , like E_V , when N and Z are changed by same factor. One question which arises, when addressing the symmetry energy, is whether there is a conceptual need for adding a *surface* symmetry term to the energy formula. Another question is how such term should enter that formula. In the literature, there are at least two ways of introducing such a term, with a surface symmetry parameter having different meanings in the two formulations.

Regarding the first question, the volume energy becomes less negative, when magnitude of nuclear asymmetry increases from zero, at a fixed A . With this, less work should be required for developing a surface, since there is less lost binding then to compensate for compared to zero asymmetry. Thus the surface tension should drop with increase in asymmetry magnitude. The quantity associated with asymmetry, shared by systems in contact in macroscopic equilibrium, such as the surface region and interior, is the asymmetric chemical potential

$$\mu_a = \frac{\partial E}{\partial(N - Z)} = \frac{1}{2}(\mu_n - \mu_p). \quad (2)$$

Under charge symmetry of nuclear interactions, with Coulomb ignored for the moment, the nuclear tension should depend only on square of μ_a and, following the above, behave for small asymmetries as

$$\sigma = \frac{\partial E_S}{\partial \Sigma} = \sigma_0 - \nu \mu_a^2, \quad (3)$$

where $\sigma_0 = a_S/4\pi r_0^2$ is the tension for symmetric nuclear matter and ν is some positive constant. When the tension depends on asymmetry, so must the surface energy E_S , cf. (3).

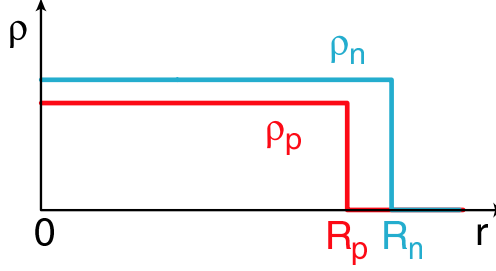


FIG. 1: Surface asymmetry can be understood in terms of different radii for proton and neutron distributions.

The next question is of the form of an energy formula which incorporates that dependence and, of course, of the consequences of that dependence.

The inverse Legendre transformation for asymmetry, from μ_a to $N - Z$, is given by

$$N - Z = \frac{\partial \Phi}{\partial \mu_a}, \quad (4)$$

where

$$\Phi = \mu_a(N - Z) - E = \mu_a(N - Z) - E_V - E_S. \quad (5)$$

Upon inserting of (5) into (4), we find

$$\frac{\partial(N - Z)}{\partial \mu_a} = 2 \frac{\partial E}{\partial \mu_a^2} = 2 \left(\frac{\partial E_V}{\partial \mu_a^2} + \frac{\partial E_S}{\partial \mu_a^2} \right). \quad (6)$$

In the equation above, $N - Z$, E , E_V and E_S are all extensive, i.e. they grow, in a characteristic fashion, as the system size grows. The equation implies that, when the surface energy depends on μ_a , the net asymmetry partitions into volume and surface portions, $N_V - Z_V$ and $N_S - Z_S$, satisfying respectively

$$\frac{\partial(N - Z)_{V,S}}{\partial \mu_a} = 2 \frac{\partial E_{V,S}}{\partial \mu_a^2}. \quad (7)$$

The surface asymmetry may be transcribed onto a difference of radii for neutron and proton distributions, which is the basis of the droplet model (to be discussed) of nuclei and is schematically indicated in Fig. 1.

Given that, at low asymmetries, due to charge symmetry, the energies must depend quadratically on asymmetry, as does the tension in Eq. (3), the second derivatives of energy in Eqs. (6) and (7) can only depend on A . In consequence, at low asymmetries, also the first derivatives of $N - Z$ in those equations must also depend solely on A . Accounting for

the dimensions and for scalings with A , we can write

$$N_V - Z_V = \frac{A}{2 a_a^V} \mu_a \quad \text{and} \quad N_S - Z_S = \frac{A^{2/3}}{2 a_a^S} \mu_a, \quad (8)$$

where a_a^V and a_a^S are constants characterizing the nuclear volume and surface, respectively, with the dimension of energy. Sum of the two asymmetries gives us the relation between μ_a and net asymmetry:

$$N - Z = N_V - Z_V + N_S - Z_S = \frac{\mu_a}{2} \left(\frac{A}{a_a^V} + \frac{A^{2/3}}{a_a^S} \right). \quad (9)$$

From Eqs. (7) and (8), we further find

$$E_V = E_V^0 + \frac{A}{4 a_a^V} \mu_a^2 = -a_V A + a_a^V \frac{(N_V - Z_V)^2}{A}, \quad (10)$$

and

$$E_S = E_S^0 + \frac{A^{2/3}}{4 a_a^S} \mu_a^2 = a_S A^{2/3} + a_a^S \frac{(N_S - Z_S)^2}{A^{2/3}}, \quad (11)$$

where $E_{V,S}^0$ are the volume and surface energies for symmetric $N = Z$ matter. It should be mentioned that there is no error in the sign difference in symmetry terms between Eqs. (11) and (3). Whereas the volume and surface energies increase with asymmetry, the surface tension decreases. The derivative of surface energy with respect to surface area, for the surface tension σ , must be taken at constant $N_S - Z_S$, which yields $\nu^{-1} = 16 \pi r_0^2 a_a^S$.

On adding up the energy contributions (10) and (11), we get for the net energy

$$E = E^0 + \frac{\mu_a^2}{4} \left(\frac{A}{a_a^V} + \frac{A^{2/3}}{a_a^S} \right) = -a_V A + a_S A^{2/3} + \frac{(N - Z)^2}{\frac{A}{a_a^V} + \frac{A^{2/3}}{a_a^S}}, \quad (12)$$

where we have eliminated μ_a in favor of $N - Z$ using (4). The nuclear energies above, quadratic in asymmetry, exhibit analogy to the capacitor energy in terms of electric charge. While asymmetry is analogous to the electric charge within this analogy, the chemical potential is analogous to the electric potential. The coefficients of proportionality between volume and surface asymmetries and chemical potential in (8) are analogs of capacitance, with the two capacitances proportional, respectively, to the volume and surface. For connected capacitors, the potentials are equal. The net symmetry partitions itself in (9), between the volume and surface, in proportion to the capacitances. Finally, net energy for connected capacitors can be represented in (12) either in terms of net potential squared multiplied by net capacitance or in terms of net asymmetry squared divided by the net capacitance¹.

¹ Beyond the quadratic approximation for the energy in asymmetry, the capacitance may be defined [26] in terms of the derivative of asymmetry with respect to the chemical potential, i.e. the l.h.s. of (6).

Upon adding the Coulomb and microscopic contributions, we now arrive at the energy formula with a mass-dependent symmetry coefficient

$$E(N, Z) = -a_V A + a_S A^{2/3} + \frac{a_a(A)}{A} (N - Z)^2 + a_C \frac{Z^2}{A^{1/3}} + E_{\text{mic}}, \quad (13)$$

where

$$a_a(A) = \frac{a_a^V}{1 + a_a^V / (a_a^S A^{1/3})}. \quad (14)$$

In the limit of large A , the asymmetry gets primarily stored within the volume and then the coefficient $a_a(A)$ tends towards a_a^V . On the other hand, in the limit of small A , the storage of asymmetry gets shifted to the surface and then the ratio $a_a(A)/A$ approaches $a_a^S/A^{2/3}$.

Although the surface symmetry effects can be important in learning on symmetry energy, as far as the net nuclear energy is concerned, those effects just correct the symmetry energy which itself is a correction to the leading term $-a_V A$ term in an nuclear energy. Additionally, since most of the measured asymmetric nuclei are heavy, those nuclei can provide little variation for $A^{1/3}$ in the symmetry-energy term. In consequence, the basic energy formula (1) can provide a fit to the measured nuclear energies that is quite satisfactory without any surface symmetry modification.

The coefficient a_a^S of surface symmetry energy is generally of interest as a fundamental quantity and because, in the context of the changing density at nuclear surface, it can provide access to the density dependence of symmetry energy in bulk nuclear matter. However, obviously, since a_a^S appears within a correction to a correction in the energy formula, it can be difficult to learn about that coefficient by fitting nuclear energy data with a formula where further types of secondary corrections may need to be included. The latter corrections may compete against each other and against the surface symmetry energy [22, 25]. This can be especially true for blind fits. The potential secondary corrections include those to the asymmetry-*dependent* Coulomb term and those to the asymmetry-*independent* part of the formula. The Coulomb energy e.g. also affects the surface asymmetry. Corrections to the asymmetry-independent part of the formula are important, possibly against expectations, because the grouping of nuclei around the line of stability, in the (N, Z) -plane, introduces mass-asymmetry correlations for the fitted data.

In this and in a subsequent paper, we shall try to understand the interplay between the dependence of bulk symmetry energy on density, density distributions in nuclei and the symmetry coefficient $a_a(A)$. On one hand, we shall try understand a connection between a_a^S

and the density dependence of symmetry energy. On the other hand, we shall try to determine $a_a(A)$ from nuclear data, refraining from a blind fit and without insisting on validity of Eq. (14). Finally, we shall seek additional information on symmetry energy within density distributions.

C. Droplet Model

A result of the form (14), for the symmetry coefficient, has first appeared in the literature in the droplet model [27] by Myers and Swiatecki. The droplet model relies on the assumption that the neutron and proton surfaces shift relative to each other as nuclear asymmetry changes. The surface energy per the elementary area of $4\pi r_0^2$ depends in the model on that shift, D_{np} , and on the relative asymmetry in nuclear interior, η_V , according to:

$$\frac{4\pi r_0^2 E_S}{\Sigma} = a_S + H \left(\frac{D_{np}}{r_0} \right)^2 + 2P \eta_V \frac{D_{np}}{r_0} - G \eta_V^2. \quad (15)$$

In the above, H , P and G are model constants and we have dropped a higher-order curvature term employed in [27]. (Strictly, the surface energy density E_S/Σ is identified in [27] as the surface tension σ , but these two are different when they depend on asymmetry, cf. Subsection II B; Eq. (15) is consistent with the *use* of the formula by the authors of [27].) When a higher-order Coulomb correction included in [27] is disregarded, the symmetry coefficient emerges such as given by Eq. (14), with the surface symmetry coefficient given by

$$a_a^S = \frac{4}{9} Q = \frac{8}{27} \frac{H^2 G}{P a_a^V}, \quad (16)$$

where Q is an auxiliary constant.

Following [24] and Subsection II B, Eq. (14) *must* emerge in the macroscopic limit at large A , for an energy analytic in asymmetry, provided underlying model assumptions represent short-range interactions obeying charge symmetry. Later in the paper, we shall encounter a greater richness of changes with asymmetry in the nuclear surface region for different Skyrme interactions, in the Hartree-Fock calculations, than envisioned in the droplet model. However, all those calculations will be consistent with the symmetry energy being quadratic in asymmetry in the macroscopic limit, with the symmetry coefficient conforming with (14) at large A .

The droplet-model energy formula eventually acquired [17] as many as 38 independent parameters that either got set by fitting nuclear energies or using auxiliary information. The general difficulty in settling on the value of a_a^S in an energy formula is illustrated by the fact that this coefficient has risen by over a factor of 2 within the history of the droplet model, from $a_a^S = 7.1$ MeV [27] to 15.7 MeV [28]. At the same time, the volume symmetry constant of the model has varied within the range of only about 25%, from $a_a^V = 28.1$ MeV [27] to $a_a^V = 36.5$ MeV [29]. A still wider range of surface symmetry coefficients is found when considering other formulas in the literature. Thus, e.g. the fits by Pomorski and Dudek [19], who have emphasized asymmetry effects, give rise to the coefficient values of $a_a^S = (\kappa_{\text{vol}} b_{\text{vol}})^2 / (\kappa_{\text{surf}} b_{\text{surf}}) = 21.3$ MeV and 50.1 MeV, in terms of these authors' notation, depending on the variant of the drop formula they employ in describing nuclear ground-state energies and fission barriers. Depending on the formula variant, the fits, at the same time, produce the values for the volume symmetry coefficient of either $a_a^V = -\kappa_{\text{vol}} b_{\text{vol}} = 28.8$ MeV or 25.4 MeV. Notably, the droplet formula [17] and the Lublin-Strasbourg formula [19] produce comparable rms deviations from the measured energies and barriers. Similarly wide variations of the surface symmetry coefficient, of nearly an order of magnitude, will be found in Sec. IV for the effective Skyrme interactions employed in the literature. The volume symmetry coefficients will, again, exhibit relatively less variation. The values of a_a^S will be found to be correlated with the density dependence of symmetry energy.

III. ENERGY FUNCTIONAL

A. Hohenberg-Kohn Functional

Here, we shall consider the nuclear energy functional in terms of neutron $\rho_n(\mathbf{r})$ and proton $\rho_p(\mathbf{r})$ densities. Given a system hamiltonian in terms of nuclear and Coulomb components,

$$\hat{H} = \hat{H}_{\text{nucl}} + \hat{H}_C, \quad (17)$$

different densities $\rho_n(\mathbf{r})$ and proton $\rho_p(\mathbf{r})$ and different values of the functional $E(\rho_n, \rho_p)$ will result, when minimizing the expectation value of the hamiltonian in the presence of different

external potentials [1], $V_n(\mathbf{r})$ and $V_p(\mathbf{r})$:

$$\langle \hat{H} + \hat{V}_n + \hat{V}_p \rangle = E(\rho_n, \rho_p) + \int d\mathbf{r} (V_n(\mathbf{r}) \rho_n(\mathbf{r}) + V_p(\mathbf{r}) \rho_p(\mathbf{r})) . \quad (18)$$

The functional E , defined in this way, is specified for integer nucleon numbers, N and Z , only. In finding the ground-state densities and energy, the functional E is minimized with respect to variations in ρ_n and ρ_p . In the context of an energy formula, we will actually be interested in the functional E averaged out and smoothed out across discrete N and Z , defined then also for fractional nucleon numbers and made analytic in the nucleon densities.

The smoothed-out functional \bar{E} will be partitioned into the parts associated with nuclear and with Coulomb interactions. The nuclear part will be further partitioned into the energy of symmetric matter and a correction associated with asymmetry:

$$\bar{E}(\rho_n, \rho_p) = E_{\text{nucl}}(\rho, \rho_{np}) + E_C(\rho, \rho_{np}) = E_0(\rho) + E_a(\rho, \rho_{np}) + E_C(\rho, \rho_{np}), \quad (19)$$

where $\rho = \rho_n + \rho_p$, $\rho_{np} = \rho_n - \rho_p$ and $E_0(\rho) \equiv E_{\text{nucl}}(\rho, 0)$.

At $\rho_{np} = 0$, the symmetry energy E_a vanishes by definition. Given that energies of nuclei, corrected for microscopic and Coulomb contributions, minimize at a lowest asymmetry, the energy E_a must be quadratic in asymmetry at low asymmetries:

$$E_a(\rho, \rho_{np}) = \int d\mathbf{r}_1 d\mathbf{r}_2 \rho_{np}(\mathbf{r}_1) \mathcal{S}(\rho, \mathbf{r}_1, \mathbf{r}_2) \rho_{np}(\mathbf{r}_2) + \mathcal{O}(\eta^4). \quad (20)$$

Because of the minimum, \mathcal{S} must be a positive-definite symmetric bilinear integral operator, with regard to its arguments \mathbf{r}_1 and \mathbf{r}_2 . This operator represents an analog of the potential matrix in electrostatics, dependent on conductor described in terms of ρ . For the purposes of assessing later the accuracy of our considerations, we have indicated the principal presence of the subsequent terms of fourth order in asymmetry and higher. At other times, we may omit underscoring the presence or order of any subsequent terms in an expansion, beyond the directly considered order.

Minimal energy \bar{E} at given N and Z will be achieved for densities ρ and ρ_{np} which satisfy the equations

$$\frac{\delta \bar{E}}{\delta \rho(\mathbf{r})} = \mu \quad (21)$$

and

$$\frac{\delta \bar{E}}{\delta \rho_{np}(\mathbf{r})} = \mu_a, \quad (22)$$

where μ and μ_a are Lagrange multipliers associated with the constraints

$$\int d\mathbf{r} \rho(\mathbf{r}) = A, \quad (23)$$

and

$$\int d\mathbf{r} \rho_{np}(\mathbf{r}) = N - Z, \quad (24)$$

respectively. The Lagrange multipliers coincide with the corresponding chemical potentials, which are derivatives of energy \bar{E} that gets minimized, $\mu = \partial\bar{E}/\partial A$ and $\mu_a = \partial\bar{E}/\partial(N - Z)$, hence the notation for multipliers. Thus, e.g. upon differentiating the energy with respect to mass number,

$$\frac{\partial\bar{E}}{\partial A} = \int d\mathbf{r} \frac{\delta\bar{E}}{\delta\rho(\mathbf{r})} \frac{\partial\rho(\mathbf{r})}{\partial A} = \mu \int d\mathbf{r} \frac{\partial\rho(\mathbf{r})}{\partial A} = \mu, \quad (25)$$

we find that the l.h.s. coincides with μ introduced as a Lagrange multiplier in (21). Since the nucleonic chemical potentials are equal to

$$\mu_{n,p} = \mu \pm \mu_a, \quad (26)$$

the system can spontaneously emit nucleons, either neutrons or protons, if

$$|\mu_a| > -\mu. \quad (27)$$

If we consider the symmetric term E_0 alone, we can expand it around the density $\rho_0(\mathbf{r})$ that minimizes E_0 amongst the densities that meet the condition (23) at a prescribed A :

$$\begin{aligned} E_0(\rho) &= E_0(\rho_0) + \mu_0 \int d\mathbf{r} \Delta\rho(\mathbf{r}) + \int d\mathbf{r}_1 d\mathbf{r}_2 \Delta\rho(\mathbf{r}_1) \mathcal{K}(\mathbf{r}_1, \mathbf{r}_2) \Delta\rho(\mathbf{r}_2) + \mathcal{O}((\Delta\rho)^3) \\ &= E_0(A) + \int d\mathbf{r}_1 d\mathbf{r}_2 \Delta\rho(\mathbf{r}_1) \mathcal{K}(\mathbf{r}_1, \mathbf{r}_2) \Delta\rho(\mathbf{r}_2) + \mathcal{O}((\Delta\rho)^3), \end{aligned} \quad (28)$$

where $\Delta\rho(\mathbf{r}) = \rho(\mathbf{r}) - \rho_0(\mathbf{r})$, $\mu_0 = dE_0/dA$, \mathcal{K} is a positive-definite operator and $\int d\mathbf{r} \Delta\rho = 0$ holds amongst the densities that meet the condition (23).

Note that, depending on context, we may use the symbol ρ_0 to denote either the function of position that minimizes the energy of a finite or semi-finite symmetric system, in the absence of Coulomb interactions, or to denote single density value that minimizes the energy of symmetric uniform matter. Use of a position argument for the quantity will obviously imply the function. The distinction may be, otherwise, made by directly naming the quantity.

B. Densities and Generalized Symmetry Coefficient

In the following, we shall suppress the Coulomb term E_C and we shall explore what consequences the discussed features of the functional \bar{E} may have on the asymmetry dependence of nuclear densities and of nuclear energy.

Thus, at given N and Z , for low asymmetry $|N - Z|$, the minimal energy may be generally represented as

$$\bar{E}(N, Z) = E_0(A) + \frac{a_a(A)}{A} (N - Z)^2 + \mathcal{O}(\eta^4), \quad (29)$$

where $a_a(A)$ is a general A -dependent symmetry coefficient. From (29), the asymmetry chemical potential, in terms of the coefficient, is

$$\mu_a = \frac{2a_a(A)}{A} (N - Z) + \mathcal{O}(\eta^3), \quad (30)$$

while the symmetric chemical potential from (29) is

$$\mu = \mu_0 + (N - Z)^2 \frac{d}{dA} \frac{a_a(A)}{A} + \mathcal{O}(\eta^4). \quad (31)$$

When the Coulomb term is suppressed, Eqs. (21) and (22) for the densities produce

$$\mu_a = 2 \int d\mathbf{r}_1 \mathcal{S}(\rho, \mathbf{r}, \mathbf{r}_1) \rho_{np}(\mathbf{r}_1) + \mathcal{O}(\eta^3), \quad (32)$$

and

$$\mu = \frac{\delta E_0}{\delta \rho(\mathbf{r})} + \int d\mathbf{r}_1 d\mathbf{r}_2 \rho_{np}(\mathbf{r}_1) \frac{\delta \mathcal{S}(\rho, \mathbf{r}_1, \mathbf{r}_2)}{\delta \rho(\mathbf{r})} \rho_{np}(\mathbf{r}_2) + \mathcal{O}(\eta^4). \quad (33)$$

An operator \mathcal{S}^{-1} inverse to \mathcal{S} ,

$$\int d\mathbf{r}_2 \mathcal{S}(\rho, \mathbf{r}_1, \mathbf{r}_2) \mathcal{S}^{-1}(\rho, \mathbf{r}_2, \mathbf{r}_3) = \int d\mathbf{r}_2 \mathcal{S}^{-1}(\rho, \mathbf{r}_1, \mathbf{r}_2) \mathcal{S}(\rho, \mathbf{r}_2, \mathbf{r}_3) = \delta(\mathbf{r}_1 - \mathbf{r}_3), \quad (34)$$

should exist as \mathcal{S} must have positive eigenvalues only. Upon applying the inverse operator to both sides of (32), we can formally solve that equation to get

$$\rho_{np}(\mathbf{r}) = \frac{\mu_a}{2} \int d\mathbf{r}_1 \mathcal{S}^{-1}(\rho, \mathbf{r}, \mathbf{r}_1) + \mathcal{O}(\eta^3). \quad (35)$$

Upon integrating both sides of (35) over space, we find for the asymmetry chemical potential

$$\mu_a = \frac{2(N - Z)}{\int d\mathbf{r}_1 d\mathbf{r}_2 \mathcal{S}^{-1}(\rho, \mathbf{r}_1, \mathbf{r}_2)} + \mathcal{O}(\eta^3). \quad (36)$$

As a consequence, the nucleon density difference from (35) can be represented as

$$\rho_{np}(\mathbf{r}) = (N - Z) \frac{\int d\mathbf{r}_1 \mathcal{S}^{-1}(\rho, \mathbf{r}, \mathbf{r}_1)}{\int d\mathbf{r}_1 d\mathbf{r}_2 \mathcal{S}^{-1}(\rho, \mathbf{r}_1, \mathbf{r}_2)} + \mathcal{O}(\eta^3). \quad (37)$$

Upon substituting (37) into the symmetry energy (20), we get

$$E_a = \frac{(N - Z)^2}{\int d\mathbf{r} d\mathbf{r}_1 \mathcal{S}^{-1}(\rho, \mathbf{r}, \mathbf{r}_1)} + \mathcal{O}(\eta^4). \quad (38)$$

Substitutions into the equation (33) for the net density, next yield

$$\mu_0 = \frac{\delta E_0}{\delta \rho(\mathbf{r})} + (N - Z)^2 \frac{\delta}{\delta \rho(\mathbf{r})} \left(\frac{1}{\int d\mathbf{r}_1 d\mathbf{r}_2 \mathcal{S}^{-1}(\rho, \mathbf{r}_1, \mathbf{r}_2)} - \frac{a_a(A)}{A} \right) + \mathcal{O}(\eta^4), \quad (39)$$

where we have used $\delta A / \delta \rho(\mathbf{r}) = 1$ and the identity

$$\int d\mathbf{r}_2 \left(\mathcal{S}(\rho, \mathbf{r}_1, \mathbf{r}_2) \frac{\delta \mathcal{S}^{-1}(\rho, \mathbf{r}_2, \mathbf{r}_3)}{\delta \rho(\mathbf{r})} + \frac{\delta \mathcal{S}(\rho, \mathbf{r}_1, \mathbf{r}_2)}{\delta \rho(\mathbf{r})} \mathcal{S}^{-1}(\rho, \mathbf{r}_2, \mathbf{r}_3) \right) = 0, \quad (40)$$

following from differentiating Eq. (34) side-by-side. With $\rho_0(\mathbf{r})$ representing the solution of

$$\mu_0 = \frac{\delta E_0}{\delta \rho(\mathbf{r})}, \quad (41)$$

we find from (39) that the net density for a finite asymmetry differs from that for symmetric matter only up to second order in asymmetry,

$$\rho(\mathbf{r}) = \rho_0(\mathbf{r}) + \mathcal{O}(\eta^2), \quad (42)$$

with the second order brought in by the second term on the r.h.s. of (39). Upon comparing the expanded energy in (29) to the combination of energies E_0 from (28) and E_a from (38), with the density $\rho_0(\mathbf{r})$ from (42), we arrive at a result for the generalized symmetry coefficient in terms of the operator \mathcal{S} ,

$$\frac{A}{a_a(A)} = \int d\mathbf{r} d\mathbf{r}_1 \mathcal{S}^{-1}(\rho_0, \mathbf{r}, \mathbf{r}_1). \quad (43)$$

Given the weak dependence on asymmetry for the net density, stated in Eq. (42), we conclude, from (35) or (37), a similarly weak dependence on asymmetry for the density difference ρ_{np} scaled by μ_a or $(N - Z)$ (or another quantity odd in asymmetry). In that context, we introduce an isovector density changing weakly with asymmetry, that will be normalized either locally or globally. Normalized locally, in terms of the intense chemical potential, the isovector density is defined as

$$\rho_a(\mathbf{r}) = \frac{2a_a^V}{\mu_a} \rho_{np}(\mathbf{r}) = \frac{a_a^V}{a_a(A)} \frac{\rho_{np}(\mathbf{r})}{\eta} + \mathcal{O}(\eta^2), \quad (44)$$

where the r.h.s. follows from (30). For an extended system at low asymmetry, the dimensionless ratio normalizing ρ_{np} on the r.h.s. of (44) can be identified with volume asymmetry η_V ,

cf. Eq. (8). The normalized chemical potential $\mu_a/2a_a^V$ differs from that asymmetry only by higher order terms and may be termed effective volume asymmetry:

$$\eta'_V \equiv \frac{\mu_a}{2a_a^V} = \frac{a_a^V}{a_a(A)} \eta + \mathcal{O}(\eta^3) = \eta_V + \mathcal{O}(\eta^3). \quad (45)$$

In the limit of symmetric matter, the isovector density becomes

$$\rho_a^0(\mathbf{r}) = 2a_a^V \left. \frac{\partial \rho_{np}(\mathbf{r})}{\partial \mu_a} \right|_{\mu_a=0} = \left. \frac{\partial \rho_{np}(\mathbf{r})}{\partial \eta_V} \right|_{\eta=0}. \quad (46)$$

Normalized globally, to integrate to a mass number A , the isovector density ρ_A is defined as

$$\rho_A(\mathbf{r}) = \frac{A}{N-Z} \rho_{np}(\mathbf{r}) \equiv \frac{\eta'_V}{\eta} \rho_a(\mathbf{r}) = \frac{a_a(A)}{a_a^V} \rho_a(\mathbf{r}) + \mathcal{O}(\eta^2). \quad (47)$$

In the limit of symmetric matter, the density normalized that way becomes

$$\rho_A^0(\mathbf{r}) = \frac{\partial \rho_{np}(\mathbf{r})}{\partial \eta}. \quad (48)$$

From (35), it follows that the isovector density ρ_a may be expressed in terms of the operator \mathcal{S} as

$$\rho_a(\mathbf{r}) = a_a^V \int d\mathbf{r}_1 \mathcal{S}^{-1}(\rho, \mathbf{r}, \mathbf{r}_1) + \mathcal{O}(\eta^2) = \rho_a^0(\mathbf{r}) + \mathcal{O}(\eta^2), \quad (49)$$

with the $\eta = 0$ limit of

$$\rho_a^0(\mathbf{r}) = a_a^V \int d\mathbf{r}_1 \mathcal{S}^{-1}(\rho^0, \mathbf{r}, \mathbf{r}_1). \quad (50)$$

From (43), it follows that the symmetry coefficient is related to the locally normalized density with

$$\frac{A}{a_a(A)} = \frac{1}{a_a^V} \int d\mathbf{r} \rho_a^0(\mathbf{r}). \quad (51)$$

The result (49) for the isovector density is a counterpart of the result (42) for the isoscalar net density. The obvious important implication of those results is that the proton and neutron densities should be describable, up to second-order in asymmetry and up to Coulomb corrections discussed in the next paper, in terms of two densities universal across an isobar chain,

$$\rho_{n,p}(\mathbf{r}) = \frac{1}{2} (\rho(\mathbf{r}) \pm \eta \rho_A(\mathbf{r})) = \frac{1}{2} (\rho(\mathbf{r}) \pm \eta'_V \rho_a(\mathbf{r})) = \frac{1}{2} (\rho_0(\mathbf{r}) \pm \eta_V \rho_a^0(\mathbf{r})) + \mathcal{O}(\eta^2). \quad (52)$$

As is apparent, the isovector density is tied to the symmetry coefficient. We shall investigate quantitatively the relation between the densities ρ and ρ_a for different interactions in half-infinite matter in the next section. It should be mentioned that, while ρ_a represents an

isovector form factor, it is, at this point, an isoscalar with regard to its transformation properties in isobar space. Using analogy with spin, that density might further be termed an isospin susceptibility.

One issue that Eq. (52) raises is that of the importance of higher-order terms in asymmetry expansion. That importance needs to be considered not just globally but locally as well. In the next section, we shall see that ρ_a is typically larger than ρ outside of the nuclear surface. Since nucleon densities must be positive, the higher-order terms must become significant, at a given η_V , at distances outside of the surface where

$$|\eta_V| \rho_a^0(\mathbf{r}) > \rho_0(\mathbf{r}). \quad (53)$$

C. Uniform Matter

In uniform matter, the energy is an integral of constant energy per unit volume e ,

$$E = \int d\mathbf{r} e(\rho_n, \rho_p) = V e, \quad \text{with} \quad e = \frac{E}{V} = \rho \frac{E}{A}, \quad (54)$$

and

$$\frac{E}{A} = \frac{E_0}{A}(\rho) + \frac{E_a}{A}(\rho, \eta) \simeq \frac{E_0}{A}(\rho) + S(\rho) \eta^2, \quad (55)$$

where S is a density-dependent symmetry coefficient. That last coefficient is on its own commonly termed the symmetry energy. An obvious test of the usefulness of the quadratic expansion of symmetry energy is whether the approximate equality,

$$\frac{E_a}{A}(\rho, 1) \stackrel{?}{\simeq} S(\rho), \quad (56)$$

holds at different densities, particularly at $\rho = \rho_0$.

To the extent that the approximation of the r.h.s. of (55) holds [30], the functions $\frac{E_0}{A}(\rho)$ and $S(\rho)$ allow for the determination, at any asymmetry in uniform matter, of nuclear energy and nuclear pressure,

$$P = \rho^2 \frac{d}{d\rho} \left(\frac{E}{A} \right) \simeq \rho^2 \frac{d}{d\rho} \left(\frac{E_0}{A} \right) + \eta^2 \rho^2 \frac{dS}{d\rho}, \quad (57)$$

and nucleonic chemical potentials,

$$\mu_{n,p} = \rho \frac{\partial}{\partial \rho_{n,p}} \left(\frac{E}{A} \right) + \frac{E}{A} = \mu \pm \mu_a, \quad (58)$$

where

$$\mu = \rho \frac{\partial}{\partial \rho} \left(\frac{E}{A} \right) + \frac{E}{A} = \frac{P}{\rho} + \frac{E}{A}, \quad (59)$$

and

$$\mu_a = \frac{\partial}{\partial \eta} \left(\frac{E}{A} \right) \simeq 2\eta S(\rho). \quad (60)$$

The pressure and chemical potentials are important in calculating neutron-star properties and in simulating supernova explosions [31].

Around ρ_0 , it is common to expand both E_0/A ,

$$\frac{E_0}{A}(\rho) = -a_V + \frac{K}{18\rho_0^2} (\rho - \rho_0)^2 + \dots, \quad (61)$$

and S ,

$$S(\rho) = a_a^V + \frac{L}{3\rho_0} (\rho - \rho_0) + \frac{K_{\text{sym}}}{18\rho_0^2} (\rho - \rho_0)^2 + \dots \quad (62)$$

Notation for the constant terms in the expansion is consistent with that in the energy formula, Sec. II. Upon employing the expansions (61) and (62), the energy per nucleon (55) may be rewritten, around its minimum, in the form

$$\frac{E}{A} = -a_V + a_a^V \eta^2 + \frac{K_{\text{eff}}}{18\rho_{\text{min}}^2} (\rho - \rho_{\text{min}})^2 + \dots, \quad (63)$$

where we retain an accuracy of the order of $\mathcal{O}(\eta^4)$ in the coefficients. Within that accuracy the density which minimizes the energy is

$$\rho_{\text{min}}(\eta) \simeq \rho_0 - \frac{3L}{K} \rho_0 \eta^2, \quad (64)$$

and the effective incompressibility is

$$K_{\text{eff}}(\eta) = K + (K_{\text{sym}} - 6L) \eta^2. \quad (65)$$

In self-bound matter, on one hand, the pressure vanishes, $P = 0$, and, on the other, the nucleonic potentials are negative. When assuming a density close to normal, from (58)-(64), one finds that the magnitude of bulk drip asymmetry η_V^d , above which nuclear matter emits nucleons, is approximately

$$\eta_V^d \simeq \frac{a_V}{2a_a^V}. \quad (66)$$

In gravitationally bound neutron-star matter, due to the fact that the energy of symmetric matter minimizes at ρ_0 , the constant L from the symmetry-energy expansion (62), largely determines the nuclear contribution to pressure in neutron-star matter around ρ_0 ,

$$P \simeq \eta^2 \rho^2 \frac{dS}{d\rho} \simeq \frac{L}{3} \rho_0 \eta^2. \quad (67)$$

Table I shows a selection of bulk nuclear parameters for the majority of Skyrme interactions employed in the literature in nuclear mean-field calculations. The force constants for most of those interactions have been compiled by Jirina Stone [32, 33]. Basic information on the determination of E_0/A and S of uniform matter for those interactions will be provided later in this section; more thorough explorations of the properties of uniform matter may be found elsewhere, e.g. in [32]. On the other hand, procedures for the determination of surface parameters and values of those parameters for the interactions will be discussed in the following section.

Variations in the bulk parameter values in Table I can serve as illustration of the status of the specific parameters. Thus, there is a general consensus in the literature regarding a_V and ρ_0 , and the respective values in the table, across the listed interactions, are $a_V = 15.9 \pm 0.3$ MeV and $\rho_0 = 0.158 \pm 0.005$ fm⁻³. Regarding variation of the energy of symmetric matter with density, recent analyses of the energies of giant isoscalar monopole resonances point [34] to nuclear incompressibilities within the range of $K = (230 - 250)$ MeV, and fewer than 30% of all the interactions in Table I give rise to incompressibilities definitely outside of that range. Some of the interactions characterized by high K -values outside of the above range have been, incidentally, purposely constructed to explore the effects of high K -values on properties of finite nuclei.

Regarding the dependence of E/A on η , the values of expansion coefficients for normal ρ_0 -matter in Table I, a_a^V , are lower by just ~ 1 MeV than the values of symmetry energy per nucleon at $\eta = 1$, $E_a/A(\rho_0, 1)$. This indicates that the quadratic expansion of energy in asymmetry is fairly accurate near ρ_0 for the Skyrme interactions. The next quartic coefficients in the expansion of E/A with respect to asymmetry must be positive for the Skyrme interactions and be of the order of 1 MeV. The inferred magnitude of quartic terms indicates that a term breaking charge invariance, that might be potentially introduced into E/A , could be more important around ρ_0 than the quartic term, for typical η of interest.

The relative variation across Table I is far greater for $a_a^V \equiv S(\rho_0)$ than for a_V . The lowest a_a^V values, of the order of 23 MeV, are close to the a_a -value inferred from the basic energy formula (1) from Sec. II, while some of the high a_a^V values in the table actually exceed 37 MeV. An even greater degree of variation is found in the table for the constants L and K_{sym} , characterizing the ρ -dependence of S . Thus, the derivative-constant L takes on positive and negative values in the table, within principally as much as 3 orders of magni-

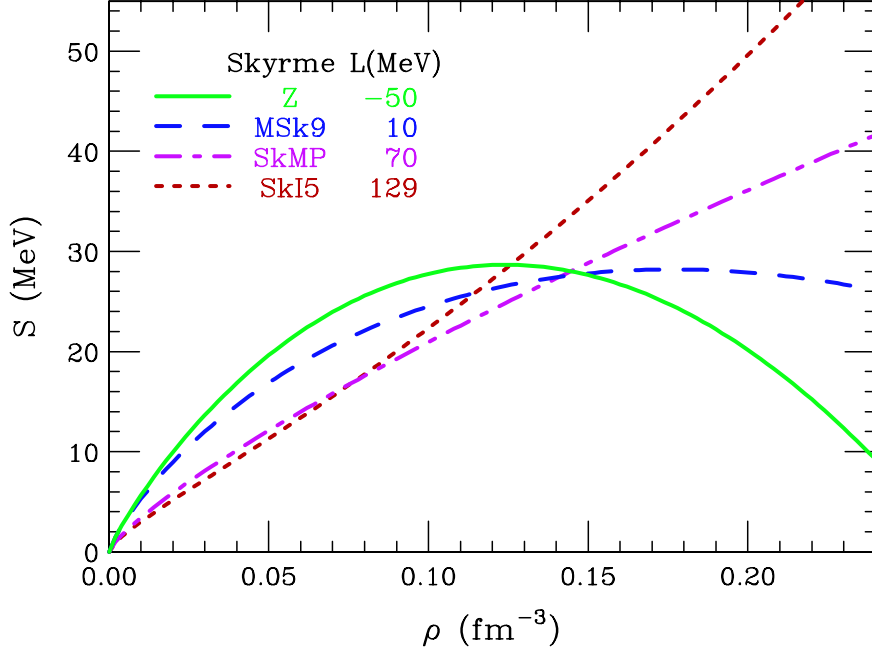


FIG. 2: Symmetry energy S as a function of density ρ , for sample Skyrme interactions characterized by widely varying derivative-parameters L .

tude; the average value of L there is 35 ± 33 MeV. The situation is found to be similar for K_{sym} that takes on both negative and positive values within 2 orders of magnitude. Functions $S(\rho)$ for the Skyrme interactions representing two more typical and two more extreme L -values are shown in Fig. 2.

While the parameters L and K_{sym} vary widely between interactions, they do so in a fairly correlated manner. The relatively tight correlation is illustrated in Fig. 3 displaying results for the Skyrme interactions, in the plane of those parameters scaled by a_a^V . The correlation may be understood as due to the fact that just one physical scale of ρ_0 governs the low-density variation of nuclear energy, limiting possible independent variations in the first and second derivatives of S at ρ_0 . If we were to approximate $S(\rho)$ -functions for the Skyrme interactions, such as those shown in Fig. 2, with parabolas, $S(\rho) \propto \rho(1 + c\rho)$, i.e. extending the expansion (62) to the whole subnormal region of densities, we would arrive at the following relation between the scaled parameters:

$$\frac{K_{\text{sym}}}{a_a^V} \approx 6 \frac{L}{a_a^V} - 18. \quad (68)$$

That relation, represented by the solid line in Fig. 3, qualitatively explains the correlation for the interactions in the figure. However, a parabola produces an incorrect linear behavior of S

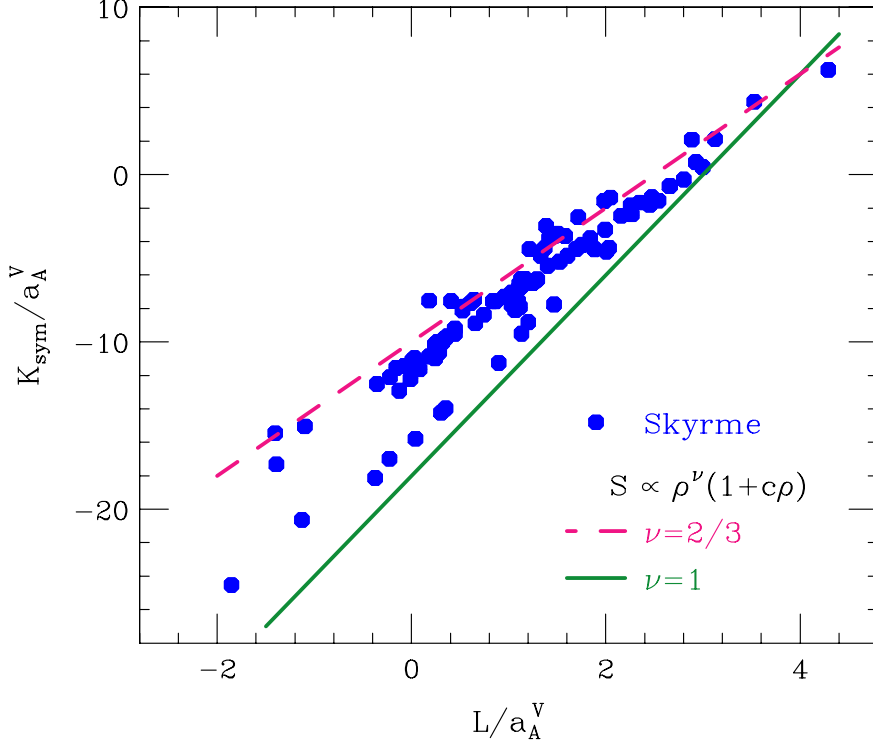


FIG. 3: Correlation between the symmetry-energy parameter-ratios K_{sym}/a_a^V and L/a_a^V . The circles represent Skyrme interactions, while the lines represent the modified power parameterization $S(\rho) \propto \rho^\nu(1 + c\rho)$.

at low ρ , where S is expected to be dominated by the Fermi-energy contribution proportional to $\rho^{2/3}$. An attempt to improve the approximation to S , using $S(\rho) \propto \rho^\nu(1 + c\rho)$, leads to the relation

$$\frac{K_{\text{sym}}}{a_a^V} \approx 6\nu \frac{L}{a_a^V} - 9\nu(\nu + 1), \quad (69)$$

represented by the dashed line in Fig. 3, for $\nu = 2/3$. It is apparent that the $\nu = 1$ and $\nu = 2/3$ relations practically bracket the correlation between the L and K_{sym} parameters, in spite of the fact that S for the Skyrme interactions differs from either of the forms used in the approximations. Practical implication of the observed correlation is that any constraining of either of the two parameter will produce constraints on the likely values of the other parameter.

With $a_V \simeq 16$ MeV, and with the average volume symmetry parameter for the Skyrme interactions being $a_a^V \sim 30$ MeV, the magnitude of drip asymmetry expected for the Skyrme interactions from the simple expression (66) is ~ 0.27 , which turns out to be close to the typical magnitude of η_V^d in Table I. The simple formula implies further an anticorrelation

between the bulk asymmetry coefficient and the drip asymmetry. Indeed, the lowest and the highest drip asymmetry values in Table I are associated with some of the highest and the lowest, respectively, volume coefficient values a_a^V in the table. Overall, the magnitudes of η_V^d in the table may seem to be low. However, these values pertain to nuclear interiors. For a given Skyrme interaction, due to asymmetry effects in the surface, nuclei may generally have a net asymmetry η larger in magnitude than η_V^d and still be stable.

TABLE I: Bulk nuclear properties for different Skyrme interactions with force constants given in the indicated references.

Name	ρ_0 (fm ⁻³)	a_V (MeV)	m^*/m	K (MeV)	a_a^V (MeV)	L (MeV)	K_{sym} (MeV)	$\frac{E_a}{A}(\rho_0, 1)$ (MeV)	η_V^d	a_S (MeV)	a_a^S (MeV)	d_0 (fm)	ΔR^0 (fm)	$\Delta_e R$ (fm)	d_a^0 (fm)	Ref.
SI	0.1553	-15.99	0.911	370.3	29.24	1.2	-461.8	30.27	0.325	17.36	26.00	0.438	0.432	0.433	0.461	[35]
SII	0.1482	-15.96	0.580	340.8	34.14	50.1	-265.1	35.75	0.274	19.38	17.54	0.517	0.718	0.761	0.439	[35]
SIII	0.1453	-15.85	0.763	355.3	28.16	9.9	-393.7	29.38	0.337	18.54	21.77	0.486	0.518	0.509	0.474	[36]
SIII _s	0.1507	-16.57	0.789	371.8	32.66	29.3	-367.7	33.60	0.299	20.06	17.70	0.492	0.653	0.717	0.412	[37]
SIV	0.1509	-15.96	0.471	324.5	31.22	63.5	-136.7	33.22	0.312	18.87	13.39	0.529	0.779	0.906	0.404	[36]
SV	0.1551	-16.05	0.383	305.7	32.83	96.1	24.2	35.32	0.312	19.16	10.27	0.553	0.941	1.231	0.368	[36]
SVI	0.1435	-15.75	0.949	363.6	26.88	-7.3	-471.3	27.86	0.354	18.10	26.27	0.466	0.428	0.404	0.496	[36]
SVII	0.1434	-15.79	1.001	366.4	26.96	-10.1	-488.9	27.89	0.354	18.11	27.43	0.462	0.415	0.388	0.500	[37]
SkT	0.1476	-15.40	0.602	333.3	24.89	28.2	-236.7	26.25	0.385	14.21	17.58	0.431	0.477	0.554	0.393	[38]
SkT1	0.1610	-15.98	1.000	236.2	32.02	56.2	-134.9	32.73	0.305	18.26	14.60	0.556	0.799	0.834	0.450	[39]
SkT2	0.1610	-15.94	1.000	235.8	32.00	56.2	-134.7	32.71	0.305	18.01	14.71	0.552	0.794	0.828	0.450	[39]
SkT3	0.1610	-15.94	1.000	235.8	31.50	55.3	-132.1	32.21	0.311	17.78	15.33	0.547	0.776	0.782	0.468	[39]
SkT4	0.1590	-15.95	1.000	235.5	35.46	94.1	-24.5	36.16	0.284	18.17	11.57	0.558	0.986	1.171	0.390	[39]
SkT5	0.1640	-16.00	1.000	201.7	37.01	98.5	-25.0	37.72	0.274	18.13	10.91	0.604	1.084	1.283	0.400	[39]
SkT6	0.1609	-15.96	1.000	236.0	29.97	30.9	-211.6	30.67	0.321	18.22	18.10	0.555	0.658	0.630	0.508	[39]
SkT7	0.1606	-15.94	0.833	235.7	29.52	31.1	-209.9	30.72	0.326	18.12	18.21	0.559	0.650	0.617	0.516	[39]

Table Continued on Next Page...

TABLE I – Continued

Name	ρ_0 (fm ⁻³)	a_V (MeV)	m^*/m	K (MeV)	a_a^V (MeV)	L (MeV)	K_{sym} (MeV)	$\frac{E_a}{A}(\rho_0, 1)$ (MeV)	η_V^d	a_S (MeV)	a_a^S (MeV)	d_0 (fm)	ΔR^0 (fm)	$\Delta_e R$ (fm)	d_a^0 (fm)	Ref.
SkT8	0.1607	-15.94	0.833	235.7	29.92	33.7	-187.6	30.77	0.322	18.13	17.88	0.559	0.657	0.637	0.509	[39]
SkT9	0.1603	-15.88	0.833	234.9	29.76	33.8	-185.7	30.60	0.323	17.79	17.81	0.555	0.654	0.636	0.508	[39]
SkTK	0.1681	-16.70	0.611	253.3	35.57	41.6	-221.9	37.35	0.275	19.78	19.46	0.579	0.696	0.685	0.512	[40]
SkM	0.1603	-15.77	0.789	216.7	30.75	49.4	-148.9	32.07	0.314	16.85	14.84	0.558	0.756	0.789	0.460	[41]
SkM1	0.1603	-15.77	0.789	216.7	25.17	-35.3	-389.0	26.53	0.414	17.46	59.67	0.575	0.180	0.161	0.729	[42]
SkMP	0.1570	-15.56	0.654	230.9	29.89	70.3	-49.8	31.26	0.336	16.58	12.06	0.549	0.850	0.950	0.423	[43]
SkMs	0.1603	-15.77	0.789	216.7	30.03	45.8	-156.0	31.39	0.322	17.46	14.48	0.575	0.765	0.790	0.470	[44]
SKa	0.1554	-15.99	0.608	263.2	32.91	74.6	-78.5	34.56	0.301	18.77	12.51	0.561	0.877	1.013	0.409	[5]
SKb	0.1554	-15.99	0.608	263.2	23.88	47.6	-78.5	25.53	0.460	18.77	10.27	0.561	0.768	0.895	0.408	[5]
SGI	0.1544	-15.89	0.608	261.8	28.33	63.9	-52.0	29.62	0.365	17.48	12.76	0.531	0.770	0.856	0.424	[45]
SGII	0.1583	-15.59	0.786	214.7	26.83	37.6	-146.0	28.10	0.365	16.10	15.11	0.538	0.660	0.679	0.464	[45]
RATP	0.1598	-16.05	0.667	239.6	29.26	32.4	-191.3	30.80	0.332	18.68	17.95	0.579	0.658	0.621	0.534	[46]
SkP	0.1625	-15.95	1.000	201.0	30.00	19.7	-266.7	31.33	0.316	18.18	18.02	0.607	0.670	0.631	0.533	[47]
E	0.1591	-16.13	0.868	333.4	27.66	-31.2	-570.8	28.83	0.359	18.94	37.62	0.485	0.321	0.280	0.576	[48]
Es	0.1628	-16.02	0.839	248.6	26.44	-36.8	-457.9	27.72	0.390	18.21	52.37	0.543	0.222	0.191	0.689	[48]
Gs	0.1576	-15.59	0.784	237.3	31.37	94.0	14.0	32.61	0.336	16.07	10.10	0.512	0.929	1.191	0.357	[48]
Rs	0.1577	-15.59	0.783	237.4	30.58	85.7	-9.1	31.82	0.340	16.06	10.59	0.512	0.888	1.106	0.366	[48]

Table Continued on Next Page...

TABLE I – Continued

Name	ρ_0	a_V	m^*/m	K	a_a^V	L	K_{sym}	$\frac{E_a}{A}(\rho_0, 1)$	η_V^d	a_S	a_a^S	d_0	ΔR^0	$\Delta_e R$	d_a^0	Ref.
	(fm ⁻³)	(MeV)		(MeV)	(MeV)	(MeV)	(MeV)	(MeV)		(MeV)	(MeV)	(fm)	(fm)	(fm)	(fm)	
T	0.1613	-15.93	1.000	235.7	28.35	27.2	-206.8	29.06	0.343	17.74	22.64	0.547	0.587	0.476	0.604	[48]
Z	0.1589	-15.97	0.842	330.3	26.82	-49.7	-657.9	27.97	0.391	17.74	51.51	0.465	0.213	0.199	0.588	[48]
Zs	0.1630	-15.88	0.783	233.4	26.69	-29.3	-401.6	28.01	0.371	17.00	46.62	0.534	0.233	0.217	0.650	[48]
Zss	0.1625	-15.96	0.775	234.9	28.80	-4.5	-332.7	30.14	0.330	17.32	29.34	0.541	0.406	0.372	0.594	[48]
SkSC1	0.1607	-15.85	1.000	234.6	28.10	0.2	-312.1	28.81	0.338	17.28	26.64	0.536	0.448	0.401	0.589	[49]
SkSC2	0.1607	-15.90	1.000	235.2	24.74	11.0	-228.3	25.44	0.401	17.45	19.73	0.540	0.515	0.477	0.535	[49]
SkSC3	0.1606	-15.85	1.000	234.5	27.01	0.8	-296.3	27.71	0.355	16.88	27.39	0.529	0.434	0.375	0.605	[49]
SkSC4	0.1606	-15.86	1.000	234.8	28.80	-2.1	-329.6	29.51	0.328	17.37	28.15	0.538	0.439	0.389	0.602	[50]
SkSC4o	0.1606	-15.84	1.000	234.5	26.98	-9.6	-337.8	27.69	0.357	17.35	30.46	0.538	0.385	0.337	0.619	[51]
SkSC5	0.1606	-15.85	1.000	234.5	30.99	-6.9	-375.2	31.69	0.300	17.28	32.03	0.536	0.415	0.368	0.627	[52]
SkSC6	0.1607	-15.92	1.000	235.5	24.57	11.0	-226.3	25.28	0.406	17.59	19.56	0.543	0.518	0.478	0.535	[52]
SkSC10	0.1607	-15.96	1.000	235.9	22.83	19.1	-172.8	23.53	0.457	17.75	15.61	0.546	0.577	0.556	0.497	[52]
SkSC11	0.1606	-15.86	1.000	234.8	28.80	-2.1	-329.6	29.51	0.328	17.37	28.15	0.538	0.439	0.389	0.602	[53]
SkSC14	0.1607	-15.92	1.000	235.5	30.00	33.2	-202.9	30.71	0.320	17.60	17.94	0.543	0.656	0.636	0.497	[51]
SkSC15	0.1607	-15.88	1.000	235.0	28.00	6.7	-284.6	28.71	0.341	17.43	23.93	0.539	0.492	0.445	0.568	[51]
Skyrme1p	0.1553	-15.99	0.911	370.3	29.35	35.3	-259.2	30.38	0.329	17.36	19.06	0.438	0.548	0.592	0.407	[54]
MSkA	0.1535	-15.99	0.794	313.3	30.35	57.2	-135.4	31.60	0.324	19.00	14.60	0.508	0.731	0.803	0.408	[55]

Table Continued on Next Page...

TABLE I – Continued

Name	ρ_0 (fm ⁻³)	a_V (MeV)	m^*/m	K (MeV)	a_a^V (MeV)	L (MeV)	K_{sym} (MeV)	$\frac{E_a}{A}(\rho_0, 1)$ (MeV)	η_V^d	a_S (MeV)	a_a^S (MeV)	d_0 (fm)	ΔR^0 (fm)	$\Delta_e R$ (fm)	d_a^0 (fm)	Ref.
SkI1	0.1604	-15.95	0.693	242.8	37.52	161.0	234.7	38.20	0.331	17.45	11.42	0.541	1.126	1.253	0.443	[56]
SkI2	0.1575	-15.77	0.685	241.0	33.38	104.3	70.7	34.02	0.316	17.03	11.68	0.537	0.951	1.096	0.412	[56]
SkI3	0.1577	-15.98	0.577	258.2	34.83	100.5	73.0	35.20	0.293	17.77	12.77	0.542	0.908	1.045	0.413	[56]
SkI4	0.1601	-15.94	0.649	248.0	29.50	60.4	-40.6	30.08	0.344	17.48	20.83	0.539	0.665	0.540	0.582	[56]
SkI5	0.1558	-15.85	0.579	255.8	36.64	129.3	159.5	37.01	0.288	17.31	10.71	0.536	1.034	1.316	0.374	[56]
SkI6	0.1591	-15.92	0.640	248.6	30.09	59.7	-47.3	30.64	0.333	17.42	19.07	0.539	0.683	0.602	0.542	[57]
SLy0	0.1603	-15.97	0.698	229.7	31.98	47.1	-116.3	32.67	0.301	18.21	16.75	0.580	0.713	0.727	0.500	[58]
SLy1	0.1603	-15.99	0.698	229.9	31.99	47.1	-116.6	32.68	0.301	18.31	16.19	0.582	0.725	0.752	0.484	[58]
SLy2	0.1605	-15.99	0.698	230.0	32.00	47.5	-115.2	32.69	0.301	18.20	17.28	0.579	0.706	0.705	0.516	[58]
SLy230a	0.1600	-15.99	0.697	229.9	31.99	44.3	-98.3	32.23	0.301	18.20	18.19	0.580	0.668	0.670	0.525	[59]
SLy3	0.1604	-15.97	0.696	229.9	31.99	45.3	-122.2	32.68	0.300	18.21	16.74	0.579	0.706	0.728	0.490	[58]
SLy4	0.1595	-15.97	0.695	230.0	32.00	46.0	-119.8	32.68	0.301	18.24	16.60	0.581	0.712	0.735	0.490	[60]
SLy5	0.1606	-15.98	0.698	230.0	32.01	48.2	-112.8	32.70	0.302	18.28	16.06	0.581	0.728	0.759	0.481	[60]
SLy6	0.1590	-15.92	0.690	229.9	31.96	47.5	-112.8	32.63	0.300	17.53	17.12	0.562	0.689	0.713	0.487	[60]
SLy7	0.1583	-15.90	0.688	229.8	31.99	47.0	-114.4	32.65	0.299	17.35	17.45	0.559	0.680	0.701	0.490	[60]
SLy8	0.1603	-15.97	0.696	229.9	32.00	47.2	-115.7	32.68	0.301	18.18	16.40	0.578	0.717	0.743	0.485	[58]
SLy9	0.1512	-15.79	0.666	229.9	31.98	54.9	-81.5	32.58	0.300	17.59	15.93	0.574	0.742	0.780	0.486	[58]

Table Continued on Next Page...

TABLE I – Continued

Name	ρ_0 (fm ⁻³)	a_V (MeV)	m^*/m	K (MeV)	a_a^V (MeV)	L (MeV)	K_{sym} (MeV)	$\frac{E_a}{A}(\rho_0, 1)$ (MeV)	η_V^d	a_S (MeV)	a_a^S (MeV)	d_0 (fm)	ΔR^0 (fm)	$\Delta_e R$ (fm)	d_a^0 (fm)	Ref.
SLy10	0.1556	-15.90	0.683	229.7	31.98	38.8	-142.3	32.62	0.297	17.05	20.23	0.549	0.607	0.608	0.518	[58]
SkX	0.1554	-16.05	0.993	271.1	31.10	33.2	-252.2	32.36	0.307	16.04	19.31	0.476	0.581	0.620	0.440	[61]
SkXce	0.1553	-15.86	1.006	268.2	30.20	33.7	-238.5	31.46	0.314	16.10	18.34	0.480	0.592	0.634	0.437	[61]
SkXm	0.1589	-16.05	0.966	238.2	31.20	32.1	-242.9	32.45	0.306	15.69	19.56	0.497	0.597	0.609	0.469	[61]
SkO	0.1605	-15.83	0.896	223.4	31.97	79.1	-43.2	32.86	0.320	17.14	14.94	0.546	0.856	0.815	0.485	[62]
SkOp	0.1602	-15.75	0.896	222.4	31.95	68.9	-78.8	32.79	0.309	16.07	15.74	0.524	0.802	0.773	0.453	[62]
SKRA	0.1595	-15.78	0.748	217.0	31.32	53.1	-139.3	32.71	0.308	16.71	14.79	0.556	0.766	0.808	0.455	[63]
MSk1	0.1575	-15.83	1.000	233.8	30.00	33.9	-200.1	30.70	0.318	17.21	18.08	0.536	0.651	0.636	0.492	[64]
MSk2	0.1575	-15.83	1.050	231.7	30.00	33.4	-203.5	30.66	0.318	17.22	18.06	0.538	0.654	0.636	0.494	[64]
MSk3	0.1578	-15.82	1.001	233.6	27.99	6.9	-284.4	28.69	0.339	17.08	24.37	0.533	0.485	0.440	0.562	[64]
MSk4	0.1575	-15.79	1.050	231.2	28.00	7.2	-284.1	28.66	0.339	17.06	24.04	0.534	0.494	0.446	0.563	[64]
MSk5	0.1575	-15.79	1.050	231.2	28.00	7.6	-282.6	28.66	0.339	17.07	23.90	0.535	0.496	0.449	0.561	[64]
MSk5s	0.1561	-15.78	0.800	243.8	28.00	7.0	-290.7	29.17	0.337	17.25	24.15	0.533	0.481	0.445	0.549	[65]
MSk6	0.1575	-15.79	1.050	231.2	28.00	9.7	-274.4	28.66	0.339	17.09	23.10	0.536	0.510	0.464	0.556	[64]
MSk7	0.1575	-15.79	1.050	231.3	27.95	9.4	-274.7	28.61	0.340	17.11	23.12	0.536	0.509	0.463	0.557	[66]
MSk8	0.1575	-15.79	1.100	229.4	27.93	8.3	-280.1	28.56	0.340	17.12	23.38	0.537	0.507	0.458	0.561	[67]
MSk9	0.1575	-15.80	1.000	233.4	28.00	10.4	-270.3	28.70	0.339	17.15	23.02	0.536	0.510	0.466	0.553	[67]

Table Continued on Next Page...

TABLE I – Continued

Name	ρ_0 (fm ⁻³)	a_V (MeV)	m^*/m	K (MeV)	a_a^V (MeV)	L (MeV)	K_{sym} (MeV)	$\frac{E_a}{A}(\rho_0, 1)$ (MeV)	η_V^d	a_S (MeV)	a_a^S (MeV)	d_0 (fm)	ΔR^0 (fm)	$\Delta_e R$ (fm)	d_a^0 (fm)	Ref.
v070	0.1575	-15.80	1.050	231.3	28.00	-3.5	-361.7	29.49	0.337	17.41	24.61	0.541	0.466	0.436	0.547	[65]
v075	0.1575	-15.80	1.050	231.3	28.00	-0.3	-342.0	29.32	0.337	17.31	24.40	0.539	0.477	0.439	0.552	[65]
v080	0.1575	-15.79	1.050	231.2	28.00	2.3	-325.7	29.18	0.337	17.18	24.30	0.536	0.483	0.441	0.555	[65]
v090	0.1575	-15.79	1.050	231.2	28.00	5.1	-304.3	28.94	0.338	17.08	24.22	0.535	0.489	0.443	0.561	[65]
v100	0.1575	-15.79	1.050	231.2	28.00	8.8	-281.5	28.75	0.339	17.02	23.68	0.534	0.502	0.453	0.560	[65]
v105	0.1575	-15.79	1.050	231.2	28.00	7.1	-284.6	28.66	0.339	17.05	24.11	0.534	0.492	0.445	0.563	[65]
v110	0.1575	-15.79	1.050	231.2	28.00	7.5	-279.7	28.59	0.339	17.11	23.78	0.535	0.496	0.451	0.559	[65]
SKz1	0.1600	-16.01	0.700	230.1	32.01	27.7	-242.5	33.60	0.294	17.35	19.03	0.554	0.616	0.641	0.490	[68]
SKz2	0.1600	-16.00	0.700	230.1	32.01	16.8	-259.8	33.27	0.293	17.34	23.95	0.554	0.523	0.509	0.549	[68]
SKz3	0.1600	-16.01	0.700	230.1	32.01	13.0	-242.0	32.77	0.293	17.35	28.05	0.554	0.465	0.435	0.596	[68]
SKz4	0.1600	-16.01	0.700	230.1	32.01	5.8	-241.0	32.35	0.293	17.35	34.04	0.554	0.393	0.358	0.643	[68]
Bsk1	0.1573	-15.80	1.050	231.4	27.81	7.2	-281.9	28.47	0.342	17.22	23.72	0.539	0.499	0.449	0.566	[69]
Bsk2	0.1575	-15.79	1.042	233.7	28.00	8.0	-297.1	29.02	0.338	17.14	23.15	0.534	0.509	0.463	0.552	[70]
Bsk2p	0.1575	-15.79	1.049	233.4	28.00	7.8	-298.1	29.02	0.338	17.11	23.20	0.534	0.508	0.462	0.553	[70]
Bsk3	0.1575	-15.80	1.123	234.8	27.94	6.8	-307.0	28.95	0.339	17.16	23.37	0.531	0.506	0.458	0.552	[71]
Bsk4	0.1575	-15.77	0.920	236.9	27.99	12.5	-266.0	28.90	0.339	16.91	23.01	0.530	0.511	0.466	0.551	[71]
Bsk5	0.1575	-15.80	0.920	237.2	28.70	21.4	-240.4	29.65	0.331	17.04	20.65	0.533	0.570	0.532	0.528	[71]

Table Continued on Next Page...

TABLE I – Continued

Name	ρ_0	a_V	m^*/m	K	a_a^V	L	K_{sym}	$\frac{E_a}{A}(\rho_0, 1)$	η_V^d	a_S	a_a^S	d_0	ΔR^0	$\Delta_e R$	d_a^0	Ref.
	(fm ⁻³)	(MeV)		(MeV)	(MeV)	(MeV)	(MeV)	(MeV)		(MeV)	(MeV)	(fm)	(fm)	(fm)	(fm)	
Bsk6	0.1575	-15.75	0.800	229.2	28.00	16.9	-215.3	28.72	0.339	16.74	22.73	0.542	0.511	0.472	0.564	[71]
Bsk7	0.1575	-15.76	0.800	229.3	28.00	18.0	-209.4	28.69	0.340	16.70	22.81	0.541	0.514	0.470	0.568	[71]
Bsk8	0.1589	-15.82	0.800	230.3	28.00	14.9	-221.0	28.70	0.341	17.12	23.13	0.549	0.506	0.462	0.578	[72]
Bsk9	0.1589	-15.92	0.800	231.5	30.00	39.9	-145.4	30.62	0.323	17.42	17.83	0.556	0.666	0.643	0.520	[72]
Bsk10	0.1593	-15.91	0.920	238.9	30.00	37.3	-195.0	31.01	0.321	17.51	17.48	0.540	0.671	0.655	0.491	[73]
Bsk11	0.1586	-15.86	0.920	238.1	30.00	38.4	-189.9	30.99	0.320	17.32	17.42	0.536	0.671	0.658	0.486	[73]
Bsk12	0.1586	-15.86	0.920	238.1	30.00	38.0	-191.4	31.00	0.320	17.30	17.51	0.535	0.668	0.655	0.487	[73]
Bsk13	0.1586	-15.86	0.920	238.1	30.00	38.8	-188.0	30.99	0.320	17.34	17.34	0.536	0.673	0.661	0.485	[73]
Bsk14	0.1586	-15.85	0.800	239.4	30.00	43.9	-152.1	30.92	0.323	17.17	17.22	0.537	0.680	0.666	0.492	[74]
SK255	0.1573	-16.33	0.797	255.0	37.40	95.1	-58.3	38.77	0.268	19.28	12.44	0.561	0.967	1.153	0.389	[75]
SK272	0.1553	-16.28	0.773	271.5	37.40	91.7	-67.8	38.71	0.264	19.21	13.48	0.545	0.916	1.068	0.395	[75]
QMC1	0.1373	-14.00	0.926	328.7	29.68	-6.7	-504.2	31.03	0.272	23.72	21.44	0.663	0.708	0.555	0.680	[76]
QMC2	0.1403	-14.29	0.834	330.1	28.70	8.7	-408.4	29.84	0.290	18.84	21.00	0.526	0.586	0.544	0.520	[76]
QMC3	0.1607	-15.98	0.825	366.9	45.78	91.8	-211.0	47.07	0.197	21.17	18.92	0.508	0.847	0.921	0.418	[76]
KDE0v	0.1608	-16.10	0.717	228.8	32.98	45.2	-144.9	33.80	0.291	17.27	18.22	0.552	0.672	0.689	0.488	[77]
KDE0v1	0.1646	-16.23	0.744	227.6	34.58	54.7	-127.2	35.34	0.281	17.66	17.25	0.558	0.730	0.757	0.474	[77]
LNS	0.1746	-15.31	0.826	210.8	33.43	61.5	-127.4	34.63	0.276	15.77	14.10	0.517	0.765	0.878	0.404	[78]

D. Local Approximation

We now consider the Hohenberg-Kohn (HK) functional in the context of uniform and near-uniform matter. For a uniform ρ , given the requirement of translation invariance, we may notice that \mathcal{S} in Eq. (20) must be a symmetric function of the difference of its arguments,

$$\mathcal{S}(\rho, \mathbf{r}, \mathbf{r}_1) = \mathcal{S}(\rho, \mathbf{r} - \mathbf{r}_1) = \mathcal{S}(\rho, \mathbf{r}_1 - \mathbf{r}). \quad (70)$$

Upon comparing (20) and (55), we arrive at the constraint in uniform matter

$$\int d\mathbf{r} \mathcal{S}(\rho, \mathbf{r}) = \int d\mathbf{r} \mathcal{S}(\rho, \mathbf{r} - \mathbf{r}_1) = \frac{S(\rho)}{\rho}. \quad (71)$$

Given the evidence for a local nature of nuclear energy functional in the energy formula and the above constraint, it should be possible to approximate the operator \mathcal{S} for uniform ρ by

$$\mathcal{S}(\rho, \mathbf{r}) \simeq \frac{S(\rho)}{\rho} \delta(\mathbf{r}), \quad (72)$$

in the action of this operator on sufficiently uniform densities ρ_{np} . Also, such an approximation should be valid for densities ρ that are not uniform generally, but are sufficiently uniform locally, with the operator then given by

$$\mathcal{S}(\rho, \mathbf{r}, \mathbf{r}_1) \simeq \frac{S(\rho(\mathbf{r}))}{\rho(\mathbf{r})} \delta(\mathbf{r} - \mathbf{r}_1). \quad (73)$$

On applying an inverse operator to \mathcal{S} for uniform ρ , to the middle and r.h.s. expressions in (71), we find a constraint on the inverse operator,

$$\int d\mathbf{r} \mathcal{S}^{-1}(\rho, \mathbf{r}) = \frac{\rho}{S(\rho)}. \quad (74)$$

A consistent approximation for the inverse operator, in matter sufficiently uniform locally, is

$$\mathcal{S}^{-1}(\rho, \mathbf{r}, \mathbf{r}_1) \simeq \frac{\rho(\mathbf{r})}{S(\rho(\mathbf{r}))} \delta(\mathbf{r} - \mathbf{r}_1). \quad (75)$$

From (49) and (74), it follows that the isovector density in uniform matter can be represented as

$$\rho_a = \frac{a_a^V}{S(\rho)} \rho + \mathcal{O}(\eta^2). \quad (76)$$

The isovector density is then seen normalized locally in such a manner that it approaches the normal density ρ_0 when isoscalar density itself approaches ρ_0 . Equation (76) is further

expected to hold in nonuniform matter that is sufficiently uniform on the scale of nonlocality in the energy functional. The contributions from such regions to $A/a_a(A)$ in (51) are then

$$\frac{A}{a_a(A)} = \int d\mathbf{r} \frac{\rho(\mathbf{r})}{S(\rho(\mathbf{r}))} + \dots, \quad (77)$$

where dots represent contributions from other regions. In (77), the contributions from locally uniform regions combine as capacitances of independent capacitors in electrostatics, with $\rho/2S(\rho)$ playing a role of local density of capacitance and $A/2a_a(A)$ playing the role of the net capacitance, cf. Eqs. (29) and (30).

One extreme limit that helps to develop an intuition, following the local approximation, is that of a constant symmetry energy, $S(\rho) \equiv a_a^V$. We find in that limit, as common sense suggests, that $a_a(A) \equiv a_a^V$, cf. (77). In the context of Eq. (14), we can see that $a_a(A)$ and a_a^V are expected to coincide when a_a^S approaches infinity. As a further implication of $S \equiv a_a^V$, we find, cf. (39), that the net nuclear density becomes identical to the density for symmetric matter up to the 4th order in asymmetry not just 2nd, $\rho(\mathbf{r}) = \rho_0(\mathbf{r}) + \mathcal{O}(\eta^4)$. For the isovector density, cf. (76), we find $\rho_a^0(\mathbf{r}) \equiv \rho_0(\mathbf{r})$ and $\rho_a(\mathbf{r}) = \rho(\mathbf{r}) + \mathcal{O}(\eta^2) = \rho_0(\mathbf{r}) + \mathcal{O}(\eta^2)$. Since the densities coincide for symmetric matter, $\rho_a^0(\mathbf{r}) \equiv \rho_0(\mathbf{r})$, the condition (53), signaling a breakdown of the quadratic approximation to the symmetry energy, is never satisfied.

These $S \equiv a_a^V$ results suggest that, for interactions for which the function S varies weakly with ρ , the isoscalar density should exhibit a weaker variation with asymmetry, than the isovector density. The result (76) suggests that the stronger variation of $S(\rho)$ with ρ , the more pronounced should be the differences between the isovector and isoscalar densities. Moreover, Eq. (77) suggests that the stronger that variation the larger should be the difference between $a_a(A)$ and a_a^V . If that difference were attributed to the nuclear surface, a larger difference would correspond to a reduced value of surface symmetry coefficient a_a^S , cf. (77). Finally, the stronger the variation of S with density, the sooner the invariance of the isoscalar density, and then of isovector density as well, should break down. Indeed, in a region where the local approximation holds, we find, from (39),

$$\frac{\delta E_0}{\delta \rho(\mathbf{r})} = \mu_0 + \eta^2 a_a(A) \left[\frac{A}{a_a(A)} \frac{da_a}{dA} + \frac{a_a(A)}{S(\rho_0(\mathbf{r}))} \left(1 - \frac{\rho_0(\mathbf{r})}{S(\rho_0(\mathbf{r}))} \frac{dS}{d\rho} \right) - 1 \right] + \mathcal{O}(\eta^4). \quad (78)$$

From (78), it appears that, simultaneously, a deviation of the local symmetry coefficient S from the global coefficient a_a , local dependence of S on ρ and the dependence of a_a on A (itself induced by the dependence of S on ρ), all conspire to produce a significant coefficient

of quadratic expansion for the isoscalar density around a given location \mathbf{r} . Further evidence, for a reduced range of validity of the implications of the second-order E_a -expansion, for a stronger ρ -variation of S , is the fact that the enhanced differences between the isovector and isoscalar densities should lead to an earlier breakdown of the condition (53), whether when staying at a given location in the matter and increasing η_V or when departing from nuclear surface at a fixed η_V .

While the ρ_0 -parameter L , Eq. (62), is commonly used to quantify the ρ -dependence of S , obviously variation of S over a wider range of subnormal densities must impact the properties of matter associated with the asymmetry. In the local expressions (76) and (77), it is seen that the inverse S is weighted with density. In the practical calculations of half-infinite nuclear matter of the next section, we find that local values of S impact the isovector density and $a_a(A)$ within the isoscalar density range of $\rho_0/4 \lesssim \rho \lesssim \rho_0$. For positions in the self-bound matter where $\rho \lesssim \rho_0/4$, the operator \mathcal{S} becomes delocalized and, thus, any potential impact of the specific values of $S(\rho)$ gets smeared out. Since any realistic $S(\rho)$ eventually tends to zero as $\rho \rightarrow 0$, a negative value of L at ρ_0 , see Fig. 2, leads in practice to an S with a weaker variation with density over the pertinent region, than a similar in magnitude but positive L .

Selected results, of the local approximation pursued here, have been arrived at in the past following the local Thomas-Fermi approximation [16, 24, 79]. Specifically, Bodmer and Usmani [79] (see also [24]) have demonstrated, in the absence of Coulomb effects, an inverse proportionality of ρ_{np} to the symmetry energy at a local net density. In [24] (see also [16] by Steiner *et al.*), the ratio $A/a_a(A)$, i.e. up to a factor the capacitance of a nuclear system for asymmetry, was found to be given by the integral on the r.h.s. of Eq. (77).

E. Functional Continuity and Kohn-Sham Methodology

In employing the Hohenberg-Kohn functional, we found it important to invoke a smoothing and interpolation procedure making the resulting functional analytic in nucleonic densities. If one were to find the Hohenberg-Kohn functional in reality, though, e.g. progressing over certain directions in the density space, the functional would be defined for discrete particle numbers only and would, otherwise, exhibit definite discontinuities across the density-ranges of interest. The latter are implied by the abrupt changes in experimental ground-state

energies, superimposed on top of a smooth variation of the energies with nucleon numbers. Those abrupt changes can be, in particular, attributed to filling of single-particle energy shells. In Kohn-Sham methodology [80], the difference between the actual (in most practice hypothetical) Hohenberg-Kohn functional, on one hand, and the kinetic energy of such form as for a noninteracting system, on the other, is represented by a continuous functional of density. The advantage of the Kohn-Sham methodology is that the assumed functional yields the exact theory in the limit of no interactions. Otherwise, discontinuities in the approximate functional, due to its kinetic part, on top of what would follow from using discrete particle numbers, may bear similarities to those for the exact Hohenberg-Kohn functional.

The Skyrme-Hartree-Fock model (SHFM), discussed in the next subsection and well-trying in nuclear physics, see e.g. [2] and [81], expands the Kohn-Sham methodology, in that the kinetic-energy terms for nucleons in the approximated functional get multiplied by factors dependent on density. The latter allows for some control over the discontinuities resulting from the functional. The remaining part of the functional is kept only minimally nonlocal through the use of lowest-order terms in density gradients. SHFM stems from modeling internucleon forces; a strategy relying from the outset on a Kohn-Sham type functional has been pioneered in nuclear physics by Fayans *et al.* [82].

In an application of the SHFM, later in the paper, to the domain of semi-infinite matter at changing asymmetry, it might seem that no smoothing of the approximate energy functional is required to make our preceding considerations, based on a functional expandable in asymmetry (cf. Eq. (20)), directly applicable. Such a conclusion might be inferred from the fact that the half-infinite matter is characterized by infinite nucleon numbers and by a continuum energy spectrum. However, it will turn out that, on account of the so-called Friedel oscillations extending from nuclear surface into the matter, the η -derivatives of nucleon density from functional minimization, of order third and higher, steadily increase with distance away from the surface. The implication of this behavior is that the expansion in asymmetry, which we have considered for the functional, must be just asymptotic in the specific domain. A direct application of our Hohenberg-Kohn considerations to SHFM for half-infinite nuclear matter, without any smoothing, could be then regarded particularly interesting as an extrapolation of our considerations. On the other hand, regarding the formal issue of smoothing and of functional analyticity, any smoothing that would lead to a smoothing of the resulting densities over a small range of Fermi wavevectors, would tame

the mentioned derivatives with respect to asymmetry. In contrast to half-infinite matter, the SHFM functional applied to uniform matter renders fully analytic results for energy without any smoothing.

F. Skyrme-Hartree-Fock Model

The Skyrme-Hartree-Fock model gets exploited in this paper in different ways. On one hand, the model has been already utilized to illustrate properties of uniform matter. On the other hand, the model will be utilized in the half-infinite matter calculations. Results of those calculations will be exploited to verify assertions concerning the Hohenberg-Kohn energy functional. Since the SHFM energy functional is expressed in terms of single-particle wavefunctions $\{\phi_\alpha\}$, rather than in terms of densities ρ_n and ρ_p , the inferences regarding the HK functional can be nontrivial.

In SHFM, the energy is

$$E = E_{\text{Skyrme}} + E_C + E_{\text{pair}}, \quad (79)$$

where the two last terms E_C and E_{pair} are, respectively, the Coulomb and pairing energies. The Skyrme functional is

$$\begin{aligned} E_{\text{Skyrme}} &\equiv \int d\mathbf{r} e_{\text{Skyrme}}(\mathbf{r}) \\ &= \int d\mathbf{r} \left\{ \frac{\hbar^2}{2m} \tau + \frac{t_0}{2} \left[\left(1 + \frac{x_0}{2}\right) \rho^2 - \left(\frac{1}{2} + x_0\right) \sum_q \rho_q^2 \right] \right. \\ &\quad + \frac{t_3}{12} \left[\left(1 + \frac{x_3}{2}\right) \rho^{\alpha+2} - \left(\frac{1}{2} + x_3\right) \rho^\alpha \sum_q \rho_q^2 \right] \\ &\quad + \frac{t_1}{4} \left[\left(1 + \frac{x_1}{2}\right) \rho\tau - \left(\frac{1}{2} + x_1\right) \sum_q \rho_q \tau_q \right] \\ &\quad + \frac{t_2}{4} \left[\left(1 + \frac{x_2}{2}\right) \rho\tau + \left(\frac{1}{2} + x_2\right) \sum_q \rho_q \tau_q \right] \\ &\quad + \frac{3t_1}{16} \left[\left(1 + \frac{x_1}{2}\right) (\nabla\rho)^2 - \left(\frac{1}{2} + x_1\right) \sum_q (\nabla\rho_q)^2 \right] \\ &\quad - \frac{t_2}{16} \left[\left(1 + \frac{x_2}{2}\right) (\nabla\rho)^2 + \left(\frac{1}{2} + x_2\right) \sum_q (\nabla\rho_q)^2 \right] \\ &\quad \left. - b_4 \rho \nabla J - b'_4 \sum_q \rho_q \nabla J_q \right\}, \end{aligned} \quad (80)$$

where the q -index summations are over neutrons and protons, $\tau = \tau_n + \tau_p$ and $\mathbf{J} = \mathbf{J}_n + \mathbf{J}_p$. Particle densities and scaled kinetic energy and spin densities are obtained from summations over the single-particle wavefunctions:

$$\rho_q(\mathbf{r}) = \sum_{\alpha} n_{\alpha}^q \phi_{\alpha}^{\dagger}(\mathbf{r}) \phi_{\alpha}(\mathbf{r}) \quad (81)$$

$$\tau_q(\mathbf{r}) = \sum_{\alpha} n_{\alpha}^q \nabla \phi_{\alpha}^{\dagger}(\mathbf{r}) \nabla \phi_{\alpha}(\mathbf{r}) \quad (82)$$

$$\mathbf{J}_q(\mathbf{r}) = \frac{1}{2i} \sum_{\alpha} n_{\alpha}^q \phi_{\alpha}^{\dagger}(\mathbf{r}) \left[(\vec{\nabla} - \overleftarrow{\nabla}) \times \boldsymbol{\sigma} \right] \phi_{\alpha}(\mathbf{r}). \quad (83)$$

Here, $\{n_{\alpha}^q\}$ are occupation numbers of the single-particle states. In less elaborate Skyrme parameterizations, the two spin-parameters are combined into one:

$$b_4 = b'_4 = t_4/2. \quad (84)$$

The gradient terms in the interaction part of the energy functional (80) (multiplied by adjustable constants), represent a simplified form of interaction nonlocalities.

Minimization of the SHFM functional (79), with respect to the wavefunctions, produces self-consistent equations for the latter

$$(h_q + U_C)(\mathbf{r}) \phi_{\alpha}(\mathbf{r}) = \epsilon_{\alpha} \phi_{\alpha}(\mathbf{r}). \quad (85)$$

In the equations, U_C is Coulomb potential and the nuclear single-particle hamiltonian h_q is of the form

$$h_q(\mathbf{r}) = -\nabla B_q(\mathbf{r}) \nabla + U_q(\mathbf{r}) - i\mathbf{W}_q(\mathbf{r}) (\nabla \times \boldsymbol{\sigma}). \quad (86)$$

The mass potential in h_q is given by

$$B_q = \frac{\hbar^2}{2m_q^*} = \frac{\hbar^2}{2m} + \frac{t_1}{4} \left[\left(1 + \frac{x_1}{2}\right) \rho - \left(\frac{1}{2} + x_1\right) \rho_q \right] + \frac{t_2}{4} \left[\left(1 + \frac{x_2}{2}\right) \rho + \left(\frac{1}{2} + x_2\right) \rho_q \right]. \quad (87)$$

and m_q^* is position-dependent effective mass. The potential U_q in (86) is

$$U_q = t_0 \left[\left(1 + \frac{x_0}{2}\right) \rho - \left(\frac{1}{2} + x_0\right) \rho_q \right] + \frac{t_3}{12} \left[(2 + \alpha) \left(1 + \frac{x_3}{2}\right) \rho^2 - \left(\frac{1}{2} + x_3\right) \left(\alpha \sum_{q'} \rho_{q'}^2 + 2\rho \rho_q \right) \right] \rho^{\alpha-1} + \frac{t_1}{4} \left[\left(1 + \frac{x_1}{2}\right) \tau - \left(\frac{1}{2} + x_1\right) \tau_q \right] + \frac{t_2}{4} \left[\left(1 + \frac{x_2}{2}\right) \tau + \left(\frac{1}{2} + x_2\right) \tau_q \right] - b_4 \nabla J - b'_4 \nabla J_q. \quad (88)$$

Finally, the form factor \mathbf{W}_q in (86) is

$$\mathbf{W}_q = b_4 \nabla \rho + b'_4 \nabla \rho_q. \quad (89)$$

Above, we suppress the terms in the SHFM functional and single-particle hamiltonian that are normally small, such as those proportional to the square of spin density.

In the context of investigating the effects of neutron-proton asymmetry, we shall introduce average and deviation-from-average quantities, for the terms in the single-particle hamiltonian and for the hamiltonian itself. These will be denoted, respectively, with either the lack of species index or with that index replaced by 'a'. (Unlike in the case of density, no special normalization will be adopted here for the quantities with the index 'a'.) Thus, e.g. for the mass potential, we will have

$$B = \frac{B_n + B_p}{2} = \frac{\hbar^2}{2m} + \frac{\rho}{16} [3t_1 + (5 + 4x_2)t_2], \quad (90)$$

and

$$B_a = \frac{B_n - B_p}{2} = \frac{\rho_{np}}{16} [(1 + 2x_2)t_2 - (1 + 2x_1)t_1]. \quad (91)$$

For the effective mass, we will have

$$m^* = \frac{1}{4} \left(\frac{1}{B_n} + \frac{1}{B_p} \right) = \frac{B}{2(B^2 - B_a^2)} \simeq \frac{1}{2B}, \quad (92)$$

where the approximation holds for low asymmetries, and

$$m_a^* = \frac{1}{4} \left(\frac{1}{B_n} - \frac{1}{B_p} \right) = -\frac{B_a}{2(B^2 - B_a^2)} = -\frac{m^* B_a}{B}. \quad (93)$$

For the optical potential, we will have, one hand, $U = (U_n + U_p)/2$ and, on the other,

$$\begin{aligned} U_a = \frac{U_n - U_p}{2} = & -\frac{t_0}{4} (1 + 2x_0) \rho_{np} - \frac{t_3}{24} (1 + 2x_3) \rho^\alpha \rho_{np} \\ & + \frac{1}{16} [(1 + 2x_2)t_2 - (1 + 2x_1)t_1] \tau_{np} - \frac{b'_4}{2} \nabla J_{np}, \end{aligned} \quad (94)$$

where $\tau_{np} = \tau_n - \tau_p$ and $\mathbf{J}_{np} = \mathbf{J}_n - \mathbf{J}_p$.

In uniform matter, the kinetic energy densities are

$$\tau_q = \frac{3}{5} \rho_q k_{Fq}^2, \quad (95)$$

with the Fermi wavenumbers given by

$$k_{Fq} = (3\pi^2 \rho_q)^{1/3}. \quad (96)$$

In symmetric matter, the partial densities are equal and, thus,

$$\rho_q = \rho/2 \quad \text{and} \quad \tau_q = \tau/2. \quad (97)$$

With $\tau_q \propto \rho_q^{5/3}$, the partial kinetic energies may be expanded in asymmetric matter around their symmetric value,

$$\tau_q = \frac{3}{10}\rho k_F^2 \left[1 \pm \frac{5}{3} \frac{\rho_{np}}{2\rho} + \frac{10}{9} \left(\frac{\rho_{np}}{2\rho} \right)^2 \pm \dots \right], \quad (98)$$

where k_F is wavevector for the symmetric matter at density ρ . Upon inserting the symmetric values into (80), the energy per nucleon of symmetric uniform matter becomes

$$\frac{E_0}{A}(\rho) = \frac{3\hbar^2}{10m} k_F^2 + \frac{3t_0}{8} \rho + \frac{t_3}{16} \rho^{\alpha+1} + \frac{3}{80} (3t_1 + 5t_2 + 4x_2 t_2) \rho k_F^2. \quad (99)$$

For a future use, from (98), the difference in partial kinetic energies may be represented at small asymmetries as

$$\tau_{np} \simeq \rho_{np} k_F^2. \quad (100)$$

Finally, upon exploiting (98) in the energy (80) for uniform matter, the density-dependent expansion coefficient in asymmetry becomes

$$S(\rho) = \frac{\hbar^2}{6m} k_F^2 - \frac{t_0}{8} (1 + 2x_0) \rho - \frac{t_3}{48} (1 + 2x_3) \rho^{\alpha+1} - \frac{1}{24} [3t_1 x_1 - (4 + 5x_2)t_2] \rho k_F^2. \quad (101)$$

As is apparent, for uniform matter the same powers of density appear in the symmetry energy S and the energy per nucleon E_0/A of symmetric matter. From the interaction constants, the dimensionless constants x_0 , x_1 and x_3 affect the strength of the three interaction-terms in S , with different density powers, without affecting E_0/A . From among the different SHFM quantities, the mass potential has a relatively simple linear density dependence. As should be obvious from Table I, the number of Skyrme interaction constants in use in the literature is large and it is, obviously, growing. For the values of constants, we refer the reader to the references indicated in the table. Otherwise, one larger compilation of constant values can be found in Ref. [32].

A combination of SHFM with the semiclassical expansion for kinetic energy [83] in terms of density,

$$\tau_q \approx \frac{3}{5} (3\pi^2)^{2/3} \rho_q^{5/3} + \frac{1}{36\rho_q} (\nabla \rho_q)^2 + \frac{1}{3} \Delta \rho_q, \quad (102)$$

valid for slowly varying densities, allows one to gain an insight into the symmetry operator \mathcal{S} and its inverse. For simplicity, we assume the spin densities \mathbf{J}_q to be zero. Upon inserting (102) into (80) and employing the identity

$$\mathcal{S}(\rho, \mathbf{r}_1, \mathbf{r}_2) = 2 \left. \frac{\delta^2 E_{\text{nucl}}}{\delta \rho_{np}(\mathbf{r}_1) \delta \rho_{np}(\mathbf{r}_2)} \right|_{\rho_{np}=0}, \quad (103)$$

we find for the operator

$$\begin{aligned} \mathcal{S}(\rho, \mathbf{r}_1, \mathbf{r}_2) &\approx \mathcal{S}_0(\rho, \mathbf{r}_1) \delta(\mathbf{r}_1 - \mathbf{r}_2) \\ &+ \int d\mathbf{r} \mathcal{S}_1(\rho, \mathbf{r}) \frac{\nabla \rho}{\rho} \cdot (\delta(\mathbf{r} - \mathbf{r}_1) \nabla \delta(\mathbf{r} - \mathbf{r}_2) + \delta(\mathbf{r} - \mathbf{r}_2) \nabla \delta(\mathbf{r} - \mathbf{r}_1)) \\ &+ \int d\mathbf{r} \mathcal{S}_2(\rho, \mathbf{r}) \nabla \delta(\mathbf{r} - \mathbf{r}_1) \cdot \nabla \delta(\mathbf{r} - \mathbf{r}_2), \end{aligned} \quad (104)$$

where

$$\begin{aligned} \mathcal{S}_0 &= \frac{S}{\rho} + \frac{1}{18\rho} \left(\frac{\nabla \rho}{\rho} \right)^2 \left\{ \frac{\hbar^2}{m} + \frac{1}{4} [(2+x_1)t_1 + (2+x_2)t_2] \rho \right\}, \\ \mathcal{S}_1 &= -\frac{1}{72\rho} \left\{ \frac{\hbar^2}{m} + \frac{1}{4} [(2+x_1)t_1 + (2+x_2)t_2] \rho \right\}, \\ \mathcal{S}_2 &= \frac{1}{72\rho} \left\{ \frac{\hbar^2}{m} - \frac{1}{16} [35(2+x_1)t_1 + 21(2+x_2)t_2] \rho \right\}. \end{aligned} \quad (105)$$

Those nonlocal gradient terms in the combination of results (104) and (105), which are multiplied by force constants, are associated with the nonlocality of interactions. On the other hand, those gradient terms, which are multiplied by \hbar^2 , are associated with quantum nonlocality. It may be noted that, for an approximately uniform ρ , the operator \mathcal{S} given by (104) becomes a function of $(\mathbf{r}_1 - \mathbf{r}_2)$ only. In addition, when both ρ and ρ_{np} onto which \mathcal{S} acts approach uniformity, then \mathcal{S} given by (104) approaches the local result (73).

IV. HARTREE-FOCK CALCULATIONS FOR HALF-INFINITE MATTER

A. Skyrme-Hartree-Fock Model for Half-Infinite Matter

With the interest in low-density features of symmetry energy, we now turn to an examination of half-infinite nuclear matter [4, 6] within SHFM. The half-infinite matter is uniform in two cartesian directions and generally nonuniform in the third that we choose to be z . Given the transverse uniformity, the solutions to the SHFM equations (85) may be looked for as the

eigenstates of transverse momentum, $\phi(\mathbf{r}) = \Psi(z) \exp(i\mathbf{k}_\perp \mathbf{r}_\perp)$. Here, \mathbf{k}_\perp is the transverse wavevector and Ψ is a spinor depending on z . In the single-particle hamiltonian (86), only the last-r.h.s. spin-orbit term has a vector character. With the form factor \mathbf{W}_q of Eq. (89) pointing in the z -direction, that spin-orbit term, acting on a wavefunction, becomes

$$-i\mathbf{W}_q(\mathbf{r}) (\nabla \times \boldsymbol{\sigma}) \phi(\mathbf{r}) = -iW_q(z) (\nabla \times \boldsymbol{\sigma})_z \phi(\mathbf{r}) = W_q(z) (\mathbf{k}_\perp \times \boldsymbol{\sigma})_z \phi(\mathbf{r}), \quad (106)$$

where

$$W_q(z) = b_4 \frac{d\rho}{dz} + b'_4 \frac{d\rho_q}{dz}. \quad (107)$$

If we next orient the x -axis along the \mathbf{k}_\perp -direction, see Fig. 4, we find that the spin-orbit term in the hamiltonian becomes proportional to the Pauli matrix along the y -direction:

$$h_q(\mathbf{r}) \phi(\mathbf{r}) = \left(-\frac{d}{dz} \frac{\hbar^2}{2m_q^*(z)} \frac{d}{dz} + \frac{\hbar^2 k_\perp^2}{2m_q^*(z)} + U_q(z) + W_q(z) k_\perp \sigma_y \right) \phi(\mathbf{r}). \quad (108)$$

With this, it turns out that the eigenstates of the hamiltonian may be searched for as the eigenstates of operator of spin projection onto the y -direction, recognized as the direction of orbital angular momentum calculated relative to the far-away interior of matter:

$$\phi_{\mathbf{k}\lambda q}(\mathbf{r}) = \psi_{k_\perp k_z \lambda q}(z) \chi_\lambda e^{i\mathbf{k}_\perp \mathbf{r}_\perp}. \quad (109)$$

Here, χ_λ is an eigenstate of σ_y ,

$$\sigma_y \chi_\lambda = \lambda \chi_\lambda, \quad (110)$$

the eigenvalues are $\lambda = \pm 1$, and $\psi(z)$ is a scalar wavefunction.

From (85) and (108)-(110), the wavefuctions ψ satisfy the differential equation

$$\epsilon_{kq} \psi_{k_\perp k_z^\infty \lambda q}(z) = \left(-\frac{d}{dz} \frac{\hbar^2}{2m_q^*(z)} \frac{d}{dz} + \frac{\hbar^2 k_\perp^2}{2m_q^*(z)} + U_q(z) + \lambda W_q(z) k_\perp \right) \psi_{k_\perp k_z^\infty \lambda q}(z). \quad (111)$$

The single-particle energy above can be represented as

$$\epsilon_{kq} = \frac{\hbar^2 k^2}{2m_{q\infty}^*} + U_{q\infty}, \quad (112)$$

where the quantities with the infinity index refer to a uniform interior of the matter far away from the surface, and where the wavevector squared is

$$k^2 = k_\perp^2 + (k_z^\infty)^2. \quad (113)$$

The last two equations principally define $k_z^\infty \geq 0$ in terms of ϵ . The z -component of the wavevector must be defined in the asymptotic region in the matter, as the z -component of

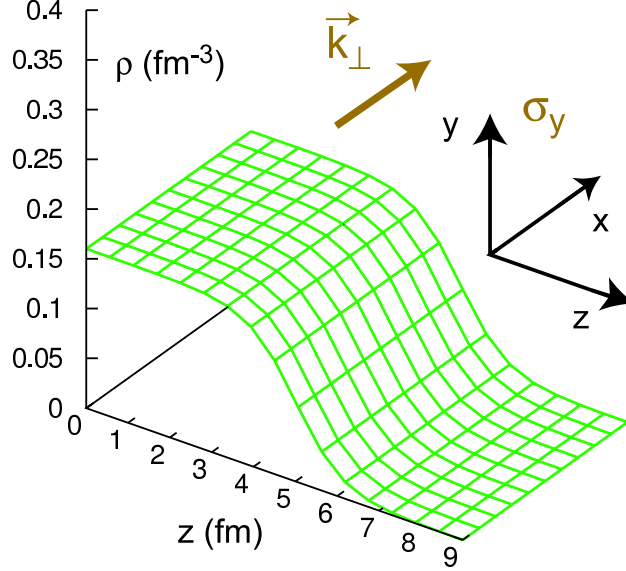


FIG. 4: Within our half-infinite matter SHFM-calculations, the z -axis is aligned with the direction of nonuniformity of matter, while the x -axis is aligned with the single-particle transverse momentum. The single-particle particle states are chosen to have a definite projection of spin onto the remaining y -axis.

single-particle momentum is generally not conserved, due to matter nonuniformity. Otherwise, in the asymptotic region, the eigenstates of single-particle hamiltonian combine waves moving towards and away from the boundary of matter, following a reflection from that boundary,

$$\psi_{k_{\perp} k_z^{\infty} \lambda q}(z) \simeq 2 \sin(k_z^{\infty} z + \delta_{k_{\perp} k_z^{\infty} \lambda q}). \quad (114)$$

Here, the individual plane waves in the combination are normalized to unity and δ is the phase of the incident relative to the reflected wave. The phase shift depends on the choice of origin for the z -axis. However, changes in the phase shift with species or with momentum, such as in $\nabla_k \delta$, do not depend on the choice of origin. The arbitrary overall phase-factor multiplying the wavefunction in (114) is chosen so as to make the wavefunction ψ real asymptotically. With the wavefunction and its derivative being real, and with the coefficients in the wave-equation (111) being real, the wavefunction ψ , after setting the phase-factor, becomes real everywhere. Far outside of the nuclear surface, in the classically forbidden region, the wavefunction must decrease exponentially with distance away from the surface,

$$\psi_{\mathbf{k} q}(z) \propto e^{-\kappa_{\mathbf{k} q} z}, \quad (115)$$

where we assume that the matter is positioned towards the negative direction of the z -axis, and

$$\kappa_{\mathbf{k}q} = \sqrt{k_{\perp}^2 - \frac{2m\epsilon_{kq}}{\hbar^2}}. \quad (116)$$

Provided self-consistent solutions for the half-infinite matter may be found, different observables can be obtained by carrying out integrations over wavefunction continuum, with the summations over discrete states, such as in (81), specifically replaced by

$$\sum_{\alpha}(\cdot) \rightarrow \sum_{\lambda} \frac{1}{(2\pi)^3} \int d\mathbf{k}_{\perp} \int_0^{\infty} dk_z^{\infty} (\cdot) = \sum_{\lambda} \frac{1}{(2\pi)^2} \int_0^1 d\cos\theta \int_0^{\infty} dk k^2 (\cdot), \quad (117)$$

in accordance with the normalization of the wavefunctions in (114). On the r.h.s., the wavevector components are $k_z = k \cos\theta$ and $k_{\perp} = k \sin\theta$. In particular, with the Hartree-Fock occupations of $n_k^q = \theta(k_F^q - k)$, the nucleon and kinetic-energy densities take, respectively, the forms

$$\rho_q(z) = \sum_{\lambda} \frac{1}{(2\pi)^2} \int_0^1 d\cos\theta \int_0^{k_F^q} dk k^2 |\psi_{k_{\perp}k_z^{\infty}\lambda q}(z)|^2, \quad (118)$$

and

$$\tau_q(z) = \sum_{\lambda} \frac{1}{(2\pi)^2} \int_0^1 d\cos\theta \int_0^{k_F^q} dk k^2 \left(k_{\perp}^2 |\psi_{k_{\perp}k_z^{\infty}\lambda q}(z)|^2 + \left| \frac{d\psi_{k_{\perp}k_z^{\infty}\lambda q}}{dz} \right|^2 \right). \quad (119)$$

Given the symmetry of half-infinite matter, only the z -component of spin density can be finite. With (83), (109) and (110), cf. Fig. 4, that component takes the form

$$J_z^q(z) = \sum_{\lambda} \frac{\lambda}{(2\pi)^2} \int_0^1 d\cos\theta \int_0^{k_F^q} dk k^2 k_{\perp} |\psi_{k_{\perp}k_z^{\infty}\lambda q}(z)|^2. \quad (120)$$

B. Numerical Solution of the SHFM Equations

As the first step, we solve the SHFM problem for nuclear matter for a certain assumed asymmetry η_V in the interior of the matter. Specifically, under the constraint of fixed η_V , with $\rho_{n,p}^V = \rho_V (1 \pm \eta_V)/2$ and employing (95) and (96), we seek ρ_V that minimizes E/A of Eq. (80) for uniform matter. That solution provides features of the semi-infinite matter in the asymptotic region.

Given the densities $\rho_{n,p}^V$ and the corresponding Fermi momenta $k_F^{n,p}$, we next discretize the wavevector space. Specifically, aiming at a calculation of the integrals (118)-(120) for observables, we discretize the space according to the abscissas $\{u_j^M\}_{j=1}^M$ for Gaussian integration

in angle,

$$\cos \theta_j = \frac{1}{2}(1 + u_j), \quad j = 1, \dots, M, \quad (121)$$

and according to the abscissas $\{t_i\}_{i=1}^N$ for Gaussian integration in wavenumber,

$$(k_{iq})^3 = \frac{1}{2}(1 + t_i) (k_{Fq})^3, \quad i = 1, \dots, N. \quad (122)$$

The choices (121) and (122) for the discretization are made to provide a uniform coverage of wavevector space, when integrations such as in (118)-(120) are approximated numerically by sums, following

$$\int_0^1 d \cos \theta \int_0^{k_F^q} dk k^2 (\cdot) = \frac{(k_{Fq})^3}{12} \int_{-1}^1 du dt (\cdot) \simeq \frac{(k_{Fq})^3}{12} \sum_{i,j} w_i^N w_j^M (\cdot). \quad (123)$$

Here, w are the respective Gaussian weights. The wavevector components for the expressions summed over on the r.h.s. of (123) are then

$$k_{zq}^{ij} = k_{iq} \cos \theta_j, \quad (124)$$

and

$$k_{\perp q}^{ij} = k_{iq} \sin \theta_j. \quad (125)$$

The wavefunction equations (111) are solved self-consistently for the chosen discrete wavevector values, at two spin orientations.

We integrate the differential equations (111), for ψ at individual wavevectors, by starting out far out from the surface. Over there, we relate the derivative to wavefunction in accordance with the asymptotic relation (115), i.e. impose the condition

$$\psi'(z) = -\kappa \psi(z). \quad (126)$$

and we move with our solution towards the matter and into its interior. Formal solutions to the differential equations (111) generally consist of two components:

$$\psi(z) = \psi^-(z) + \psi^+(z). \quad (127)$$

In the above, the ψ^- component drops in magnitude when moving away from the nuclear surface, according to the asymptotics of Eq. (115). That component represents, up to a factor, the solution we are looking for. On the other hand, the ψ^+ component grows when moving away from the surface, behaving as

$$\psi^+(z) \propto e^{+\kappa z}. \quad (128)$$

Have we moved away from the surface in integration, any inaccuracy in (126) compared to an exact relation for ψ^- , or any inaccuracies in the integration, would admix the ψ^+ component to our numerical solution. The ψ^+ component would eventually begin to dominate over ψ^- due to its exponential growth. However, if we move towards the matter, the opposite takes place, i.e. any ψ^+ admixture fades away due to its exponential decrease. For such reasons, in fact, it is not very important to insist on (126) in the starting conditions, as long as any results very close to the starting point are not utilized. E.g. one could start integration with $\psi' = 0$. Due to the linearity of the wavefunction equation, further, the starting magnitude of the wavefunction is not even important, i.e. e.g. $\psi = 1$ could be principally used. This is because the wavefunction normalization can be reset after the integration arrives into the interior of matter, by imposing the condition

$$|\psi_{\mathbf{k}}(z)|^2 + \left| \frac{1}{k_z^\infty} \frac{d\psi_{\mathbf{k}}}{dz} \right|^2 = 4, \quad (129)$$

following (114). In practice, because of the Friedel oscillations that will be discussed, which die off slowly in z , we prefer to impose the condition (129) with the l.h.s. in the condition averaged over a distance in z of $\sim \pi/k_F$.

An attractive high-accuracy method for solving second-order differential equations, such as the Schrödinger equation, of fifth order in the employed step, is the Cowell-Numerov (CN) method [84, 85, 86]. High order of a method generally allows for large steps in integration preventing accumulation of rounding errors, when numerous small steps need to be taken. The CN method applies directly, though, to the equations where the second derivative is expressed exclusively in terms of the independent variable and the integrated function. For those Skyrme interactions in Table I, for which $m^*/m \neq 1$, the position-dependent effective mass in the wavefunction equation (111) introduces, however, the first-order derivative of wavefunction into the single-particle equation, preventing a direct application of the CN method. With $B_q(z) = \hbar^2/2m_q(z)$, we specifically get for the derivative term in (111):

$$\frac{d}{dz} B \frac{d}{dz} \psi = B \frac{d^2 \psi}{dz^2} + \frac{dB}{dz} \frac{d\psi}{dz}. \quad (130)$$

A straightforward work-around has been put forward by Dobaczewski *et al.* [87]. Thus, on introducing

$$v_{k_\perp k_z^\infty \lambda q}(z) = B_q^{1/2}(z) \psi_{k_\perp k_z^\infty \lambda q}(z), \quad (131)$$

the r.h.s. of (130) can be rewritten as

$$B^{1/2} \frac{d^2 v}{dz^2} + \frac{1}{2B^{3/2}} \left[\frac{1}{2} \left(\frac{dB}{dz} \right)^2 - B \frac{d^2 B}{dz^2} \right] v = B^{-1/2} \left(\frac{d^2 v}{dz^2} - \Delta U v \right), \quad (132)$$

where

$$\Delta U_q(z) = \frac{1}{2} \frac{d^2 B_q}{dz^2} - \frac{1}{4B_q(z)} \left(\frac{dB_q}{dz} \right)^2. \quad (133)$$

Upon rewriting of the derivative term in (132), the first-order derivative disappears from the expression at the cost of the appearance of a term linear in the function, but the latter is not a problem for the CN method. Upon inserting the derivative term into (111), the differential equation for v takes the form

$$\epsilon_{kq} v_{k_\perp k_z \lambda q}(z) = \left(-\frac{\hbar^2}{2m_q^*(z)} \frac{d^2}{dz^2} + \frac{\hbar^2 k_\perp^2}{2m_q^*(z)} + U_q^{\text{eff}}(z) + \lambda W_q(z) k_\perp \right) v_{k_\perp k_z \lambda q}(z), \quad (134)$$

where

$$U_q^{\text{eff}}(z) = U_q(z) + \Delta U_q(z). \quad (135)$$

The equation for v above can now be solved with the CN method and ψ can be obtained from v following (131). The asymptotic $z \rightarrow \pm\infty$ behaviors are of the same type for v as for ψ , as B approaches a constant either inside or outside of the matter.

In the discretization of wavevector space, we typically utilize abscissa numbers of $M \sim 14$ and $N \sim 28$. The typical spatial step that we employ, when integrating the wavefunction equations with the CN method, is $\Delta z = 0.02$ fm. We start from a distance z_{max} displaced from the matter surface position of z_0 by $z_{\text{max}} - z_0 \simeq 14$ fm and we continue the integration of the wavefunction equations down to a position z_{min} in the matter, away from the surface by $z_0 - z_{\text{min}} \simeq 16$ fm. After each solution pass, the local particle and kinetic energy densities, of Eqs. (118) and (119), are updated, with the integrals (117) in the densities represented in terms of the summations (123).

For initialization of the solution iterations, starting densities must be assumed and we employ the combination of Fermi shapes:

$$\rho_{n,p}(z) = \frac{1}{2} [\rho^F(z) + \overline{\rho_{np}^F}(z)], \quad (136)$$

where

$$\rho^F(z) = \frac{\rho_V}{1 + \exp[(z - z_0)/d]}, \quad (137)$$

and

$$\overline{\rho_{np}^F}(z) = \text{sgn}(\rho_{np}^V) \min(|\rho_{np}^F(z)|, \rho(z)), \quad (138)$$

with

$$\rho_{np}^F(z) = \frac{\rho_n^V - \rho_p^V}{1 + \exp[(z - z_0 - \Delta R_a)/d_a]}. \quad (139)$$

In the above, z_0 is the starting position of nuclear surface, d is the diffuseness of isoscalar density, ΔR_a is the displacement of isovector density relative to the isoscalar density, and d_a is the diffuseness of isovector density. The role of Eq. (138) is to ensure that the magnitude of asymmetry does not exceed 1 locally. The initial kinetic energy densities for the wave equations are estimated from the densities using Eq. (102). The spin densities are at first assumed to vanish [6] and are thereafter found to rise to finite values during iterations. The surface diffuseness is first taken in the initialization equal to $d \sim 0.55$ fm. After self-consistency is first reached for symmetric matter, the value of d is read off from the obtained $\rho(z)$ and that value is then used to initialize a restarted set of iterations for the given interaction. For calculations of asymmetric matter, the initial values used are $\Delta R_a = 0.6$ fm (cf. Table I) and $d_a = d$. After the self-consistency is first reached for a small asymmetry η_V , the values of ΔR_a and d_a are read off from the small- η_V solution and used subsequently in the initialization of all other calculations of asymmetric matter for the specific interaction.

Within iterations for self-consistency, an attempt to use directly output densities from an I 'th solution iteration, $[\rho]_{\text{out}}^I$ and $[\tau]_{\text{out}}^I$, as input densities to the $(I+1)$ 'th iteration, generally introduces problems of two types. One problem is an undesired gradual shift of the solution in the direction outside of matter, towards a boundary of the computational region. Another problem are instabilities. To remedy both problems while optimizing convergence, as an input to the subsequent iteration, we employ, see also [6], a linear combination of the preceding input and of the shifted output,

$$[\rho_q(z)]_{\text{in}}^{I+1} = \beta(z) [\rho_q(z + u_I)]_{\text{out}}^I + [1 - \beta(z)] [\rho_q(z)]_{\text{in}}^I, \quad (140)$$

with the same $\beta(z)$ and u_I for ρ_q and τ_q . In the practice of setting the value of u_I , we found the requirements of either an unchanged nucleon number within the computational region, or of a fixed position for the net density reaching half of its asymptotic value, to be comparably effective in speeding up the iteration convergence and in preventing the undesired drift. The factor β has been made to vary smoothly across the computational

region, and to reach larger values, up to 0.4, outside of the matter and smaller inside the matter. For two of the Skyrme parameterizations, Skz0 and Skzm1 [68], we could not arrive at consistency at finite asymmetry, no matter what $\beta(z)$ we employed. For any of the Skyrme parametrizations, the use of an excessive $z_0 - z_{\min}$ might induce long-wavelength instabilities in the solution, inside the matter, evidenced by a convergence of the solution iterations, but to slightly different density shapes $\rho_{n,p}(z)$ in the matter, depending on the step Δz and on the starting position z_{\min} . Except for the immediate vicinity of the boundaries of the computational region, the solutions for interactions represented in Table I, for our choices of $z_{\min, \max}$ and Δz , are stable with respect to variations in the boundaries and in step magnitude. When comparing to each other our solutions for different interactions and different asymmetries in the next section, we reposition the solutions, so that the location where the net density drops to half of its asymptotic value does not change from one solution to another, $\rho(z_0) = \rho_V/2$.

C. Role of the Spin-Orbit Coupling

Figure 5 shows the typical central potential U , spin-orbit form factor W_z and net density ρ , arrived at in the course of solving the SHFM equations until consistency, in symmetric half-infinite nuclear matter. As seen in the figure, the density ρ and potential U exhibit different diffusenesses, with ρ being steeper. Otherwise, consistently with (89) and with general physical requirements, the spin-orbit form factor W_z is finite only in the surface region. With this, it can affect macroscopic features of the nuclear surface.

Quantitatively, with $k_{\perp} \lesssim k_F \approx 1.33 \text{ fm}^{-1}$, the spin-orbit term $k_{\perp} W_z$ is small in the wavefunction equation (111), lower by as much as a factor of ~ 4 or more at the maximum of its magnitude compared to the central potential U , see Fig. 5. The sign of W_z makes the spin-orbit potential attractive for spins parallel to the orbital angular momentum, $\lambda = +1$, and repulsive for antiparallel, $\lambda = -1$. On account of the potential, nucleons with $\lambda = +1$ get, on the average, displaced outward relative to the nucleons with $\lambda = -1$, as illustrated in terms of the respective densities in Fig. 5. This displacement, in turn, produces a positive spin density J_z in the surface region, cf. (120). A finite spin density modifies the central potential which involves a divergence of that density, see Eq. (88). With $b_4 + b'_4/2 > 0$ for a Skyrme parameterization, the correction to the central potential is attractive in the more

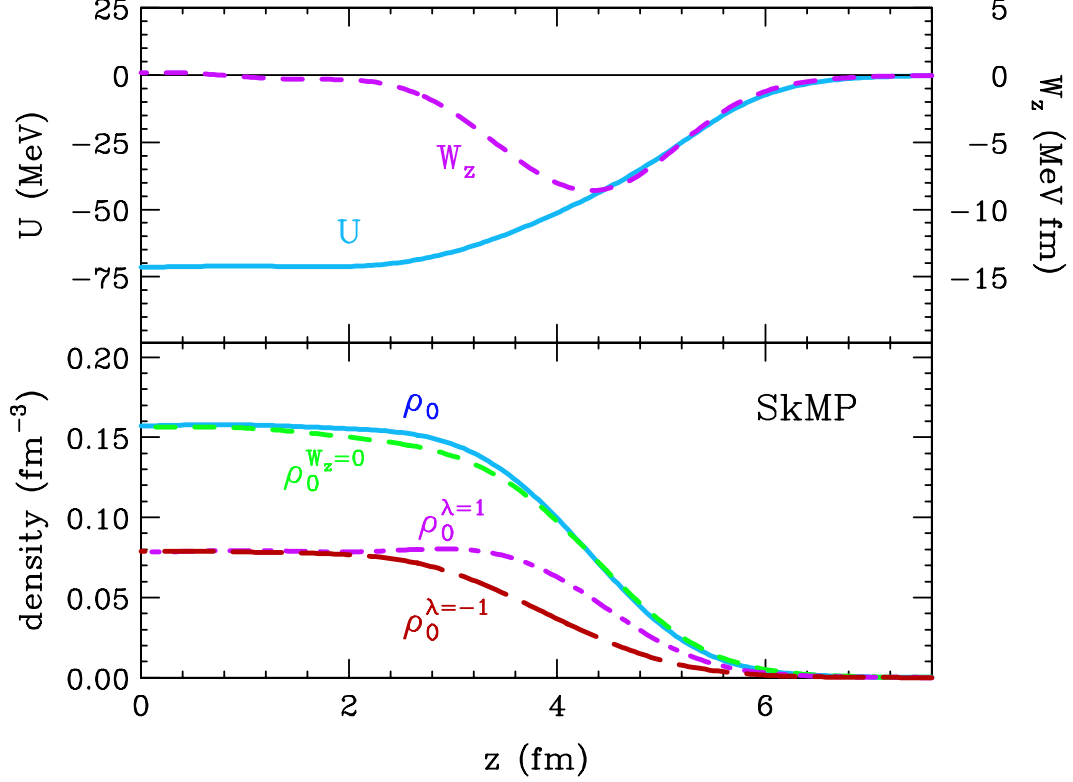


FIG. 5: Results of reaching self-consistency in symmetric half-infinite matter for the SHFM equations with the SkMP interaction, shown as a function of position along the axis perpendicular to the surface. The top panel displays the central potential U and the spin-orbit form factor W_z . The bottom panel displays the net nucleon density ρ_0 and partial densities of nucleons with spin parallel $\rho_0^{\lambda=1}$ and antiparallel $\rho_0^{\lambda=-1}$ to orbital momentum. Also displayed is the net density $\rho_0^{W_z=0}$ obtained when the spin-orbit potential is put to zero, $W_z = 0$.

inner part of the surface and repulsive in the outer. This steepens the central potential and, in consequence, makes the net density steeper in the surface region compared to the case when the spin-orbit term is ignored, see Fig. 5 where the density arrived at without the spin-orbit term is also shown.

A steeper profile of net density due to the spin-orbit term has been first predicted by Stocker, within a variational consideration [88]. Details behind his prediction, however, differ from our results. Thus, he has anticipated a steeper density-profile for $\lambda = -1$ than $\lambda = 1$ nucleons, while we find the opposite to hold, see Fig. 5. We next turn to the systematics of density with changing asymmetry. We will come back to the role of spin-orbit coupling in the surface region in the context of coefficients characterizing surface energy.

D. Densities for Different Asymmetries

In Section III, we have indicated that, in consequence of the quadratic dependence of E_a on $\rho_{np}(\mathbf{r})$, the normalized difference of nucleon densities for a given mass number, $\rho_{a(A)}(\mathbf{r})$, as well as the net density, $\rho(\mathbf{r})$, should both weakly depend on asymmetry. Figures 6 and 7 show, respectively, the isoscalar and isovector densities from solving the SHFM equations for half-infinite matter at several η , for sample Skyrme parameterizations. It is apparent in the figures that the anticipated scaling is generally very well satisfied. The scaling behavior holds even at $\eta = 0.3$ for the MSk9 and SkMP interactions, when the drip asymmetries for those interactions are close-by, at $\eta_V^d = 0.339$ and 0.336 , respectively. For the SkI5 interaction, the asymmetry $\eta = 0.3$ is already above the drip asymmetry of 0.288 and the corresponding densities are not displayed in the figures. A closer examination of the densities in Figs. 6 and 7 reveals that, in the interior of matter, the scaling worsens a bit with an increase in the *magnitude* of L and, in the density tails, the scaling worsens with an increase in the *value* of L . These findings are consistent with the expectations developed in Subsection III D. Regarding implications of Eq. (78), the overall symmetry coefficient for half-infinite matter is identical to that for the volume, $a_a \equiv a_a^V$. Consistently either then with (78) or with (64), in the interior of the matter in Fig. 6, the net density goes up or down depending on the sign of L , to the order of η^2 . Further, consistently with the expectations developed in the context of the local approximation in Subsection III D, in the density tails, the scaling is seen to be a bit worse satisfied for the isovector densities in Fig. 7, than for the isoscalar densities in Fig. 6. Nonetheless, one can claim that, in the end, the scaling for the isovector densities is more impressive than for isoscalar. This is because the isoscalar densities are rather bland across the interactions and they are forced to take on a value of $\rho_V/2$ at z_0 . In contrast to the isoscalar, the isovector densities exhibit much variation across the interactions and, for each interaction, the scaling needs to be exclusively due to an approximately invariant interdependence between the isovector and isoscalar densities and cannot be attributed to any imposed auxiliary condition.

Figure 8 next compares the isoscalar and isovector densities in symmetric half-infinite matter, for the same sample interactions. For each interaction, the isovector density is generally pushed out relative to the isoscalar density. Amongst the interactions, for the Z interaction with the most negative L , though, the two densities are rather close to each other.

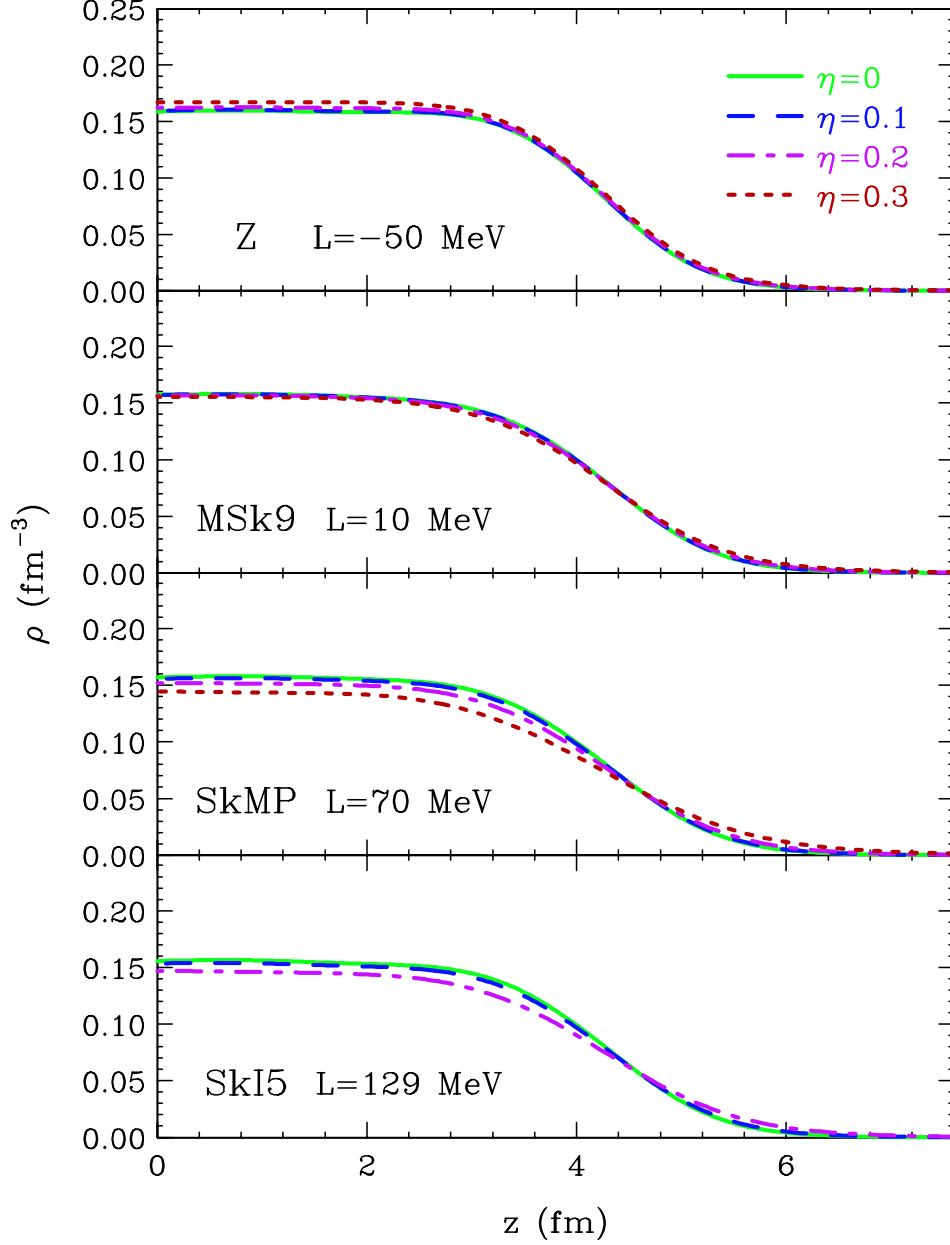


FIG. 6: Net density profiles at different asymmetries in half-infinite nuclear matter within SHFM, for sample interactions. For the SkI5 interaction, the asymmetry of 0.3 is already past the drip value of $\eta_V^d = 0.288$ and the corresponding profile is not shown. The $\eta = 0$ SkMP density is the same as the ρ_0 -density in Fig. 5.

As L increases, the densities separate more and more, with the most pronounced differences between these densities appearing for the SkI5 interaction in the figure. The growing difference with growing L again conforms with the expectations developed in Subsection III D.

Given the qualitative utility of the local approximation, it can be of interest to test that

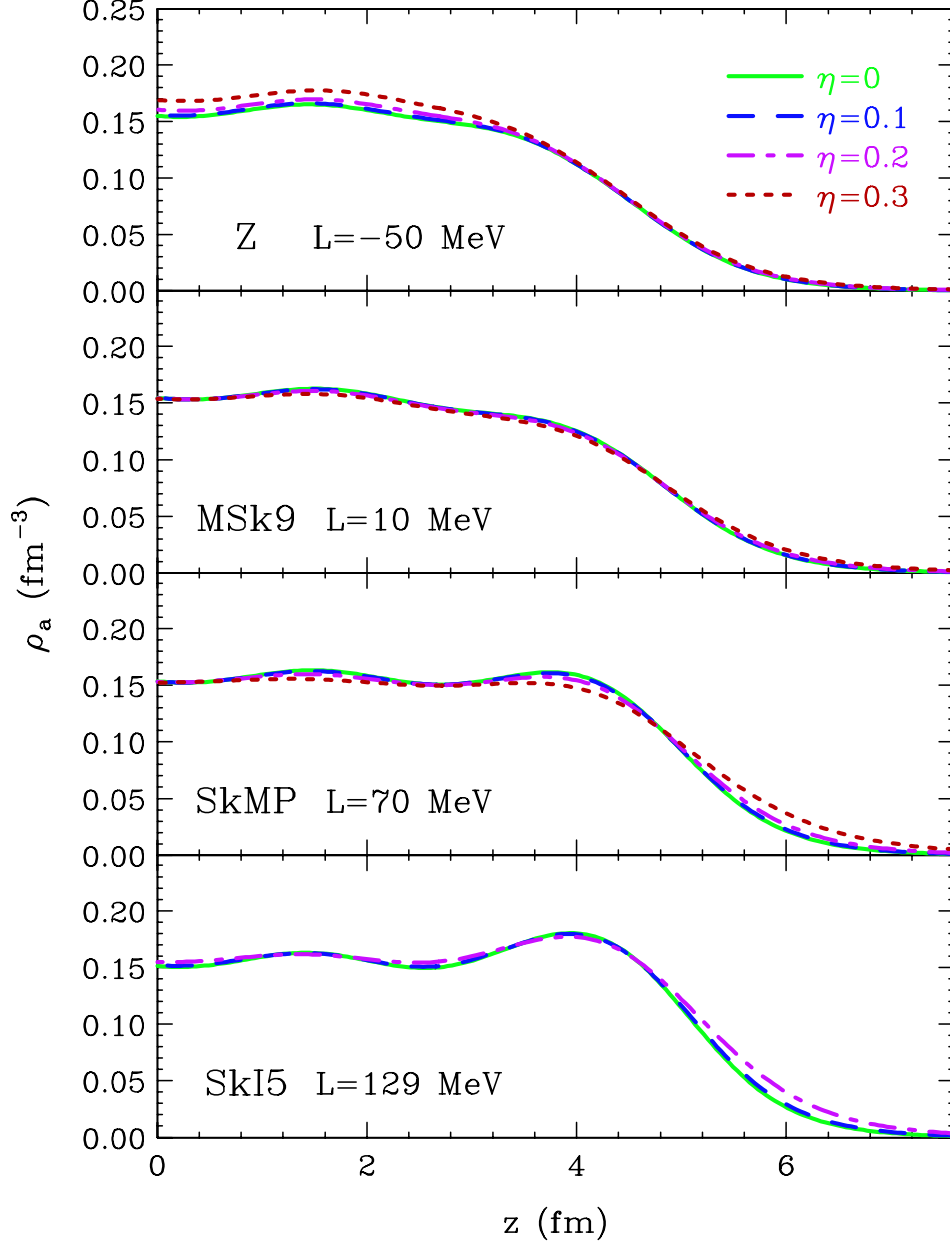


FIG. 7: Profiles of the isovector density, Eq. (44), at different asymmetries in half-infinite nuclear matter within SHFM, for sample interactions. For the SkI5 interaction, the asymmetry of 0.3 is already past the drip value of $\eta_V^d = 0.288$ and the corresponding profile is not shown. The abscissa scale is numerically identical to that in Fig. 6.

approximation quantitatively. For that purpose, in addition to the already displayed $\eta = 0$ isoscalar and isovector densities, we plot in Fig. 8 the local approximation to the isovector density, of Eq. (76). It can be seen that the actual isovector density $\rho_a^0(z)$ oscillates around the local approximation at the higher isoscalar densities, down to the net density reaching

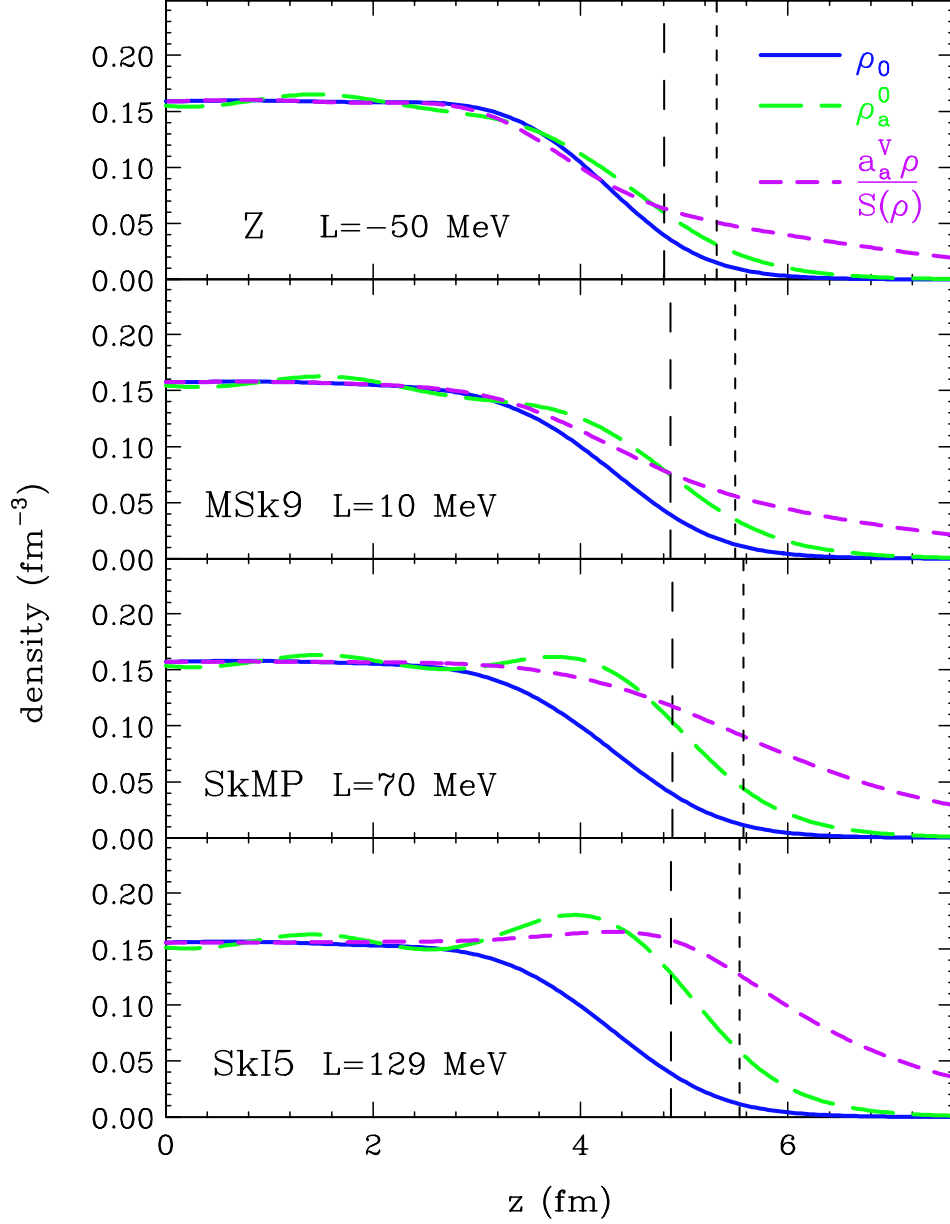


FIG. 8: Comparison of isoscalar and isovector densities, and of the local approximation to the isovector density, in symmetric half-infinite nuclear matter within SHFM, for sample interactions. The longer- and shorter-dashed vertical lines for the specific interaction indicate, respectively, the location where the net density is equal to the quarter of normal density and the location of a classical return point for the Fermi wavevector directed along the z -axis, when the spin-orbit potential is disregarded.

about a quarter of the normal density, $\rho_0/4$, for the interactions in the figure. At lower net densities in the matter, the actual density and the approximation separate from each other, with the local approximation thereafter strongly overestimating $\rho_a^0(z)$. It follows that, for arguments \mathbf{r} of the SHFM-operator \mathcal{S} such that $\rho(\mathbf{r}) < \rho_0/4$, this operator becomes significantly nonlocal.

Increasingly nonlocal character of the operator \mathcal{S} , with a drop of density in the surface, is expected on the basis of the result (104). In that result, see (105), the gradient corrections proportional to t_1 and t_2 represent effects of the range of interaction, while the corrections proportional to \hbar^2 represent quantal nonlocalities. It is seen in the expressions (105) that the \hbar^2 correction-terms will dominate over the finite-range terms at sufficiently low densities and eventually also overwhelm the zeroth-order term. Overall, it appears that the nonlocalities enhance the operator \mathcal{S} in the far-out surface region making its inverse reduced and producing physically expected exponential fall-off for the isovector density ρ_a .

The close proximity of the isovector density ρ_a to the local approximation, for the wide range of higher densities, opens up a chance of determining details in the density dependence of symmetry energy, from the systematics of proton densities alone. Correspondingly, it becomes of interest to understand better both the agreement of isovector density with the local expectation and the deviations. For this, we turn, in the following, to the Wentzel-Kramers-Brillouin-Jeffreys (WKBJ) approximation for the single-particle wavefunctions.

E. WKBJ Analysis

The wavelength for the oscillations of isovector density in Fig. 8, around the local approximation, can be easily recognized as that expected for the Friedel oscillations [89], $\lambda = \pi/k_F \simeq \pi/(1.33 \text{ fm}^{-1}) = 2.36 \text{ fm}$. Corresponding oscillations can also be detected in the isoscalar density, but they are there of a considerably lesser amplitude than in the isovector density. Friedel oscillations generally arise when a disturbance of the system, forcing nonuniformity, such as the surface, acts to synchronize the density oscillations for individual component wavefunctions. Other than generating the oscillations, the specific synchronization of components due to the surface acts also to slow down the rise of density with distance away from the surface, when moving into the interior of matter. The Friedel oscillations are much stronger for the isovector density, due to the dominant contribution of

the states near the Fermi surface, to the difference of neutron and proton densities.

To understand the oscillations mathematically, we invoke approximate WKB solutions to the SHFM equations (111). In the classically allowed region, where the equation

$$\epsilon_{kq} = \frac{\hbar^2 k_{k_\perp \lambda q}^2(z) + \hbar^2 k_\perp^2}{2m_q^*(z)} + U_q(z) + \lambda W_q(z) k_\perp, \quad (141)$$

has real solutions $k^z(z)$, the WKB solutions are of the form

$$\psi_{k_\perp k_z^\infty \lambda q}(z) \simeq 2 \sqrt{\frac{v_z^\infty}{v_z(z)}} \sin \left(\int_z^{z_{k_\perp k_z^\infty \lambda q}} dz' k_{k_\perp k_z^\infty \lambda q}^z(z') + \frac{\pi}{4} \right). \quad (142)$$

In the above, $z_{k_\perp k_z^\infty \lambda q}$ is the classical return point ending the classically allowed region that is assumed to extend here up to infinity in the negative z -direction, and v_z is the z -component of the velocity, $v_z = \hbar^{-1} \partial \epsilon / \partial k_z = \hbar k_z / m^*$. In the classically forbidden region, where (141) has purely imaginary solutions, the WKB wavefunctions are of the form

$$\psi_{k_\perp k_z^\infty \lambda q}(z) \simeq \sqrt{\frac{v_z^\infty}{|v_z(z)|}} \exp \left(- \int_{z_{k_\perp k_z^\infty \lambda q}}^z dz' |k_{k_\perp k_z^\infty \lambda q}^z(z')| \right). \quad (143)$$

Those wavefunction forms actually apply some distance away from the return point. Deep into the forbidden region, the wavefunctions are exponentially depressed and, in the considerations below, we will just put them to zero beyond the return point. With this, the density of nucleons q , at position z , becomes

$$\begin{aligned} \rho_q(z) &\simeq \frac{4}{(2\pi)^3} \sum_\lambda \int dk_z^\infty d\mathbf{k}_\perp \frac{v_z^\infty}{v_z(z)} \sin^2(\dots) \\ &= \frac{4}{(2\pi)^3} \sum_\lambda \int dk_z d\mathbf{k}_\perp \sin^2(\dots) \\ &= \frac{2}{(2\pi)^3} \sum_\lambda \int dk_z d\mathbf{k}_\perp \left[1 + \sin \left(2 \int_z^{z_{k_\perp k_z^\infty \lambda q}} dz' k_{k_\perp k_z^\infty \lambda q}^z(z') \right) \right]. \end{aligned} \quad (144)$$

In obtaining the second to the last expression, we have converted the wavevector integration from one over the asymptotic to one over the *local* wavevector-components. It should be noted that those wavevector integrations are confined to a half of the Fermi sphere. In arriving at the last expression, we have used the identity $\sin^2(\alpha + \frac{\pi}{4}) = \frac{1}{2} + \frac{1}{2} \sin(2\alpha)$. Effects of the spin-orbit term on nucleon densities cancel out to the lowest order. For that reason and also to make the local Fermi sphere isotropic, those effects will be further disregarded.

In consequence, the density of nucleons q becomes

$$\begin{aligned}\rho_q(z) &\simeq \frac{4}{(2\pi)^3} \int_{k < k_{Fq}(z)} d\mathbf{k} \left[1 + \sin \left(2 \int_z^{z_{k_\perp k_z^\infty q}} dz' k_{k_\perp k_z^\infty q}^z(z') \right) \right] \\ &= \frac{k_{Fq}^3(z)}{3\pi^2} + \frac{1}{2\pi^3} \int_{k < k_{Fq}(z)} d\mathbf{k} \sin \left(2 \int_z^{z_{k_\perp k_z^\infty q}} dz' k_{k_\perp k_z^\infty q}^z(z') \right).\end{aligned}\quad (145)$$

With the disregard of the spin-orbit term, the local Fermi wavevectors in (145) follow from

$$\mu_q = \frac{\hbar^2 k_{Fq}^2(z)}{2m_q^*(z)} + U_q(z). \quad (146)$$

If we were to consider the general case of mass potential B , we would need to decompose the local kinetic energy τ_q in a similar manner to (145). However, since our primary goal is to gain an insight, we shall confine ourselves to the case of $m^* \equiv m$, avoiding the need for specific decomposition.

Mathematically, the Friedel oscillations can be tied to the sine term on the r.h.s. of (145) or (144). Integration over wavevector components for that term leads to an averaging of the sine over argument values. While, in general, wide-range variations of the argument will make that average approach zero, any residue of averaging is likely to reflect possible nonuniformities in the integration, as far as values of the sine argument are concerned. An obvious discontinuity is the termination of integration at k_{Fq} , producing oscillations of the form $\sin(2k_{Fq}z + \delta)$. Otherwise, the local amplitude of oscillations depends on the distance from the surface. The larger the distance, the faster will be the variation of the argument of sine in (144), with the variation of wavevector, and the more suppressed will be the contribution of the sine to a density. Furthermore, different amplitudes will emerge for different types of densities. Thus, isoscalar density involves 3-dimensional integrals over parameters affecting the sine argument, cf. (145). However, isovector density involves differentiation of nucleonic densities with respect to asymmetry, cf. (46), which produces a sine-function integral reduced in the dimension to 2. In effect of the reduced averaging of the sine function, the Friedel oscillations turn out to be significantly larger, and they fall off slower with distance, in the isovector than in the isoscalar density.

Considering the vicinity of zero asymmetry for the functions, we now represent nucleon densities as

$$\rho_q(z) = \frac{k_{Fq}^3(z)}{3\pi^2} (1 + \mathcal{G}_q(z)), \quad (147)$$

where

$$\mathcal{G}_q(z) \simeq \frac{3}{2\pi k_{Fq}^3(z)} \int_{k < k_{Fq}(z)} d\mathbf{k} \sin \left(2 \int_z^{z_{k_\perp k_z^\infty q}} dz' k_{k_\perp k_z^\infty q}^z(z') \right). \quad (148)$$

The net nucleon density at $\eta = 0$ is then

$$\rho_0(z) = \frac{2k_F^3(z)}{3\pi^2} (1 + \mathcal{G}(z)). \quad (149)$$

We write, moreover, the μ_a -derivative of ρ_{np} at $\eta = 0$, for use in the isovector density (46), as

$$\frac{\partial \rho_{np}(z)}{\partial \mu_a} = 2 \frac{\partial \rho_n(z)}{\partial \mu_a} = \frac{2k_F^2(z)}{\pi^2} (1 + \mathcal{F}(z)), \quad (150)$$

where, with (147),

$$\mathcal{F}(z) = \mathcal{G}(z) + \frac{k_F(z)}{3 \left(\frac{\partial k_{Fn}}{\partial \mu_a} \right)} \frac{\partial}{\partial \mu_a} \mathcal{G}_n(z). \quad (151)$$

On evaluating the μ_a -derivative of both sides of Eq. (146) for neutrons, and on using Eqs. (46), (58), (94), (101), (149) and (150), we arrive at the following expression for the isovector density

$$\rho_a^0 = \frac{a_a^V \rho}{S(\rho)} \frac{1}{1 + \frac{\hbar^2 k_F^2}{6mS} \frac{\mathcal{G}-\mathcal{F}}{1+\mathcal{F}}} \approx \frac{a_a^V \rho}{S(\rho)} \left(1 + \frac{\hbar^2 k_F^2}{6mS} \mathcal{F} \right). \quad (152)$$

The last approximation is valid at large distances from the surface, in the classically allowed region, where we expect $1 \gg \mathcal{F} \gg \mathcal{G}$.

Equation (152) represents the isovector density in terms of the local approximation to that density combined with an oscillatory correction. Coefficient for the correction, whether examined in the denominator of the middle expression or on the r.h.s. of (152), involves the ratio of the kinetic contribution to symmetry energy to the net symmetry energy. Correspondingly, the Friedel oscillations are expected to be stronger for interactions with lower symmetry-energy values around the normal density, which indeed appears to be the case for the examples in Fig. 8. For the simplistic model of a step-like barrier at z_0 , representing a rapidly rising isoscalar optical potential U , the functions \mathcal{G} and \mathcal{F} may be arrived at in the following analytic forms:

$$\mathcal{G}(z) = \frac{3}{4k_F^2(z_0 - z)^2} \left[\cos(2k_F(z_0 - z)) - \frac{\sin(2k_F(z_0 - z))}{2k_F(z_0 - z)} \right], \quad (153)$$

$$\mathcal{F}(z) = -\frac{1}{2k_F(z_0 - z)} \sin(2k_F(z_0 - z)). \quad (154)$$

Following those results, oscillations in the isovector density, governed by \mathcal{F} , should die out rather slowly with the distance $(z_0 - z)$, as distance inverse, which appears to be borne out

by the results in Fig. 8. On the other hand, oscillations in the isoscalar density should die out rather quickly, as distance inverse squared, consistently with the previous qualitative expectations and with practical findings.

A couple of other observations can be made in connection with the considerations above. Thus, it is apparent that the region of potential validity of the local approximation in the $\eta \rightarrow 0$ matter is necessarily limited by the farthest lying classical return point for symmetric matter. At the general level, this criterion is consistent with the expectation that the range effects must be ignorable for the approximation to apply. An interesting aspect of this criterion is, however, that it is independent of the symmetry energy and tied only to the features of symmetric matter. Indeed, in spite of the widespread variation of the symmetry energy in Fig. 8, the position where local approximation breaks down, in terms of net density, remains approximately the same. The farthest return point is of course that for a Fermi wavevector directed along the z -axis and, for reference, we indicate the location of those points in Fig. 8. The return points for lower wavenumbers or for wavevectors not pointing along the z -axis are closer to the interior of the matter; the coarse end-location for the validity of the local approximation, of isoscalar density being about $\rho_0/4$, represents the return point for a Fermi wavevector directed at about 35° to the z -axis.

Another observation, related to the preceding considerations, pertains to the η -systematics of the tails of isoscalar and isovector densities. The *relative* variation of density in those tails appears to be significant with higher η in Figs. 6 and 7, for at least two of the sample interactions, SkMP and SkI5. Features of the tails combine the effects of symmetry energy close to the classical return points and the effects of chemical potentials on the forbidden region. Figure 9, which displays details of different densities on a logarithmic scale, at different η for two of the sample interactions, MSk9 and SkMP, can serve as an illustration in the discussion of understanding of the tails. At $\rho \gtrsim \rho_0/4$, larger deviations of symmetry energy from a_a^V , for SkMP than for MSk9 interaction, and larger $dS/d\rho$, yield both stronger changes in the isoscalar $\rho(\mathbf{r})$ with η^2 for SkMP, as expected from Eqs. (39) and (78). Changes within the second order in one of the densities, such as for SkMP, generally impact the other density within that order. Regarding the forbidden region, insights come from the behavior of the WKBJ wavefunctions far into the forbidden region, described in Eq. (143). With integrations in the wavevector space over squared wavefunctions producing densities, it is apparent that the neutron and proton densities need to fall off primarily exponentially in

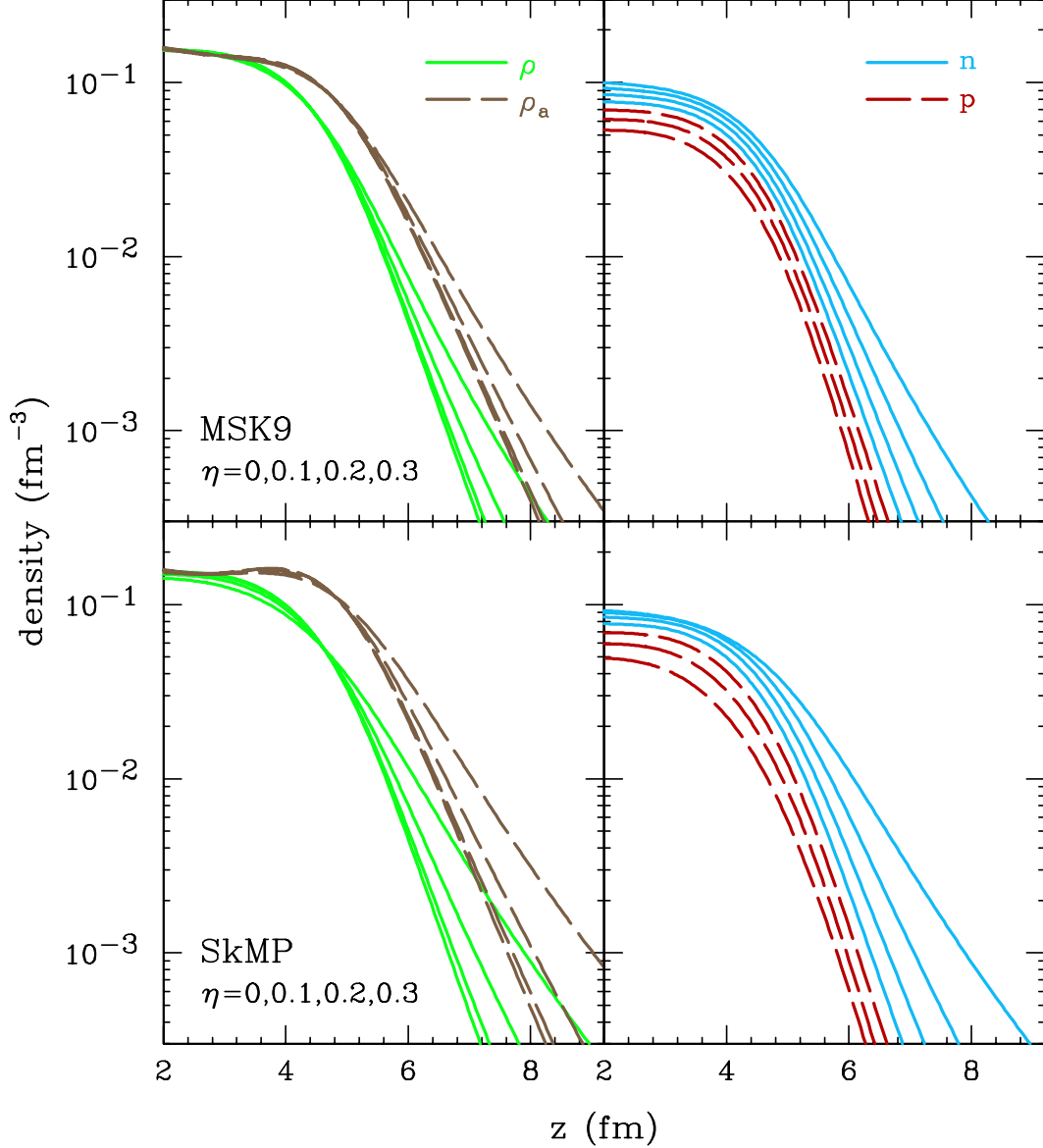


FIG. 9: Densities on a logarithmic scale, in the surface region of half-infinite nuclear matter, for sample MSk9 and SkMP interactions in the top and bottom panels, respectively. The abscissa scale is numerically identical to that in Figs. 6, 7 and 8. The left panels show the approximately invariant densities, isoscalar (solid lines) and isovector (dashed), with the order from left to right in the tails corresponding to $\eta = 0, 0.1, 0.2$ and 0.3 , respectively. The right panels show proton densities (dashed lines) for, respectively, $\eta = 0.3, 0.2$ and 0.1 , from left to right in the tail, and neutron densities (solid) for, respectively, $\eta = 0, 0.1, 0.2$ and 0.3 , from left to right in the density tail.

the far-out forbidden region, as $\exp(-2\kappa_{Fq} z) \equiv \exp(-z/d_q)$, where $\kappa_{Fq} = \sqrt{-2m\mu_q}/\hbar$ and, thus, $d_q \sim 0.57$ fm for $\mu_q \sim 16$ MeV. For $\eta \geq 0$ then, on account of the neutron contribution, with neutron chemical potential being greater or equal to the proton potential, the isoscalar and isovector densities should fall off as $\exp(-2\sqrt{-2m\mu_n} z/\hbar)$. Given a milder neutron than proton slope for $\eta > 0$, in fact, sufficiently far out, the neutron density needs to eventually strongly dominate over the proton density. Looking at the tails of proton and neutron densities in Fig. 9, far from the surface, it is seen that these densities indeed eventually begin to fall off exponentially, by about e per 0.6 fm at $\eta = 0$. As has been anticipated, the fall-off slopes are always about the same for ρ and ρ_a at a given η , and, at $\eta \geq 0$, about the same for these two densities and ρ_n . As neutron chemical potential increases with an increase in η , the slope of fall-off of the densities becomes milder. When one moves then farther and farther out of the matter, for $\eta > 0$, the accumulated effects of changed density slope, while possibly small on absolute scale, can become arbitrarily large on the scale of density scaled with the density for $\eta = 0$. However, besides slopes, the behavior of densities in the allowed region matters as well for the forbidden region, in setting of the initial conditions for the fall-off. Incidentally, as critical asymmetries nearly coincide for MSk9 and SkMP, see Table I, there is a similarity in evolution of μ_n with changes in η , for the two interactions. That similarity implies a degree of similarity in the slopes alone, that can be checked in Fig. 9.

F. Coefficients Characterizing Nuclear Surface Energy, a_S and a_a^S

For a self-sustained system in the absence of long-range interactions, the energy associated with a boundary can be simply defined as the difference between the actual energy and the energy expected if the boundary were not there,

$$E_S = E - \left(\frac{E}{A}\right)_V A = \int d\mathbf{r} \left[e_{\text{Skyrme}}(\mathbf{r}) - \left(\frac{E}{A}\right)_V \rho(\mathbf{r}) \right]. \quad (155)$$

The last expression has been arranged to make the integration over depth within the matter finite in the limit of $A \rightarrow \infty$, when the net energy can be represented in Skyrme form. In the case of half-infinite matter, Eq. (155) yields surface energy per unit area of the form

$$\frac{E_S}{\Sigma} = \int dz \left[e_{\text{Skyrme}}(z) - \left(\frac{E}{A}\right)_V \rho(z) \right]. \quad (156)$$

From the energy per unit area, principally, the coefficients a_S and a_a^S in an energy formula may be inferred. Specifically, with the area of $\Sigma \simeq 4\pi r_0^2 A^{2/3}$ for a large spherical nucleus

at $\eta \rightarrow 0$, we find, from (11), that the coefficients are related to the energy of half-infinite matter with

$$\begin{aligned} 4\pi r_0^2 \frac{E_S}{\Sigma} &= a_S + \frac{\mu_a^2}{4 a_a^S} + \mathcal{O}(\eta^4) \equiv a_S + \frac{(a_a^V)^2}{a_a^S} (\eta'_V)^2 + \mathcal{O}(\eta^4) \\ &= a_S + \frac{(a_a^V)^2}{a_a^S} \eta_V^2 + \mathcal{O}(\eta^4). \end{aligned} \quad (157)$$

In practice, some problems emerge when trying to utilize Eqs. (156) and (157) directly for determination of the coefficients characterizing nuclear surface.

Thus, while the subintegral function in (156) nominally approaches zero with increasing depth into the matter, i.e. $z \rightarrow -\infty$ in our convention, in practice it is not possible to employ (156) down to any depth in matter. This is because errors on the values of $e(z)$ and $\rho(z)$, from numerical integration of the SHF equations, do not vanish with increasing depth. If the use of (156) were insisted upon down to any depth in the matter, the accumulated effects of errors across the volume would eventually overpower any surface contribution to the sought integral. Outside of the matter, errors from the integration of the SHF equations surge, at least relatively, close to the start of integration. In consequence, in integrations across surface of half-infinite matter, when seeking E_S/Σ or other surface quantities, we employ a profile function $P(z)$ to control errors accumulating with distance away from the surface, by choosing to approximate integration such as in (156) with

$$\frac{E_S}{\Sigma} \simeq \int dz P(z) \left[e_{\text{Skyrme}}(z) - \left(\frac{E}{A} \right)_V \rho(z) \right]. \quad (158)$$

The profile function takes on the values

$$P(z) = \begin{cases} 1, & \text{at } |z - z_0| < z_P \\ 0, & \text{at } |z - z_0| > z_P + \Delta z_P \end{cases}. \quad (159)$$

where z_0 represents surface location. We further make $P(z)$ vary smoothly between z_P and $z_P + \Delta z_P$ aiming at a reduction of the error in integration associated with an interplay between the termination of integration and the Friedel oscillations in nucleon and energy densities inside the matter. We typically employ $z_P \sim 6$ fm and $\Delta z_P \sim 6$ fm. Results that will be presented, obtained using P , are stable with respect to variations in z_P and Δz_P around our choices.

When trying to extract the a_a^S coefficient from Eq. (158), an additional to the above problem arises, particularly serious for interactions with negative L . Thus, when extracting a_a^S , the energy values at small η must be considered. This makes the contribution of

surface-symmetry energy to the net energy to be of net third-order in smallness, with one order due to the surface-to-volume ratio and with the two remaining orders due to the asymmetry. For a negative L , the surface contribution to the net symmetry energy is particularly small. The problem can be circumvented by employing Eq. (51) for calculating a_a^S , rather than (156). Namely, upon adding and subtracting A/a_a^V from the right-hand side of (51), for large but finite spherical system of mass number A , we find

$$\frac{A}{a_a(A)} = \frac{A}{a_a^V} + \frac{1}{a_a^V} \int d\mathbf{r} (\rho_a^0(\mathbf{r}) - \rho^0(\mathbf{r})) \simeq \frac{A}{a_a^V} + \frac{A^{2/3}}{a_a^S}. \quad (160)$$

From the above, we find that the surface symmetry coefficient may be expressed as

$$\frac{1}{a_a^S} = \frac{4\pi r_0^2}{a_a^V} \int dz (\rho_a^0(z) - \rho^0(z)), \quad (161)$$

where the r.h.s. integration is over the direction perpendicular to the surface. In practical calculations with Eq. (161), we also employ a profile function such as in (158). Reaching a desired accuracy for a_a^S with (161) requires operating within two orders of smallness, rather than three, due to surface-to-volume ratio and due to difference $\rho_n - \rho_p$, of the order of η , in calculating ρ_a^0 . With the typical values of asymmetry that can be afforded in our extractions of a_a^S , $\eta \simeq (0.03-0.15)$, the error on a_a^S turns out actually to be (1–2) orders of magnitude smaller when using (161) than when using (156). In the following, we will extract the coefficients a_S and a_a^S , relying on the formulas above, and we will compare the results to those of preceding Hartree-Fock calculations for half-infinite matter by Kohler [5] and by Farine, Pearson *et al.* [7, 8, 90]. Also, we shall compare the extracted coefficients to those deduced from spherical Hartree-Fock calculations [96] for large, up to $A \sim (10^5 - 10^6)$, systems.

Interestingly, our Eq. (161) is equivalent to a droplet-model expression considered in the context of their calculations by Farine, Cote and Pearson [7, 8] (see [3] for a functional derivation by Farine), and ultimately exploited [91] in the context of Farine’s code, where

$$\frac{1}{a_a^S} = \frac{3}{2a_a^V r_0} \lim_{\eta_V \rightarrow 0} \frac{1}{\eta_V} \int dz \left\{ \frac{\rho_n(z)}{\rho_n^V} - \frac{\rho_p(z)}{\rho_p^V} \right\}. \quad (162)$$

The equivalence of the results (162) and (161) can be seen by noting that at low volume asymmetries, $\eta_V \rightarrow 0$, the asymptotic nucleon densities become $\rho_q^V \simeq 3(1 \pm \eta_V/2)/(8\pi r_0^3)$,

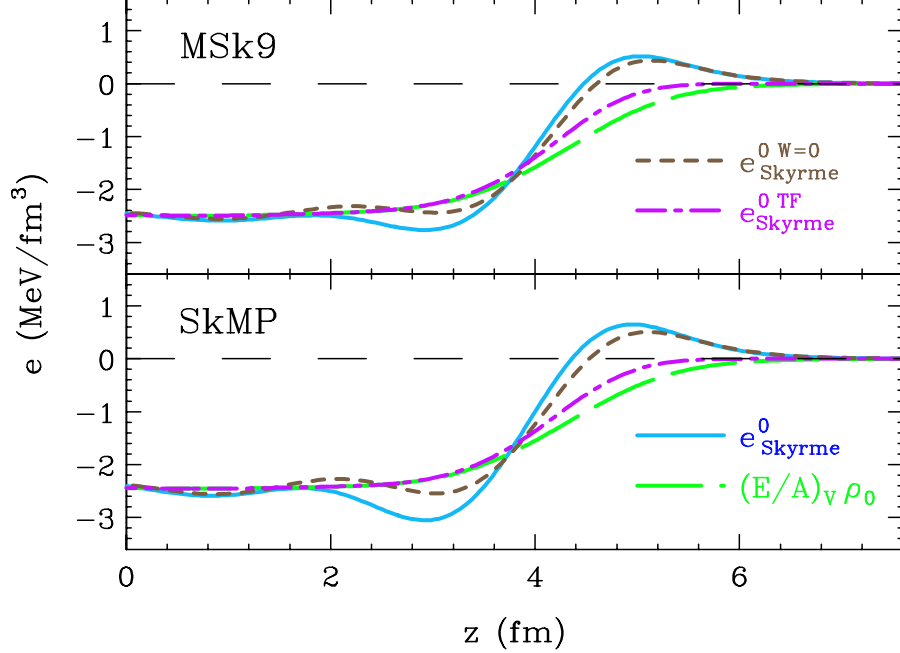


FIG. 10: Different energy densities in the surface region of symmetric half-infinite nuclear-matter, for sample Skyrme interactions. Shown are the Skyrme energy density in the standard SHFM calculations, e_{Skyrme}^0 from Eq. (80), the energy density from the calculations with spin-orbit term ignored, $e_{\text{Skyrme}}^{0 W=0}$, the energy density in the Thomas-Fermi approximation with gradient terms ignored, $e_{\text{Skyrme}}^{0 \text{TF}}$, and, finally, the energy density expected if the energy per nucleon were constant, $(E/A)_V \rho_0$. The abscissa scale is numerically identical to that in Figs. 6, 7 and 8.

allowing to rewrite the r.h.s. of (162) as

$$\begin{aligned} \frac{1}{a_a^S} &= \frac{4\pi r_0^2}{a_a^V} \lim_{\eta_V \rightarrow 0} \frac{1}{\eta_V} \int dz \left\{ \frac{\rho_n(z)}{1 + \eta_V} - \frac{\rho_p(z)}{1 - \eta_V} \right\} \\ &= \frac{4\pi r_0^2}{a_a^V} \lim_{\eta_V \rightarrow 0} \int dz \left\{ \frac{\rho_n(z) - \rho_p(z)}{\eta_V} - \rho(z) \right\}, \end{aligned} \quad (163)$$

where the r.h.s. yields next the r.h.s. of (161), cf. Eq. (46). Notably, because of the Friedel oscillations, Farine *et al.* ended up never employing Eq. (162) directly in their analyses. Instead, they have examined the separation between neutron and proton surfaces at finite η_V , with which separation they have replaced the integral that appears on the r.h.s. of Eq. (162). With this, they proceeded along the lines of the droplet model [27], see also [5].

Figure 10 displays different energy densities in the surface region of symmetric half-infinite nuclear matter, for two sample Skyrme interactions, MSK9 and SkMP. Those densities include the two energy densities, e_{Skyrme}^0 and $(E/A)_V \rho_0$, of which the integrated difference

yields the surface energy (156), and they further include the energy density $e_{\text{Skyrme}}^{0W=0}$ calculated with the spin-orbit term suppressed and, finally, the energy density calculated in the Thomas-Fermi approximation, $e_{\text{Skyrme}}^{0\text{TF}}$. In obtaining the last energy density, the density of kinetic energy is taken in the local approximation of Eq. (95) and the gradient terms in any *density* are ignored.

For moderately subnormal nucleon densities in Fig. 10, the energy densities $(E/A)_V \rho_0(z)$ and $e_{\text{Skyrme}}^{0\text{TF}}(z)$ are not much different from each other. This just reflects the fact that the energy per nucleon minimizes in uniform matter at normal density and, in consequence, it changes little with moderate deviations of density from normal. Across nucleon densities, the energy density $e_{\text{Skyrme}}^0(z)$ oscillates in the figure in the vicinity of $e_{\text{Skyrme}}^{0\text{TF}}(z)$. Dominant and positive contribution to the difference of energy densities $e_{\text{Skyrme}}^0 - (E/A)_V \rho_0$, in the expression (156) for the surface energy, is seen to come from the far-out tail of the density distribution, from essentially the classically forbidden region. In fact, in the outmost tail, the potential energy approaches zero faster than does the kinetic energy, making the net energy density even positive. The positive contribution to the difference in (156) is next, in the matter direction, much reduced by the negative contribution from just moderately subnormal nucleon densities in the density tail. When moving further in position into interior of the matter, the energy densities in the difference in (156) and, correspondingly, the difference itself oscillate in a Friedel fashion, with a wavelength of $\sim \pi/k_F \simeq 2.4$ fm. The precise location of maxima and minima in e_{Skyrme}^0 , and in the energy difference, depends on the choice that was made for the kinetic energy density. Thus, when expressing the kinetic energy density in terms of a square of wavefunction gradient in (82), the kinetic energy oscillates approximately out of phase with respect to the density. If the kinetic energy were expressed, though, in terms of a laplacian, rather than gradient squared, the oscillations of kinetic-energy density would have been approximately in phase with the nucleon density.

Surface energy coefficients, calculated by integrating the $\eta = 0$ difference of energy densities in (158), to obtain the energy for elementary surface area,

$$a_S = 4\pi r_0^2 \frac{E_S^0}{\Sigma}, \quad (164)$$

are provided for various Skyrme interactions in Table I. The value distribution, across interactions, is rather narrow, with the average coefficient value of 17.6 MeV combined with the standard deviation of 1.1 MeV.

An interesting issue is how the surface coefficient may be affected by the effects of a spin-orbit coupling acting in the surface region. Looking at the Skyrme energy functional (80), where nucleon densities multiply spin-density divergencies in the coupling, we see that this coupling allows a nuclear system to lower its energy by developing spin densities. Divergence of a spin density obviously integrates to zero. However, energy of a system can change when positive and negative divergence values are correlated with different magnitudes of nucleon densities. For positive b_4 -coefficient values in the functional (80), the energy gets lowered when a spin density directed outward develops in the surface region. In that case, the divergence is positive in the inner part of the surface and negative in the outer allowing the energy density to drop more in the inner than in the outer part of the surface. The polarization in the system is moderated, in particular, by the kinetic energy density that grows, but only quadratically, with spin density. For reference, in addition to other energy densities in Fig. 10, we show there also the Skyrme energy density $e_{\text{Skyrme}}^{0W=0}$ obtained when suppressing the spin-orbit coupling. It is seen that, indeed, inclusion of the coupling lowers energy density more in the inner part of the surface than in the outer. Lowering of the system energy leads to lowering of the surface coefficient. Notably, inclusion of the coupling affects also $(E/A)_V \rho$ in the difference of energy densities for the surface energy (158), but not as strongly as e_{Skyrme} there, cf. Fig. 5. Quantitatively, for the surface coefficients of the interactions illustrated in Fig. 10, we find $a_S^{W=0} = 18.7 \text{ MeV}$ for both the MSk9 and SkMP, when the spin-orbit coupling is suppressed. With the coupling, we find $a_S = 17.1$ and 16.6 MeV , respectively, for the the MSk9 and SkMP interactions, see Table I. A $\sim 10\%$ magnitude in reduction of a_S is typical for the Skyrme parameterizations, when switching on the spin-orbit coupling, see also the forthcoming Table II. To our knowledge, Stocker [88] was the first to assess the sign and magnitude of the change in the surface symmetry coefficient when including the spin-orbit coupling in the surface description.

Besides the values of a_S , Table I gives, further, the surface symmetry coefficients a_a^S obtained by integrating the $\eta = 0$ difference of isovector and isoscalar densities in Eq. (161). As might be expected from Fig. 8, where the relation between isoscalar and isovector densities varies widely from one interaction to another, the values of a_a^S vary widely between individual interactions, from 10 to 60 MeV. Figure 11 illustrates next the changes in surface energy (158) of an elementary area $4\pi r_0^2$, with changing asymmetry, for the sample Skyrme interactions. Magnitude of the changes in energy should be compared to the magnitude of

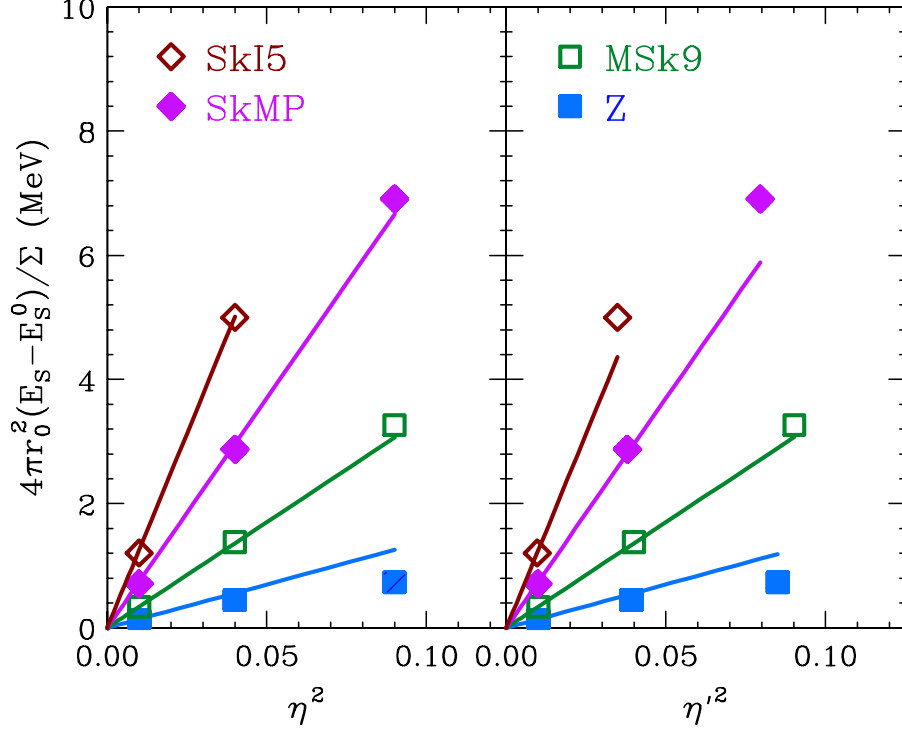


FIG. 11: Symbols represent change in the surface energy of an elementary area, from (158), for different Skyrme parameterizations, plotted vs square of asymmetry: volume asymmetry in the left panel and effective volume asymmetry, $\eta'_V \equiv \mu_a/(2a_a^V)$, in the right panel. Lines represent expectations based on Eq. (157), with surface symmetry coefficients taken from Eq. (161).

the surface coefficient (164), of the order of 17 MeV for the Skyrme interactions. Note that the rise of surface energy with asymmetry in a finite nucleus would be accompanied by a drop in the volume symmetry energy, compared to a system with no surface, due to asymmetry moving out to the surface region. As evident in Fig. 8, the surface energy generally changes quadratically with asymmetry. At small asymmetries, barely visible deviations from the lines, representing expectations from Eqs. (157) and (161), stem from numerical inaccuracies, primarily arising from the use of Eq. (158) to calculate the surface energy. At higher asymmetries generally true fourth-order terms in asymmetry come into play. In particular, some differences between the regularities in the left and right panels become apparent at higher η and L ; these are due to the differences that, depending on interaction, develop between η_V and η'_V at higher asymmetries, as a consequence of fourth-order terms in the energy of uniform matter.

For the Skyrme parameterizations with $b_4 = b'_4$, cf. Eq. (84), the spin-orbit coupling

has even less effect on a_a^S than on a_S . Unlike a_S , the coefficient a_a^S increases rather than decreases with the switching on of the spin-orbit coupling, usually by less than 10% and often by much less. Notably, though, at constant volume asymmetry, the increase in a_a^S implies dropping of the surface energy, cf. (157), just as a decrease in a_S does. Without the coupling, we find e.g. $a_a^{SW=0} = 22.5$ and 11.1 MeV, respectively, for the MSk9 and SkMP parameterizations, and $a_a^S = 23.0$ and 12.1 MeV, respectively, for these parameterizations, with the coupling. Additional exemplary results from $b_4 = b'_4$ Skyrme parameterizations can be found in the forthcoming Table II. For parameterizations with different b_4 and b'_4 , the spin-orbit coupling may have a stronger effect on the a_a^S coefficient, than for $b_4 = b'_4$, seemingly due to a strengthening of the spin-isospin correlations in the surface region. E.g. for the SkO parameterization, we find $a_a^{SW=0} = 13.2$ MeV and $a_a^S = 14.9$ MeV, without and with the coupling, respectively. For SkI4, we find $a_a^{SW=0} = 17.5$ MeV and $a_a^S = 20.8$ MeV.

G. Comparison to Coefficient Values in the Literature

Our results for the coefficients of surface energy are next compared in Table II to the results obtained by others in the literature within the SHFM calculations of asymmetric systems. Specifically, our coefficients are compared to those obtained within the calculations of semi-infinite matter, done by Kohler [5] and by Pearson *et al.* [6, 8, 71, 72, 90, 91, 92, 93, 94]. The latter results stem predominantly from the code by Farine [95]. The dependence of the surface energy on asymmetry has been expressed in the past calculations of semi-infinite matter in terms of the coefficient Q from the droplet model, cf. Subsection II C. That coefficient differs from a_a^S by simple factor, cf. (16), allowing for a simple transcription of the results obtained for semi-infinite matter. The calculations by Kohler were done without spin-orbit coupling and, in comparisons to his results, we have suppressed that coupling as well. In addition, in Table II, our coefficients for the surface are compared to those deduced in the calculations of spherical nuclei with large mass, up to $A \sim (10^5 - 10^6)$, by Reinhard *et al.* [96]. Those authors have assessed the coefficients of expansion of energy in powers of $A^{-1/3}$ and η^2 , for different interactions. If we expand the symmetry coefficient (14) in $A^{-1/3}$, we find that we can compute a_a^S from the coefficient a_{ssym} in [96], with

$$a_a^S = -\frac{(a_a^V)^2}{a_{\text{ssym}}}. \quad (165)$$

As will be mentioned later, in addressing the likely coefficient values, the expansion of the symmetry coefficient (14) lacks justification for nuclear masses encountered in nature.

TABLE II: Comparison of coefficients characterizing nuclear surface energy, from SHFM calculations of nuclear systems by different authors, with sources for outside results provided in the superscripts. The surface symmetry coefficient a_a^S is related to the coefficient Q , stemming from the droplet model, with $a_a^S = 4Q/9$, and to coefficient a_{ssym} in the large- A expansion of nuclear energy [96], with $a_a^S = -(a_a^V)^2/a_{\text{ssym}}$.

Name	a	Value (MeV)			
		Kohler	Pearson <i>et al.</i>	Reinhard <i>et al.</i>	Our
SII	$a_S^{W=0}$	19.8 ^[5]			20.20
	$a_a^{SW=0}$	11.6 ^[5]			17.27
	a_S		19.8 ^[8]		19.38
	a_a^S		17.8 ^[8]		17.54
SIII	$a_S^{W=0}$	19.6 ^[5]	19.9 ^[6]		19.85
	$a_a^{SW=0}$	21.3 ^[5, 8]			21.79
	a_S		18.8 ^[8]		18.54
	a_a^S		23.1 ^[8]		21.77
SIV	a_S		19.6 ^[8]		18.87
	a_a^S		15.1 ^[8]		13.39
SV	$a_S^{W=0}$	19.6 ^[5]			20.44
	$a_a^{SW=0}$	4 ^[5]			9.95
	a_S		19.8 ^[8]		19.16
	a_a^S		11.1 ^[8]		10.27
SVI	a_S		18.3 ^[8]		18.10
	a_a^S		26.7 ^[8]		26.27
SkMs	a_S		18.0 ^[90]	17.6 ^[96]	17.46
	a_a^S		26.7 ^[90]	17.4 ^[96]	14.48

Table Continued on Next Page...

TABLE II – Continued

Name	a	Value (MeV)			
		Kohler	Pearson <i>et al.</i>	Reinhard <i>et al.</i>	Our
SKa	$a_S^{W=0}$	19.8 ^[5]			19.97
	$a_a^{SW=0}$	9.3 ^[5]			12.06
SKb	$a_S^{W=0}$	19.8 ^[5]			19.97
	$a_a^{SW=0}$	7.6 ^[5]			10.03
SkP	a_S			18.2 ^[96]	18.18
	a_a^S			20.0 ^[96]	18.02
SkI3	a_S			18.0 ^[96]	17.77
	a_a^S			16.2 ^[96]	12.77
SkI4	a_S			17.7 ^[96]	17.48
	a_a^S			25.6 ^[96]	20.83
SLy4	a_S			18.4 ^[96]	18.24
	a_a^S			19.0 ^[96]	16.60
SLy6	a_S		17.74 ^[91]	17.7 ^[96]	17.53
	a_a^S		14.8 ^[91]	20.0 ^[96]	17.12
SkO	a_S			17.3 ^[96]	17.14
	a_a^S			17.6 ^[96]	14.94
BSk1	a_S		17.54 ^[91]	17.5 ^[96]	17.22
	a_a^S		20.3 ^[91]	21.5 ^[96]	23.72
BSk2	a_S		17.54 ^[71, 91, 92]		17.14
	a_a^S		20.4 ^[91] , 30.2 ^[71, 92]		23.15
BSk3	a_S		17.5 ^[71, 92]		17.16
	a_a^S		29.8 ^[71, 92]		23.37
BSk4	a_S		17.3 ^[71]		16.91
	a_a^S		33.8 ^[71]		23.01
BSk5	a_S		17.5 ^[71]		17.04
	a_a^S		23.1 ^[71]		20.65

Table Continued on Next Page...

TABLE II – Continued

Name	a	Value (MeV)			
		Kohler	Pearson <i>et al.</i>	Reinhard <i>et al.</i>	Our
BSk6	a_S		17.18 ^[71, 72, 91]	17.3 ^[96]	16.74
	a_a^S		19.9 ^[91] , 23.7 ^[72] , 36.9 ^[71]	23.8 ^[96]	22.73
BSk7	a_S		17.3 ^[71, 91]		16.70
	a_a^S		20.1 ^[91] , 35.6 ^[71]		22.81
BSk8	a_S		17.64 ^[72, 91, 93]		17.12
	a_a^S		20.2 ^[91, 93] , 24.0 ^[72]		23.13
BSk9	a_S		17.92 ^[91, 93]		17.42
	a_a^S		15.8 ^[91, 93]		17.83
BSk10	a_S		18.0 ^[73]		17.51
	a_a^S		15.6 ^[73]		17.48
BSk11	a_S		17.7 ^[73]		17.32
	a_a^S		15.6 ^[73]		17.42
BSk12	a_S		17.7 ^[73]		17.30
	a_a^S		16.0 ^[73]		17.51
BSk13	a_S		17.7 ^[73]		17.34
	a_a^S		15.6 ^[73]		17.34
BSk14	a_S		17.6 ^[74, 94]		17.17
	a_a^S		15.6 ^[74, 94]		17.22

When carrying a case-by-case examination of the entries in Table II, it becomes apparent that results for the surface coefficient a_S agree fairly well between different authors. As to results for the surface symmetry coefficient a_a^S , a degree of agreement is found in many cases but in a number of other cases there is a disagreement by factors even in excess of 1.5. The status of the two coefficients in the literature is further illustrated with two panels in Fig. 12. For different Skyrme parameterizations with or without spin-orbit coupling, the values obtained in the literature are plotted in those panels against our values. In case of an ideal agreement, the results should line up with the diagonal lines in the panels.

In assessing the level of agreement between the results in literature, on the basis of the figure, it should be noted that the range of values displayed in the panel for a_S is lower by one order of magnitude than in the panel for a_a^S .

Regarding the three author groups, we appear to have the best overall agreement with Reinhard *et al.* [96]. Their results, though, are also later than most of other results that we compare against. On the average, their results for a_S are higher by just ~ 0.25 MeV than ours for the coefficient. The results by Pearson *et al.*, for the surface coefficient, appear systematically shifted by a bit more, ~ 0.4 MeV, which still represents just 2% of coefficient value. By contrast, in the overall assessment, the agreement between the results for a_a^S turns out to be somewhat unsatisfactory, given the discrepancies encountered that are of the same order as coefficient values. In practice, this demonstrates the difficulty in working with contributions to system properties that are small due to their simultaneous association with surface and with asymmetry. That difficulty is further underscored by the fact that Pearson *et al.* have quoted significantly different values characterizing surface symmetry energy, for the same interaction, in different publication years, cf. Table II.

Realizing the fragility of their results for the coefficient characterizing surface symmetry-energy, Pearson *et al.* have eventually reassessed the procedures for extracting the coefficient values, specifically in Appendix A of Ref. [91]. They have examined there the stability of extracted coefficient values, when changing asymmetry in the extraction. From the three tested procedures tested, they have found the one based on Eq. (162) to be the most stable and, thus, preferred. Note that before [7], for the sake of result stability, Pearson *et al.* have found it beneficial to approximate the integral on the r.h.s. of (162), with a displacement of densities. While there is a significant improvement in the agreement of our results with those of Pearson *et al.* following the reassessment [74, 91, 91, 94], disagreements between the two sets still can reach the order of 20%, cf. Table II. Reinhard *et al.* [96] have employed a strategy close to that in Eq. (157) and disagreements between their and our a_a^S -coefficient values reach $\sim 25\%$.

Our own tests of the stability of our results for a_a^S from Eq. (161), with respect to different technical aspects of calculations, indicate that errors of those coefficient values do not exceed 0.5%. The aspects of calculations that have been varied include the already mentioned mesh in wavevector space, step of integration in space, and the profile function in space. In the context of the investigations in [91], it may be still worthwhile to compare the

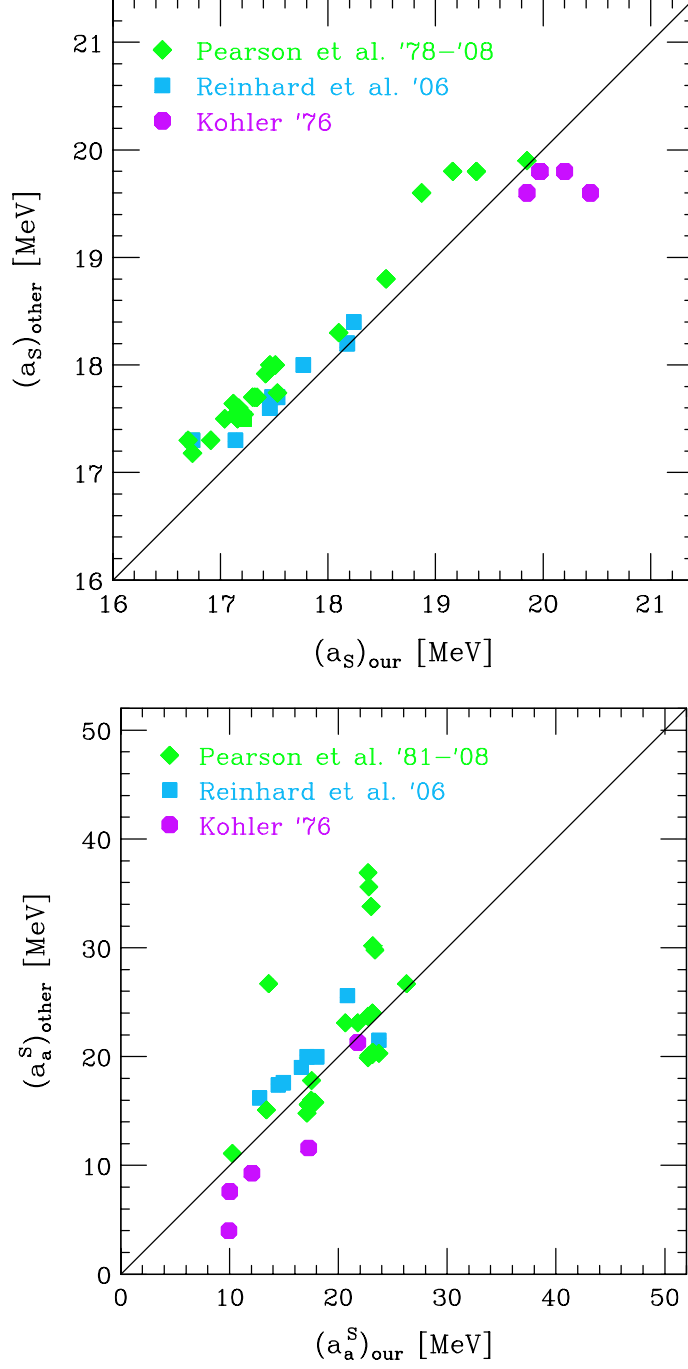


FIG. 12: Comparison of the values of coefficients characterizing nuclear surface energy in our calculations and elsewhere in the literature [5, 6, 8, 71, 72, 73, 74, 90, 91, 92, 93, 94, 96]. The first and second panels show, respectively, the comparison of surface coefficients a_S and of surface symmetry coefficients a_a^S . Respective coefficient values are given in Table II and the comparisons of coefficients with and without spin-orbit coupling are lumped together. In the case of an ideal agreement, the results, as plotted, should line up with the diagonals in the panels.

results on a_a^S obtained with different methods. We have mentioned that errors for a method involving dividing out two powers of η , can exceed errors for a method involving dividing out just one power, by (1–2) orders of magnitude, for the small values of η we employ. Partly, this can be compensated by employing a higher η in extracting a_a^S with the inferior method: when one is resigned to a larger error, effects of any anharmonicity of the symmetry energy in η matter less. Overall, though, when the quality of calculations increases, errors decrease, whether for the more favored or the more inferior method of a_a^S extraction. Thus, differences between the results obtained with different methods can be exploited in general assessment of calculations.

As to the intrinsic comparisons, Fig. 11, for one, can be used for testing visually the consistency between Eqs. (157) and (161) in our calculations, for the several interactions in that figure. Otherwise, Table III shows the values of a_a^S extracted with three different methods from our half-infinite matter calculations, when employing Eq. (161), Eq. (157) and also Eq. (11). The last two methods both involve dividing out factors of the second order in asymmetry and, thus, are both expected to provide inferior results to the first method that is our standard. Our calculations for the table have been done for those Skyrme parameterizations for which Pearson *et al.* have also done calculations with different methods. Their results are also shown in Table III, for comparison. The largest deviation between the preferred and an inferior method in Table III is 7% for our calculations and 34% for Pearson *et al.*

H. Further Discussion of the Isovector Density ρ_a^0 and of the Coefficient a_a^S

As we have shown, in the classically allowed region of the surface, $\rho \gtrsim \rho_0/4$, the isovector density ρ_a follows closely the expectation of Eq. (76) from uniform matter, with ρ_a inversely proportional to the symmetry energy $S(\rho)$ at a given net density ρ . The form of the adherence to the expectation, and the partial consequences of that adherence, are the following for the specific limits of $S(\rho)$. When the symmetry energy remains significant at subnormal densities, for low positive or even negative values of the dimensionless parameter-ratio L/a_a^V , the isovector density ρ_a stays close to the isoscalar density ρ over a significant portion of the classically allowed region of nuclear surface, as expected from Eq. (76). Outside of the classically allowed region, both densities drop rapidly to zero, in an approximately expo-

TABLE III: Values of surface symmetry coefficient, extracted following different indicated equations from the SHFM calculations of half-infinite nuclear matter, done for the different indicated Skyrme parameterizations. The results that were ultimately decided to be superior by the respective authors are represented in the roman font and other results are represented in italic.

Name	a_a^S [MeV]					
	Our			Pearson <i>et al.</i>		
	Eq. (11)	Eq. (161)	Eq. (157)	Eq. (162) ^a	Eq. (157)	Ref.
SII	<i>16.63</i>	17.54	<i>18.26</i>	15.1	<i>17.8</i>	[8]
SIII	<i>20.83</i>	21.77	<i>22.75</i>	19.1	<i>23.1</i>	[8]
SIV	<i>12.88</i>	13.39	<i>14.27</i>	12.9	<i>15.1</i>	[8]
SV	<i>10.40</i>	10.27	<i>10.80</i>	8.9	<i>11.1</i>	[8]
SVI	<i>26.13</i>	26.27	<i>26.66</i>	32.4	<i>26.7</i>	[8]
BSk8	<i>22.80</i>	23.13	<i>23.32</i>	20.0	<i>13.3</i>	[91]

^aAn additional approximation is employed [7].

ponential fashion. On the other hand, when, for high L/a_a^V -ratio, the symmetry energy drops rapidly with density at subnormal densities, the isovector density ρ_a remains significantly higher than ρ , across the classically allowed region, cf. Fig. 8. For the exponential fall-off of the densities in the classically forbidden region, the starting value for ρ_a is then further significantly higher than for ρ , extending the region where ρ_a dominates over ρ , cf. Fig. 9. Note that, while L/a_a^V ratio is suitable for characterizing the *shape* of $S(\rho)$, due to small variations of a_a^V relative to variations of L between different interactions, the relative magnitudes of L and the relative magnitudes of L/a_a^V are usually interchangeable when comparing different interactions.

In Table I different parameters can be found, quantifying characteristics of the densities ρ_0 and ρ_a^0 , including respective diffuseness parameters, d_0 and d_a^0 . The isoscalar diffuseness d_0 is of obvious importance as quantifying the pace, independent of the symmetry energy, at which the isoscalar density approaches zero. We define each diffuseness parameter in

terms of the derivative of respective density at half of asymptotic value:

$$\frac{\rho_0}{4d_0} = \left. \frac{d\rho_0}{dz} \right|_{\rho_0(z)=\rho_0/2} \quad \text{and} \quad \frac{\rho_0}{4d_a^0} = \left. \frac{d\rho_a^0}{dz} \right|_{\rho_a^0(z)=\rho_0/2}. \quad (166)$$

We elect such a definition over the more common relation of diffuseness to the surface thickness as distance over which the density drops from 90% to 10% of asymptotic value. This is because of our intention to have consistent definitions for ρ and ρ_a and because of the potentially complicated features of ρ_a around normal density. The latter features are due to the relation of ρ_a to symmetry energy and due to amplified Friedel oscillations in ρ_a , as compared to ρ , cf. Fig. 8. For the isoscalar density, the definitions in terms of derivative and surface thickness yield nearly identical results.

The isoscalar diffuseness parameters tend to be fairly consistent between different Skyrme interactions, averaging at 0.541 fm in Table I, with an rms deviation of 0.031 fm. When a larger deviation from the average is found for an interaction in Table I, a correlated change, compared to other interactions, is typically found to occur in other distance parameters for the surface. For the lowest L -values, for which the $\rho_0/2$ -position of the isovector density lies within the classically allowed region, the isovector diffuseness needs obviously to depend on the shape of the dependence of symmetry energy on density, cf. Eq. (76). At any fixed shape for the symmetry energy, such as characterized by the ratio L/a_a^V , though, the isovector diffuseness should further scale in proportion to the isoscalar diffuseness that sets the scale for variation of isoscalar density in space. Figure 13 shows the correlation between, on one hand, the isovector diffuseness from the SHFM calculations, scaled with the isoscalar diffuseness, and, on the other, the slope parameter L scaled with a_a^V . A quite tight correlations is observed between the scaled parameters, with a linear fit to the results yielding

$$d_a^0 \simeq d_0 (1.062 - 0.117 L/a_a^V). \quad (167)$$

Interestingly, the tight correlation extends well into the region of the isovector $\rho_0/2$ -point lying beyond the $\rho_0/4$ -point in isoscalar density, representing the start of a classically forbidden region. Figure 13 shows also the correlation between the isovector diffuseness d_a^0 and slope L , when the parameter scaling is removed. The lack of scaling results in a deterioration of the correlation; analogous deteriorations may be found for other tight correlations in the paper, when scalings implied by the physics are removed.

More significant than the difference in diffusenesses, between the isovector and isoscalar

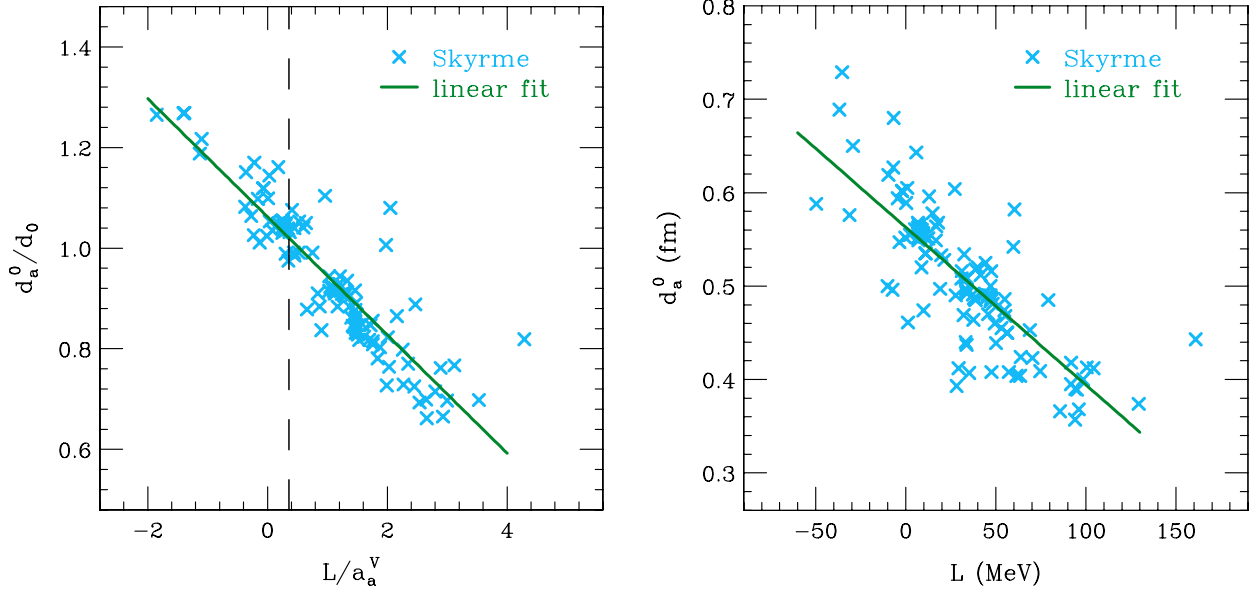


FIG. 13: Correlation between the diffuseness d_a^0 of isovector density in symmetric half-infinite matter and the slope parameter L of symmetry energy in uniform matter. In the first panel, the isovector diffuseness d_a^0 and the slope parameter L are scaled, respectively, with the diffuseness d_0 of isoscalar density and with the value a_a^V of symmetry energy at ρ_0 . No scalings are applied in the second panel. Symbols in the panels represent results for Skyrme interactions in Table I. Solid lines represent linear fits to the results for Skyrme interactions. The dashed vertical line in the first panel separates coarsely those interactions, to the left of the line, for which the $\rho_0/2$ -point in isovector density appears in the classically allowed region, from those interactions, to the right of the line, for which the $\rho_0/2$ -point appears in the classically forbidden region.

densities, is the overall displacement of those densities relative to each other. This displacement can be quantified in different ways. One possible quantification is in terms of the displacement ΔR^0 of the $\rho_0/2$ -density points for isovector and isoscalar densities, at $\eta = 0$, see Table I. Another possible quantification is in terms of the ratio of symmetry coefficients a_a^V/a_a^S , proportional to the integral over the difference of those densities at $\eta = 0$, in the direction perpendicular to nuclear surface, cf. Eq. (161). To the extent that the densities could be both described in terms of Fermi functions or, otherwise, were simply translations one of another, the ratio of coefficients could, following (161), be approximated with

$$\frac{a_a^V}{a_a^S} \simeq \frac{3 \Delta R^0}{r_0}. \quad (168)$$

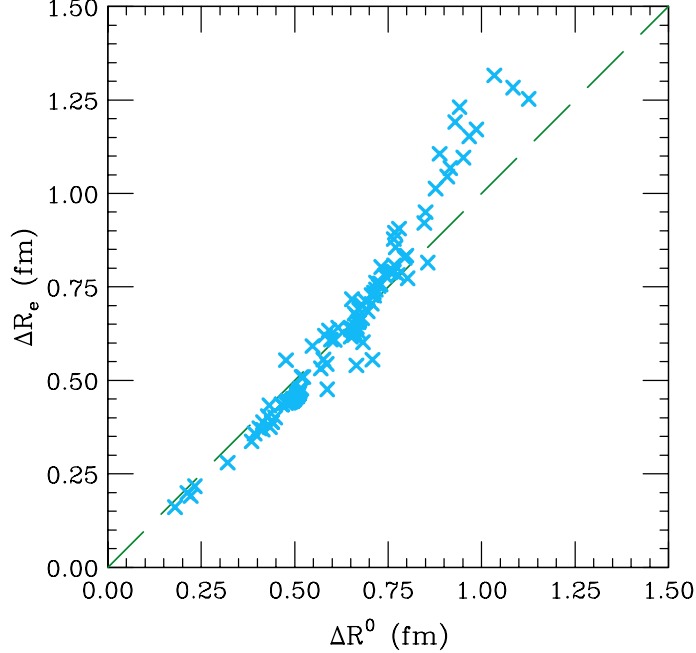


FIG. 14: Correlation between, on one hand, the relative displacement ΔR^0 of isovector and isoscalar densities in half-infinite symmetric matter, from the $\rho_0/2$ -points, and, on the other hand, the effective displacement $\Delta_e R = (a_a^V/a_a^S)(r_0/3)$. Symbols represent the variety of Skyrme interactions from Table I. The diagonal dashed line serves to guide the eye.

Following (168), we define an effective displacement in terms of the coefficient ratio as

$$\Delta_e R = \frac{r_0}{3} \frac{a_a^V}{a_a^S}, \quad (169)$$

which is provided in Table I in addition to ΔR^0 . Surface displacement ΔR^0 is found to range in the table from 0.21 to 1.13 fm. Figure 14 shows the correlation between the two displacements, for the Skyrme interactions. Over much of the range of variation, the displacements are rather close to each other. Only for the highest displacement values, $\Delta_e R$ tends to prevail over ΔR^0 .

Judging from the local approximation, and from Fig. 8, the most significant differences between the isovector and isoscalar densities should be associated with the highest L -values. Indeed, high L -values imply a rapid drop of symmetry energy at subnormal densities and, correspondingly, high isovector compared to isoscalar density values. Correlation between, on one hand, the symmetry parameter ratio a_a^V/a_a^S , proportional to the integral over density difference, cf. Eq. (161), and, on the other hand, the scaled slope parameter L/a_a^V , is shown in Fig. 15. The lowest values of the symmetry parameter ratio, of the order of 0.4, are

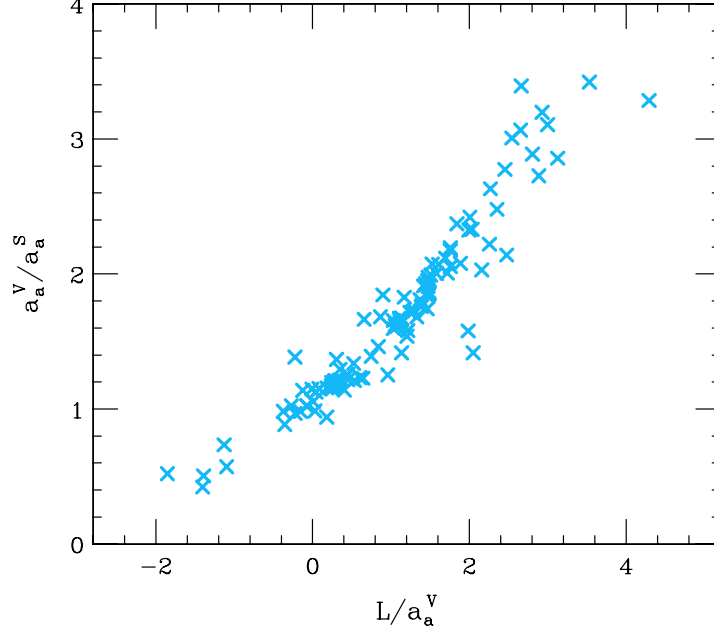


FIG. 15: Ratio of symmetry energy coefficients a_a^V/a_a^S , for different Skyrme interactions, plotted vs the slope parameter L of the symmetry energy, scaled with the value of symmetry energy a_a^V .

indeed found for the lowest values of scaled L , and the highest values of the ratio, of the order of 3.4, are found for the highest values of L . In more detail, the isovector density is expected to stay elevated, following the symmetry energy in the local approximation of Eq. (76), down to the isoscalar classical-return density of $\sim \rho_0/4$. With this, a correlation can be expected between the displacement ΔR^0 of the isovector from isoscalar surfaces and the value of symmetry energy at $\rho_0/4$. Figure 16 shows the correlation between ΔR^0 scaled with isoscalar diffuseness and the symmetry energy at $\rho_0/4$, scaled with a_a^V . The correlation is the tightest from among those explored here for surface properties. Linear fit to the correlation, represented by a solid line in Fig. 16, produces

$$\Delta R^0 \simeq d_0 (2.71 - 3.42 S(\rho_0/4)/a_a^V). \quad (170)$$

The dashed line in Fig. 16 represents prediction based on the simplified geometric consideration illustrated in Fig. 17, where the densities are taken to vary linearly with position. That consideration yields

$$\Delta R^0 \simeq d_0 + d_a^0 (a_a^V/S(\rho_0/4) - 2), \quad (171)$$

and, for Fig. 16, we use $d_a^0 \simeq d_0 (0.336 - 1.336 S(\rho_0/4)/a_a^V)$ from fitting the correlation of d_a^0 with symmetry energy. While the formula from the simple consideration begins to

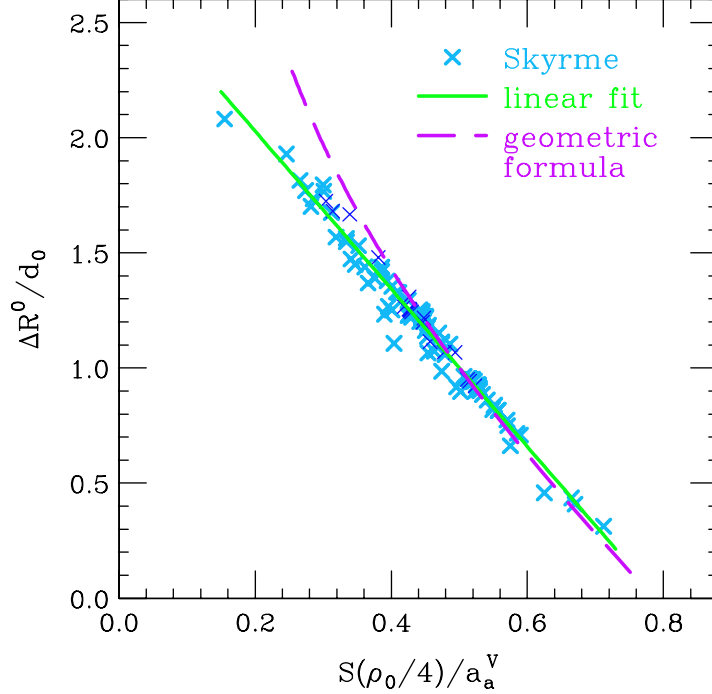


FIG. 16: Displacement of isovector- relative to isoscalar-density in symmetric half-infinite matter, plotted vs value of symmetry energy at $\rho_0/4$. The displacement and the energy value at $\rho_0/4$ are scaled, respectively, with the isoscalar diffuseness and the symmetry-energy value at ρ_0 . Symbols represent results for Skyrme interactions from Table I. Solid line represents a linear fit to the Skyrme results. Dashed line represents predictions of formula (171) based on simplified geometric considerations.

overestimate the shift for the symmetry energies with a strongest density-dependence, it is apparent that the simple consideration grasps the essence of impact of the low-density symmetry-energy on the shift.

Rounding up the set of correlations between surface characteristics and features of symmetry energy in uniform matter, Fig. 18 shows the displacement of the isovector- relative to isoscalar-surface for the Skyrme interactions, as a function of scaled slope parameter. Quality of this correlation does not change significantly when the shift is scaled with diffuseness, so we present the correlation without such a scaling, as possibly simpler to use. With the correspondence between the displacement ΔR^0 and the effective displacement $\Delta_e R$ proportional to a_a^V/a_a^S , cf. Fig. 14, Fig. 18 is a counterpart of Fig. 15. Linear fit to the Skyrme

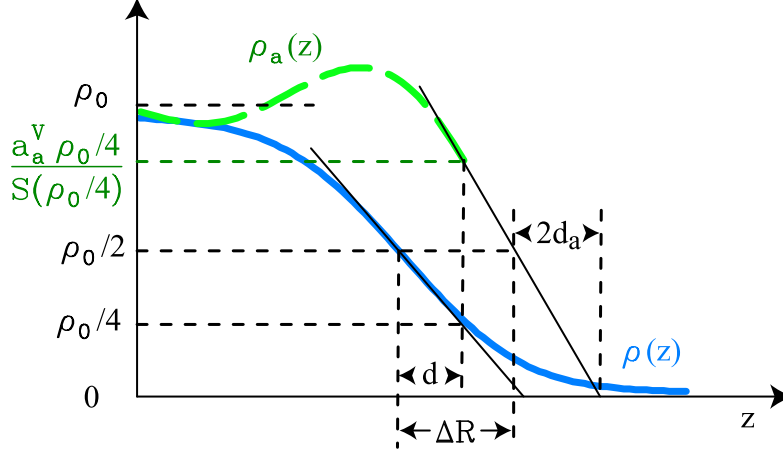


FIG. 17: Geometric construction behind Eq. (171). In the surface region, the dependence of isoscalar density and of the isovector density on position, beyond the breakdown of local approximation for ρ_a^0 , is approximated in a linear form, with the slope expressed in terms of the respective diffuseness.

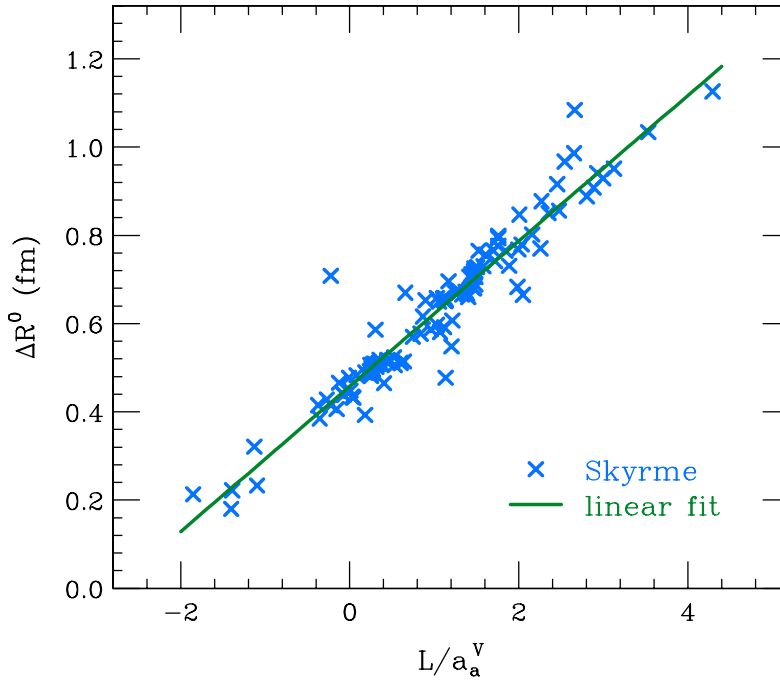


FIG. 18: Displacement of isovector- relative to isoscalar-surface in semi-infinite nuclear-matter, plotted vs normalized slope-parameter of symmetry energy. Symbols represent results for the Skyrme interactions of Table I. The line represents a linear fit to the Skyrme results.

results, which is indicated in Fig. 18, produces

$$\Delta R^0 \simeq (0.458 + 0.165 L/a_a^V) \text{ fm} . \quad (172)$$

I. Some Context

In discussing the isovector and isoscalar densities in the preceding subsection, we have concentrated on the shift of these densities relative to each other and on their diffusenesses. To the extent to which ρ_a^0 and ρ_0 might be approximated in terms of Fermi functions, these characteristics could suffice for describing the average sizes of asymmetry skins in nuclei. The skin sizes have been, so far, the prime aspect of nuclear density distributions linked in the literature to the density dependence of symmetry energy.

Specifically, in the context of asymmetry skins, let us consider neutron and proton rms radii for a nucleus of mass A . From (52), we find for the mean squared proton radius:

$$\langle r^2 \rangle_p = \langle r^2 \rangle + \frac{Z - N}{2Z} (\langle r^2 \rangle_a - \langle r^2 \rangle) , \quad (173)$$

where

$$\langle r^2 \rangle = \frac{1}{A} \int dV r^2 \rho(\mathbf{r}) , \quad (174)$$

and

$$\langle r^2 \rangle_a = \frac{\int dV r^2 \rho_a(\mathbf{r})}{\int dV \rho_a(\mathbf{r})} \equiv \frac{1}{N - Z} \int dV r^2 \rho_{np}(\mathbf{r}) . \quad (175)$$

With the $N \leftrightarrow Z$ interchange on the r.h.s. of (173) yielding the neutron instead of the proton mean squared-radius, the difference between nucleon squared-radii may be represented as

$$\langle r^2 \rangle_n - \langle r^2 \rangle_p = \frac{A(N - Z)}{2NZ} (\langle r^2 \rangle_a - \langle r^2 \rangle) . \quad (176)$$

From the above, we finally get for the size of asymmetry skin

$$\langle r^2 \rangle_n^{1/2} - \langle r^2 \rangle_p^{1/2} \simeq \frac{A(N - Z)}{4NZ} \frac{\langle r^2 \rangle_a - \langle r^2 \rangle}{\langle r^2 \rangle^{1/2}} . \quad (177)$$

It turns than out that the size of asymmetry skin directly probes the difference in mean squared radii for the isovector and isoscalar densities. When a density can be approximated in the Fermi form, the mean squared radius can be expressed in terms of the $\rho_0/2$ -position combined with diffuseness. Looking at Figs. 6 and 7, it is apparent that isoscalar densities are more likely to be well described in terms of a Fermi shape than isovector, particularly

for the most extreme symmetry energies, characterized by either very low or very high slope-parameters L .

Outside of the scope of this paper, analyses of data point to a symmetry energy in uniform matter that is characterized by a slope in the upper range of the values possible for Skyrme interactions, especially for the slope scaled with a_a^V . Thus, e.g. the analysis of excitation energies of isobaric analog states [97, 98] yields independent values of a_a^V and a_a^S . While the volume symmetry coefficient from this type of analysis, $a_a^V \simeq (31.5\text{--}33.5)\text{ MeV}$, comes out quite in the middle of values found for the Skyrme interactions, the surface symmetry coefficient, $a_a^S \simeq (9.5\text{--}12)\text{ MeV}$, comes out right at the lower end of values encountered for the Skyrme interactions. The coefficient ratio from that analysis is in the range $a_a^V/a_a^S \simeq (2.8\text{--}3.3)$. That ratio produces the effective surface displacement in the range of $\Delta_e R = (r_0/3)(a_a^V/a_a^S) \simeq (1.06\text{--}1.26)\text{ fm}$. Moreover, Figs. 14 and 15 yield the respective ranges of $\Delta R^0 \simeq (0.85\text{--}1.05)\text{ fm}$ and $L/a_a^V \simeq (2.4\text{--}3.4)$ or $L \simeq (78\text{--}111)\text{ MeV}$. The analysis [97, 98] is relatively model-independent, provided curvature effects play little role for heavier nuclei. If the latter were not the case, though, a bit softer symmetry energy would need to be deduced.

The large displacement for the isovector surface, inferred above, would give rise to large predicted asymmetry skins, cf. Eq. (177), towards the top of those that appear possible within the Skyrme-Hartree-Fock descriptions [97, 99]. Notably, still higher sizes of asymmetry skins can be encountered in the relativistic mean-field descriptions of nuclear systems, along with higher values of the L -parameter than encountered for the Skyrme parameterizations [99]. Aiming at constraints beyond those in [97, 98], on the symmetry energy in uniform matter, we intend to develop strategies for the constraints, further in this series, exploiting available experimental information on nucleonic densities, along the lines of developments of the present paper. Otherwise, the isovector density, as a fundamental quantity, deserves attention on its own when analyzing data on nucleonic densities.

V. CONCLUSIONS

In this paper, we have considered nuclear energy in the macroscopic limit for a nucleus. Further, we have considered the Hohenberg-Kohn functional for a nuclear system, in terms of proton and neutron densities. Finally, we have carried out Skyrme-Hartree-Fock calculations

of half-infinite particle-stable nuclear-matter. In each case, we have concentrated on the role of neutron-proton asymmetry in the system and on the symmetry energy.

In discussing nuclear energy in the macroscopic limit, we have shown that surface symmetry-energy emerges, as an unavoidable ingredient of the net nuclear energy, from simultaneous considerations of nuclear surface and symmetry energies. A consequence of this conclusion is that the net nuclear surface and volume energies combine in the similar manner as energies of connected capacitors in electrostatics. The role of charge flowing and distributing itself between the capacitors, is taken over by the asymmetry that distributes itself between the nuclear interior and surface, in proportion to volume and surfaces capacitances. The capacitances for the interior and surface are proportional, respectively, to the volume and surface area and are inversely proportional to the volume and surface symmetry coefficients.

When considering a continuous limit of the Hohenberg-Kohn functional, we have broken up the nuclear part of the functional into the functional for symmetric matter and a symmetry term that is bilinear, in the lowest order, in the difference of neutron and proton densities. The kernel \mathcal{S} in the symmetry term is generally nonlocal and depends on the net density. In the limit of weak nonuniformities, the kernel may be approximated in a local form as a δ -function multiplying symmetry energy in uniform matter, divided by local density. We have shown that, up to Coulomb corrections and terms of second order in asymmetry, the net nucleonic density and shape of the neutron-proton density difference are invariant, in the continuous limit, across an isobaric chain. The neutron-proton density difference, in particular, is expressible in terms of the inverse operator \mathcal{S} for the symmetric matter. In this context, we have introduced an isovector density, as a scaled neutron-proton density difference, and a counterpart to the net density, also termed isoscalar density. The neutron and proton densities can be expressed as a combination of those nearly invariant isoscalar and isovector densities. When the local approximation for \mathcal{S} holds, the isovector density is proportional to the isoscalar density divided by the value of symmetry energy for uniform matter. A generalized symmetry coefficient can be introduced for a nuclear system and can be expressed in terms of the inverse operator \mathcal{S} . The coefficient turns out, further, to be inversely proportional to the volume integral of the isovector density. Contributions to the net capacitance of the system, for asymmetry, can be expressed in terms of the volume integral of the difference of isovector and isoscalar densities.

We have carried out Skyrme-Hartree-Fock calculations of symmetric and asymmetric semi-infinite nuclear matter, with a significantly higher accuracy than in the past. The accuracy is important when trying to extract subtle symmetry effects associated with the nuclear surface. We have calculated symmetric surface and surface-symmetry characteristics for nearly all Skyrme parameterizations that have been proposed in the literature. In the calculations, we have verified the near-invariance of the isoscalar and isovector densities, first inferred within the considerations relying on the Hohenberg-Kohn functional. We have found that, up to the Friedel oscillations, the isovector density follows the expectation from the local approximation, down to about a quarter of normal density. Within the WKBJ approximation, we have shown that the isovector density is expected to follow the local approximation within the classically allowed region for single-particle wavefunctions. In the far-out forbidden region, on the other hand, the density fall-off is governed by separation energy. We have extracted displacements of isovector- relative to isoscalar-density as well diffuseness values for the two densities. By integrating differences of the two densities for symmetric matter, we have determined values of the surface symmetry coefficient for different Skyrme parameterizations. Consistently with qualitative expectations, we found the displacements and volume-to-surface symmetry-coefficient ratios to be strongly correlated with the density dependence of symmetry energy in uniform matter. The faster the symmetry energy drops at subnormal densities, the larger the relative displacement of the two densities and the larger the coefficient ratio.

One exciting possibility, emerging as a consequence of our investigations, is that, due to the invariance of two fundamental densities, isoscalar and isovector, features of the symmetry energy could be investigated by studying systematics of proton distributions alone, without reference to neutron distributions. Such an investigation requires, however, a careful separation and/or circumvention of shell, pairing, Coulomb and deformation effects on the proton distribution for finite nuclei. The obvious difficulty of such separation may be compensated by the rather extensive knowledge of proton densities.

Acknowledgments

The authors are grateful to J. Rikovska Stone for supplying them with values of force constants for the majority of Skyrme interactions employed in this work. They further

thank H. S. Kohler, W. Nazarewicz and J. M. Pearson for comments related to the paper. This work was supported by the National Science Foundation under Grants PHY-0551164, PHY-0555893, PHY-0606007 and PHY-0800026.

-
- [1] P. Hohenberg and W. Kohn, Phys. Rev. 136 (1964) B864.
- [2] P.-G. Reinhard, in *Computational Nuclear Physics 1: Nuclear Structure*, edited by K. Langanke, J. A. Maruhn and S. E. Koonin, pp. 29–50 (Springer-Verlag, New York), 1991.
- [3] M. Farine, Z. Phys. A 321 (1985) 265.
- [4] H. S. Kohler, Nucl. Phys. A 139 (1969) 353.
- [5] H. S. Kohler, Nucl. Phys. A 258 (1976) 301.
- [6] J. Cote and J. M. Pearson, Nucl. Phys. A 304 (1978) 104.
- [7] M. Farine, J. Côte and J. M. Pearson, Nucl. Phys. A 338 (1980) 86.
- [8] M. Farine, J. Côte and J. M. Pearson, Phys. Rev. C 24 (1981) 303.
- [9] M. D. Estal, M. Centelles and X. Vinas, Nucl. Phys. A 650 (1999) 443.
- [10] M. Brack, C. Guet and H. B. Hakansson, Phys. Rept. 123 (1985) 275.
- [11] W. D. Myers, W. J. Swiatecki and C. S. Wang, Nucl. Phys. A 436 (1985) 185.
- [12] K. Kolehmainen, M. Prakash, J. M. Lattimer and J. R. Treiner, Nucl. Phys. A 439 (1985) 535.
- [13] J. Treiner and H. Krivine, Ann. Phys. 170 (1986) 406.
- [14] M. Centelles, M. D. Estal and X. Vinas, Nucl. Phys. A 635 (1998) 193.
- [15] W. D. Myers and W. J. Świątecki, Phys. Rev. C 63 (2001) 034318.
- [16] A. W. Steiner, M. Prakash, J. M. Lattimer and P. J. Ellis, Phys. Rept. 411 (2005) 325, nucl-th/0410066.
- [17] P. Moller, J. R. Nix, W. D. Myers and W. J. Swiatecki, At. Data Nucl. Data Tables 59 (1995) 185, nucl-th/9308022.
- [18] H. Koura, M. Uno, T. Tachibana and M. Yamada, Nucl. Phys. A 674 (2000) 47.
- [19] K. Pomorski and J. Dudek, Phys. Rev. C 67 (2003) 044316, nucl-th/0205011.
- [20] G. Royer and C. Gautier, Phys. Rev. C 73 (2006) 067302.
- [21] J. Mendoza-Temis *et al.*, Nucl. Phys. A 799 (2008) 84.
- [22] M. W. Kirson, Nucl. Phys. A 798 (2008) 29.
- [23] A. N. Tikhonov, Sov. Math. Dokl. 4 (1963) 1035, originally in Dokl. Akad. Nauk SSSR 151 (1963) 501-504.
- [24] P. Danielewicz, Nucl. Phys. A727 (2003) 233, nucl-th/0301050.

- [25] A. E. L. Dieperink and P. V. Isacker, *Eur. Phys. J. A* 32 (2007) 11.
- [26] S. Kubis, *Phys. Rev. C* 76 (2007) 025801.
- [27] W. D. Myers and W. J. Swiatecki, *Ann. Phys.* 55 (1969) 395.
- [28] W. D. Myers and W. J. Swiatecki, *Phys. Rev. C* 62 (2000) 044610.
- [29] W. D. Myers and W. J. Swiatecki, *Ann. Phys.* 84 (1974) 186.
- [30] W. Zuo, I. Bombaci and U. Lombardo, *Phys. Rev. C* 60 (1999) 024605.
- [31] J. M. Lattimer and M. Prakash, *Phys. Rept.* 442 (2007) 109, astro-ph/0612440.
- [32] J. Rikovska Stone *et al.*, *Phys. Rev. C* 68 (2003) 034324.
- [33] J. Rikovska Stone, private communication, 2007.
- [34] G. Colo *et al.*, *Phys. Rev. C* 70 (2004) 024307, nucl-th/0403086.
- [35] D. Vautherin and D. M. Brink, *Phys. Rev. C* 5 (1972) 626.
- [36] M. Beiner, H. Flocard, N. van Giai and P. Quentin, *Nucl. Phys. A* 238 (1975) 29.
- [37] M. J. Giannoni and P. Quentin, *Phys. Rev. C* 21 (1980) 2076.
- [38] C. M. Ko, H. C. Pauli, M. Brack and G. E. Brown, *Nucl. Phys. A* 236 (1974) 269.
- [39] F. Tondeur, M. Brack, M. Farine and J. M. Pearson, *Nucl. Phys. A* 420 (1984) 297.
- [40] J. Treiner and H. Krivine, *J. Phys. G* 2 (1976) 285.
- [41] H. Krivine, J. Treiner and O. Bohigas, *Nucl. Phys. A* 336 (1980) 155.
- [42] J. M. G. Gomez and M. Casas, *Few-Body Syst. Suppl.* 8 (1995) 374.
- [43] L. Bennour *et al.*, *Phys. Rev. C* 40 (1989) 2834.
- [44] J. Bartel *et al.*, *Nucl. Phys. A* 386 (1982) 79.
- [45] N. van Giai and H. Sagawa, *Phys. Lett. B* 106 (1981) 379.
- [46] M. Rayet, M. Arnould, G. Paulus and F. Tondeur, *Astron. Astrophys.* 116 (1982) 183.
- [47] J. Dobaczewski, H. Flocard and J. Treiner, *Nucl. Phys. A* 422 (1984) 103.
- [48] J. Friedrich and P.-G. Reinhard, *Phys. Rev. C* 33 (1986) 335.
- [49] J. M. Pearson *et al.*, *Nucl. Phys. A* 528 (1991) 1.
- [50] Y. Aboussir, J. M. Pearson, A. K. Dutta and F. Tondeur, *Nucl. Phys. A* 549 (1992) 155.
- [51] J. M. Pearson and R. C. Nayak, *Nucl. Phys. A* 668 (2000) 163.
- [52] M. Onsi, H. Przysiezniak and J. M. Pearson, *Phys. Rev. C* 50 (1994) 460.
- [53] R. C. Nayak and J. M. Pearson, *Phys. Rev. C* 52 (1995) 2254.
- [54] C. J. Pethick, D. G. Ravenhall and C. P. Lorenz, *Nucl. Phys. A* 584 (1995) 675.
- [55] M. M. Sharma, G. Lalazissis, J. König and P. Ring, *Phys. Rev. Lett.* 74 (1995) 3744.

- [56] P.-G. Reinhard and H. Flocard, Nucl. Phys. A 584 (1995) 467.
- [57] W. Nazarewicz *et al.*, Phys. Rev. C 53 (1996) 740.
- [58] E. Chabanat, *Interactions effectives pour des conditions extremes d'isospin*, Ph.D. thesis, University Claude Bernard Lyon-1, Lyon, France, 1995.
- [59] E. Chabanat *et al.*, Nucl. Phys. A 627 (1997) 710.
- [60] E. Chabanat *et al.*, Nucl. Phys. A 635 (1998) 231.
- [61] B. Alex Brown, Phys. Rev. C 58 (1998) 220.
- [62] P.-G. Reinhard *et al.*, Phys. Rev. C 60 (1999) 014316.
- [63] M. Rashdan, Mod. Phys. Lett. A 15 (2000) 1287.
- [64] F. Tondeur, S. Goriely, J. M. Pearson and M. Onsi, Phys. Rev. C 62 (2000) 024308.
- [65] J. M. Pearson and S. Goriely, Phys. Rev. C 64 (2001) 027301.
- [66] S. Goriely, F. Tondeur and J. M. Pearson, At. Data Nucl. Data Tables 77 (2001) 311.
- [67] S. Goriely, M. Pearson and F. Tondeur, Nucl. Phys. A 688 (2001) 349.
- [68] J. Margueron, J. Navarro and N. Van Giai, Phys. Rev. C 66 (2002) 014303.
- [69] M. Samyn *et al.*, Nucl. Phys. A 700 (2002) 142.
- [70] S. Goriely *et al.*, Phys. Rev. C 66 (2002) 024326.
- [71] S. Goriely, M. Samyn, M. Bender and J. M. Pearson, Phys. Rev. C 68 (2003) 054325.
- [72] M. Samyn, S. Goriely, M. Bender and J. M. Pearson, Phys. Rev. C 70 (2004) 044309.
- [73] S. Goriely, M. Samyn and J. Pearson, Nucl. Phys. A 773 (2006) 279.
- [74] S. Goriely, M. Samyn and J. M. Pearson, Phys. Rev. C 75 (2007) 064312.
- [75] B. K. Agrawal, S. Shlomo and V. Kim Au, Phys. Rev. C 68 (2003) 031304.
- [76] P. A. M. Guichon and A. W. Thomas, Phys. Rev. Lett. 93 (2004) 132502.
- [77] B. K. Agrawal, S. Shlomo and V. K. Au, Phys. Rev. C 72 (2005) 014310.
- [78] L. G. Cao, U. Lombardo, C. W. Shen and N. V. Giai, Phys. Rev. C 73 (2006) 014313.
- [79] A. R. Bodmer and Q. N. Usmani, Phys. Rev. C 67 (2003) 034305.
- [80] W. Kohn and L. J. Sham, Phys. Rev. 140 (1965) A1133.
- [81] K. Bennaceur and J. Dobaczewski, Comput. Phys. Commun. 168 (2005) 96, nucl-th/0501002.
- [82] S. A. V., T. S. V. and F. S. A., Yad. Fiz. 48 (1988) 1661.
- [83] D. A. Kirzhnits, *Field Theoretical Methods in Many Body Systems* (Pergamon, Oxford), 1967.
- [84] P. H. Cowell and A. C. D. Crommelin, *Investigation of the motion of Halley's comet from 1759 to 1910, Appendix to the volume of Greenwich Observations for the year 1909* (Neill &

- Co. Ltd., Edinburgh), 1910.
- [85] B. V. Noumerov, Publications de l'Observatoire Astrophysique Central de Russie II (1923) 188.
 - [86] B. V. Noumerov, Monthly Notices Roy. Astr. Soc. 84 (1924) 592.
 - [87] J. Dobaczewski, H. Flocard and J. Treiner, Nucl. Phys. A 422 (1984) 103.
 - [88] W. Stocker, Nucl. Phys. A 159 (1970) 222.
 - [89] J. Friedel, Adv. Phys. 3 (1954) 446.
 - [90] M. Farine, J. M. Pearson and F. Tondeur, Nucl. Phys. A 615 (1997) 135.
 - [91] M. Samyn, S. Goriely and J. M. Pearson, Phys. Rev. C 72 (2005) 044316.
 - [92] M. Samyn, S. Goriely and J. M. Pearson, Nucl. Phys. A 725 (2003) 69.
 - [93] S. Goriely, M. Samyn, J. M. Pearson and M. Onsi, Nucl. Phys. A 750 (2005) 425.
 - [94] S. Goriely and J. M. Pearson, Phys. Rev. C 77 (2008) 031301.
 - [95] M. Farine, Ph.D. thesis, University of Montreal, Montreal, Quebec, Canada, 1981.
 - [96] P.-G. Reinhard, M. Bender, W. Nazarewicz and T. Vertse, Phys. Rev. C 73 (2006) 014309.
 - [97] P. Danielewicz, Nuclear symmetry energy: from nuclear extremes to neutron- star matter, 2004, unpublished, nucl-th/0411115.
 - [98] P. Danielewicz and J. Lee, AIP Conf. Proc. 947 (2007) 301, arXiv 0708.2830.
 - [99] S. Typel and B. A. Brown, Phys. Rev. C 64 (2001) 027302.